The Miocene Tatatila–Las Minas IOCG skarn deposits (Veracruz) as a result of adakitic magmatism in the Trans-Mexican Volcanic Belt

Los depósitos de tipo skarn IOCG miocénicos de Tatatila–Las Minas (Veracruz) como resultado del magmatismo adakítico de la Faja Volcánica Trans-Mexicana

Edith **Fuentes-Guzmán**[1,2,3], Eduardo **González-Partida**[4], Antoni **Camprubí**[1,3*], Geovanny **Hernández-Avilés**[2], Janet **Gabites**[5], Alexander **Iriondo**[4,6], Giovanni **Ruggieri**[7], Margarita **López-Martínez**[8]

[1] Instituto de Geología, Universidad Nacional Autónoma de México. Ciudad Universitaria, 04510 Coyoacán, CDMX, Mexico.

[2] Programa de Posgrado en Ciencias de la Tierra, Universidad Nacional Autónoma de México. Ciudad Universitaria, 04510 Coyoacán, CDMX / Boulevard Juriquilla 3001, 76230 Juriquilla, Querétaro, Mexico.

[3] Laboratorio Nacional de Geoquímica y Mineralogía (LANGEM). Ciudad Universitaria, 04510 Coyoacán, CDMX, Mexico.

[4] Centro de Geociencias, Universidad Nacional Autónoma de México. Boulevard Juriquilla 3001, 76230 Juriquilla, Querétaro, Mexico.

[5] Pacific Centre for Isotopic and Geochemical Research, Department of Earth, Ocean and Atmospheric Sciences, University of British Columbia; Earth Sciences Building, 2207 Main Mall, Vancouver, V6T 1Z4, British Columbia, Canada.

[6] Department of Geosciences, University of Arizona. 1040 E 4th Street, 85721, Tucson, Arizona,USA.

[7] Istituto di Geoscienze e Georisorse, Consiglio Nazionale delle Ricerche. Via G. Moruzzi 1, 56124 Pisa, Italy.

[8] Centro de Investigación Científica y Estudios Superiores de Ensenada. Carretera Tijuana-Ensenada km. 107, 22860 Ensenada, Baja California, Mexico.

* Corresponding author: (A. Camprubí)
camprubi@comunidad.unam.mx

How to cite this article:
Fuentes-Guzmán, E., González-Partida, E., Camprubí, A., Hernández-Avilés, G., Gabites, J., Iriondo, A., Ruggieri, G., López-Martínez, M., 2020, The Miocene Tatatila–Las Minas IOCG skarn deposits (Veracruz) as a result of adakitic magmatism in the Trans-Mexican Volcanic Belt: Boletín de la Sociedad Geológica Mexicana, 72 (3), A110520. http://dx.doi.org/10.18268/BSGM2020v72n3a110520

Manuscript received: October 28, 2020
Corrected manuscript received: May 1, 2020
Manuscript accepted: May 10, 2020

Peer Reviewing under the responsibility of Universidad Nacional Autónoma de México.

ABSTRACT

The Cu- and Au-rich Tatatila–Las Minas IOCG skarn deposits in Veracruz (central-east Mexico) are circumscribed to the earliest stages of the Trans-Mexican Volcanic Belt (TMVB) and stand for a metallogenic province directly linked to its tectonomagmatic dynamics. This is the first well-documented case for such metallogenic province. These deposits were formed as skarns between rocks of the Mesozoic carbonate series and Miocene intermediate to acid hypabyssal rocks. New U-Pb zircon and $^{40}Ar/^{39}Ar$ ages provide evidence for four epochs of magmatic activity in the area: (1) early Permian (Artinskian), in association with the Paleozoic basement, (2) late Oligocene to early Miocene suite of pre-TMVB intrusive rocks, (3) middle to late Miocene suite of early TMVB-related intrusive rocks, and (4) Pliocene intrusive and extrusive rocks of the TMVB, possibly associated with the Los Humeros post-caldera stage. The obtained ages range between 24.60 ± 1.10 and 19.04 ± 0.69 Ma for stage 2, and between 16.34 ± 0.20 and 13.92 ± 0.22 Ma for stage 3. Stage 2 corresponds to a magmatic stage unheard of in the area, until this study. Only stage 3 rocks are associated with the IOCG skarn mineralization, with retrograde stages dated at 12.44 ± 0.09 (chromian muscovite, phyllic association) and 12.18 ± 0.21 Ma (zircon, potassic association). Therefore, the ages of stage-3 intrusive rocks are interpreted to date the formation of

RESUMEN

Los skarns IOCG ricos en Cu y Au de Tatatila–Las Minas en Veracruz (centro-oriente de México) están circunscritos a los estadíos más tempranos de la Faja Volcánica Transmexicana (FVTM) e indican directamente la existencia de una provincia metalogenética vinculada a su dinámica tectonomagmática. Este es el primer caso bien documentado para dicha provincia metalogenética. Estos depósitos se formaron como skarns entre rocas de la secuencia carbonatada del Mesozoico y rocas hipabisales indermedias a ácidas del Mioceno. Los nuevos fechamientos U-Pb en zircón y $^{40}Ar/^{39}Ar$ evidencian la existencia de cuatro épocas de actividad magmática en el área: (1) en el Pérmico temprano (Artinskiano), en asociación con el basamento paleozoico de las secuencias del Mesozoico, (2) un conjunto de intrusivos pre-FVTM entre del Oligoceno tardío y el Mioceno temprano, (3) un conjunto de intrusivos del Mioceno medio y tardío asociados a la FVTM, y (4) rocas intrusivas extrusivas del Plioceno de la FVTM, posiblemente asociadas a los depósitos del estadio post-caldera de Los Humeros. Las edades obtenidas varían entre 24.60 ± 1.10 y 19.04 ± 0.69 Ma para el estadío 2, y entre 16.34 ± 0.20 y 13.92 ± 0.22 Ma para el estadío 3. El estadío 2 corresponde a una etapa magmática hasta el presente estudio desconocida en el área. Sólo las rocas del estadío 3 están asociadas a las mineralizaciones de skarn IOCG, cuyas etapas retrógradas han sido fechadas en 12.44 ± 0.09 (moscovita crómica, asociación fílica) y 12.18 ± 0.21 Ma (zircón, asociación potásica). Por tanto, las edades de las rocas intrusivas del estadío 3 se interpretan como parte de las asociaciones de skarn prógrado (mayormente, de ~15.4 a <14 Ma).

http://dx.doi.org/10.18268/BSGM2020v72n3a110520

the prograde skarn associations (mostly ~15.4 to <14 Ma). The petrogenetic affinity of stage-2 and stage-3 rocks is about the same—the main difference has to do with higher Y and Yb contents in stage-3 rocks (although no affinity with within-plate granites was found), which is suggestive of an interaction of their parental magmas with alkaline magmas that most likely belong to the conterminous and contemporaneous Eastern Mexico Alkaline Province. Petrological indicators (elemental and isotopic) in Cenozoic rocks consistently point to intermediate to acid, metaluminous, I- and S-type rocks that were emplaced in a subduction-related continental arc, within the medium- to high-potassium calc-alkaline series, with high-silica adakitic signatures due associated to deep-sourced magmas that underwent crustal contamination to some degree. The various possible sources for the magmas with adakitic signature in this context can be narrowed down to two of them that are not mutually exclusive: adakitic derived from subducted slab melting and melting-assimilation-storage-homogenization (MASH)-derived adakites. Both sources are, in principle, capable of generating magmas that would eventually produce magmatic-hydrothermal mineralizing systems with an associated variety of ore deposit types, including IOCG. Also, both possible sources for adakites are compatible with the renewed steepening of the subducted slab after a period of flat subduction, for the earliest stage in the evolution of the TMVB.

Keywords: IOCG, adakites, Miocene, Trans-Mexican Volcanic Belt, skarn, magmatic-hydrothermal, iron oxides.

La afinidad petrogenética de las rocas correspondientes a los estadíos 2 y 3 es prácticamente la misma—su principal diferencia estriba los contenidos más altos de Y e Yb en rocas del estadío 3 (aunque no se encontró afinidad alguna con granitos de intraplaca), lo cual sugiere la interacción de sus magmas primigenios con magmas alcalinos que posiblemente pertenecieron a la contigua y contemporánea Provincia Alcalina Oriental Mexicana. Los indicadores petrogenéticos (elementales e isotópicos) en las rocas del Cenozoico apuntan consistentemente a rocas intermedias a ácidas, metalumínicas, de tipo I y S, emplazadas en un arco continental debido a subducción y pertenecen a las series calci-alcalinas de potasio medio a alto, con (mayormente) firmas de adakitas altas en sílice debidas a un origen profundo de magmas que experimentaron cierto grado de contaminación cortical. La diversidad de posibles orígenes para las fimas adakíticas en este contexto pueden reducirse a sólo dos de ellas, que no son mutuamente exclusivas: adakitas derivadas de la fusión de la placa subducida y adakitas derivadas de procesos tipo fusión-asimilación-almacenamiento-homogeneización (MASH, por sus siglas en inglés). Ambas fuentes, en principio, poseen la capacidad de generar magmas que eventualmente pudieran producir sistemas mineralizantes magmático-hidrotermales con una cierta variedad de tipos de depósitos minerales asociados, incluyendo depósitos IOCG. Además, ambas posibles fuentes de adakitas son compatibles con la reverticalización de la placa subducida tras un periodo de subducción plana para el estadío más temprano en la evolución de la FVTM.

Palabras clave: IOCG, adakitas, Mioceno, Faja Volcánica Transmexicana, skarn, magmático-hidrotermal, óxidos de hierro.

1. Introduction

Recent assessment has shown that the metallogenic potential of the mid-Miocene to Holocene Trans-Mexican Volcanic Belt (TMVB) and the potential of Miocene to Holocene ore deposits in Mexico are greater than previously believed (Camprubí, 2009, 2013; Clark and Fitch, 2009; Poliquin, 2009; Jansen *et al.*, 2017; Camprubí *et al.*, 2019, 2020; Fuentes-Guzmán *et al.*, 2020). The metallogeny of Miocene to Holocene epochs in Mexico is, in fact, distributed across several regions, namely (1) the southernmost part of the Sierra Madre Occidental, in association with its last ignimbritic flare-up, (2) the Trans-Mexican Volcanic Belt (TMVB), (3) the southern part of the Eastern Mexico Alkaline Province (EMAP) and northern Chiapas, (4) the easternmost part of the Sierra Madre del Sur (in Oaxaca), and (5) the Gulf of California. As (a) the easternmost ending of the TMVB coincides with the N-S geographic distribution of the EMAP, (b) the metallogeny of the TMVB is still poorly understood, and (c) there is a wide variety of types of ore deposits across the EMAP—including, skarns, metalliferous porphyries, epithermal deposits, IOCG deposits and carbonatites—, the identification of whether an ore deposit in such a region is geologically associated with the TMVB or the EMAP is not a straightforward task.

The Tatatila–Las Minas district in Veracruz State is located precisely in the region in which the TMVB and the EMAP overlap geographically, in the Palma Sola area. The ore deposits in the

http://dx.doi.org/10.18268/BSGM2020v72n3a110520

Tatatila–Las Minas have a magmatic-hydrothermal origin and are essentially Cu-Au iron oxide skarns, part of the IOCG "clan", and epithermal deposits (Camprubí, 2013). Therefore, in order to investigate the origin of these deposits, the first necessary step would be to elucidate their genetic affinity with either magmatic province. Camprubí (2013) deduced a plausible age of ~11 Ma and some affinity with alkaline magmatism for the deposits in the Tatatila–Las Minas district, based on Negendank *et al.* (1985) and Ferrari *et al.* (2005a), which linked the Palma Sola massif with the EMAP. However, the middle Miocene to Recent alkaline and calc-alkaline volcanism of the Palma Sola area was ascribed to the TMVB, and to the subduction along the Pacific trench, as in Besch *et al.* (1988), Gómez-Tuena *et al.* (2003), and Orozco-Esquivel *et al.* (2007). The relevance of the EMAP, besides its petrotectonic affinity, as a major metallogenic province was already stressed by Camprubí (2009, 2013). However, the age of magmatism with which these ore deposits were plausibly associated corresponds well to the middle and late Miocene arc at the beginning of the TMVB (~19 to 10 Ma; Gómez-Tuena *et al.*, 2005, 2007).

In summary, we may use as a starting hypothesis the fact that neither the EMAP nor the TMVB are implausible magmatic provinces to have produced the parental magmatism to the Tatatila–Las Minas deposits. The implications for regional mineral exploration that may arise from either possibility are very different, nonetheless. In this paper, we analyze the petrologic affinity of the hypabyssal intrusive bodies with which the formation of the IOCG deposits of the Tatatila–Las Minas district is associated. This will enable a discrimination between the ascription of these deposits to the metallogeny of the TMVB or the EMAP. The proximal-to-source character of these magmatic-hydrothermal deposits (i.e., iron skarns) allows to soundly elucidate the linkage between the magmatism and the hydrothermal activity that generated the deposits. In addition, this paper contributes to a long-standing program that aims to the geochronological characterization of Mexican mineral deposits and the geologic events with which they are genetically associated (Camprubí *et al.*, 2015, 2016a, 2016b, 2017, 2018, 2019, 2020; Farfán-Panamá *et al.*, 2015; Martínez-Reyes *et al.*, 2015; González-Jiménez *et al.*, 2017a, 2017b; Enríquez *et al.*, 2018; Fuentes Guzmán *et al.*, 2020) to better constrain the metallogenic evolution of Mexico, as documented by Camprubí (2009, 2013, 2017).

2. Geological setting

The Tatatila-Las Minas mining district is located in the central-eastern part of the state of Veracruz (Figure 1) within the Palma Sola massif. It is characterized by the intrusion of Neogene stocks. Stock compositions are described to vary between gabbro and granodiorite, with dominantly monzodioritic to dioritic compositions, and intruded middle Jurassic, red beds and lower Cretaceous carbonate rocks. The latter rocks are part of the continental to marine sequences of the Sierra Madre Oriental that were deformed during the orogenic pulses of the Mexican Fold-and-Thrust Belt between the late Cretaceous and the Paleocene (Centeno-García, 2017; Fitz-Díaz *et al.*, 2018; and references therein). The Middle Jurassic red bed sequence in the area correlates with the Cahuasas Formation, and is overlain by carbonates and lutites of the Pimienta (Tithonian-Barriasian) and Orizaba (Albian-Cenomanian) formations. The host carbonate series in the study area consists essentially of platform carbonates that correspond to the Orizaba Formation (Ortuño-Arzate *et al.*, 2005). The Lower Cretaceous sequence unconformably overlies Permo-Triassic schists intruded by granitic rocks. The latter can be mistaken for Neogene intrusive bodies with similar compositions, as the thick vegetation cover commonly hinders their visualization and the identification of the lithologic contacts; both groups of intrusive rocks come in contact by faulting in the northern-

http://dx.doi.org/10.18268/BSGM2020v72n3a110520

most termination of the mineralized area (Figure 1). The Mesozoic sedimentation was controlled by the horst-and-graben configuration that resulted from the opening of the Gulf of Mexico during the breakup of Pangea (Martini and Ortega-Gutiérrez, 2018), thus developing simultaneously shallow platforms and relatively deep open-sea facies, hence the Córdoba platform (Ortuño-Arzate *et al.*, 2005) on which the upper Jurassic and Lower Cretaceous sedimentary units developed.

Neogene intrusive bodies generated typical skarn associations, with prograde mineralization by contact metamorphism (Ca silicate-rich) that was followed by retrograde IOCG-type hydrothermal stages of mineralization (Figure 2). Such intrusive bodies made up a NE-SW striking ~20 km long and ~10 km wide intrusive ensemble whose composition varies from gabbro to granodiorite, with dominantly monzodioritic to dioritic compositions (see below) with phaneritic textures. These rocks typically contain hornblende, biotite, pyroxenes, apatite and zircon this two as accessory mineral (Figure 3). Some andesite dykes, up to 30 m long and ~2 m thick crosscut the intrusive ensemble and predate the mineralization. A sequence of andesitic, basaltic and dacitic hypabyssal, this with porphyritic texture include plagioclase phenocrysts and volcanic rocks postdates the mineralization and the emplacement of the associated intrusive rocks, and comprises a variety of depos-

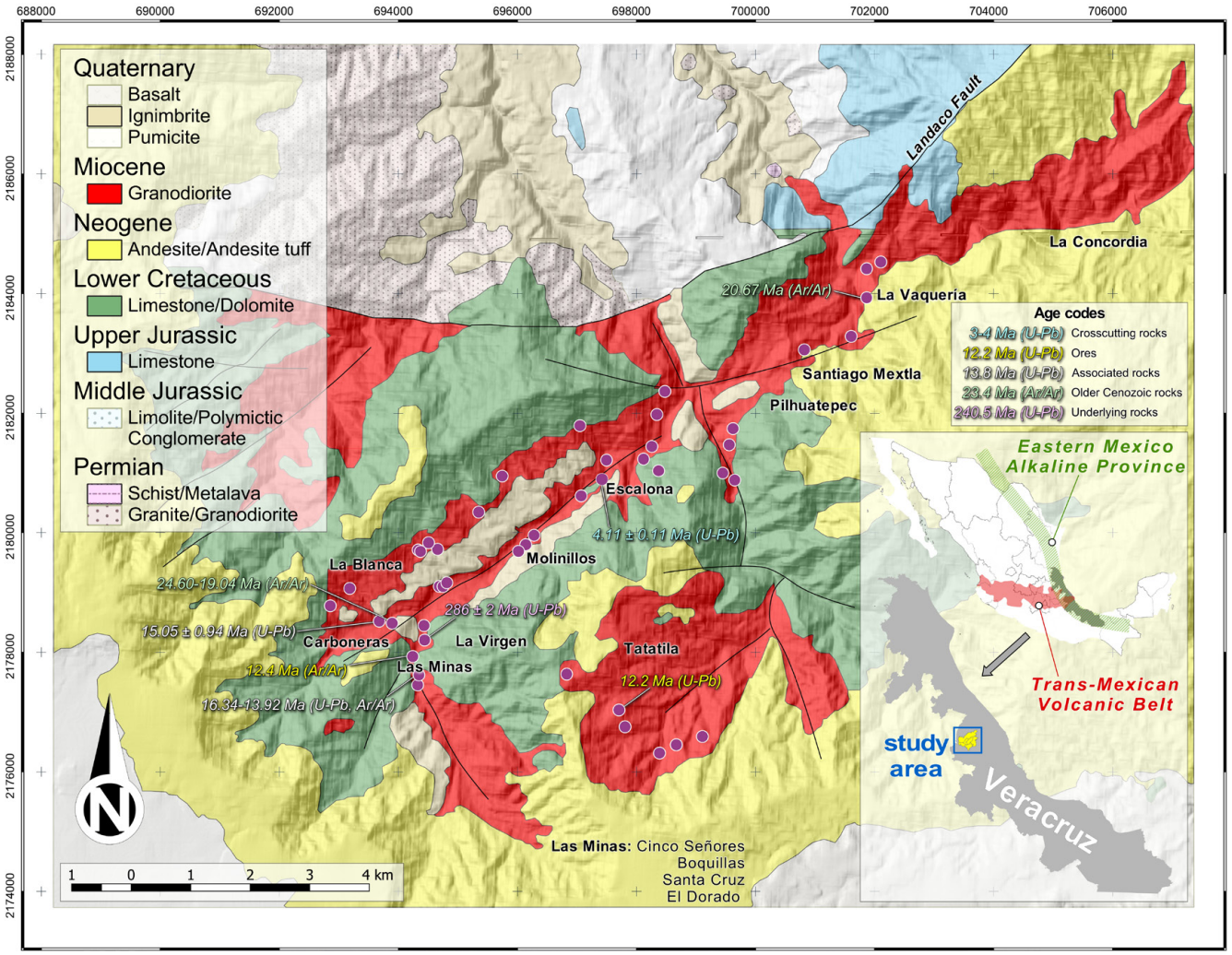

Figure 1 Geological map of the Tatatila–Las Minas mining district, east of the Palma Sola massif. Adapted from Servicio Geológico Mexicano (2007, 2010). Purple circles denote the location of samples on which this study is based, with indication of the obtained ages.

http://dx.doi.org/10.18268/BSGM2020v72n3a110520

its, including volcanic conglomerates, tuffs, ash-fall and pyroclastic deposits. Such rocks are interpreted as distal Pliocene deposits associated with the post-caldera deposits of Los Humeros caldera (Carrasco-Nuñez *et al.*, 2018; Dorantes-Castro, 2016; Sarabia-Jacinto, 2017). Ages for the Palma Sola area to the east of the Tatatila-Las Minas area were 14.6 ± 0.3 (U-Pb, zircon) and 11 ± 0.87 Ma (K-Ar, biotite), were reported by Poliquin (2009) and Murillo-Muñetón and Torres-Vargas (1987), respectively. These correspond to the ensemble of hypabyssal and volcanic rocks that allowed Camprubí (2013) to deduce a tentative age of ~11 Ma for these ore deposits, which is also constrained by the formation of capping volcanic rocks between 9 and 6.6 Ma. Contact metamorphism and mineralization of the fresh carbonate rocks can be observed in the conspicuous formation of marble in a 300 to 400 m wide zone that shows an outward decreasing degree of recrystallization. Skarn associations are distributed in the classic zonation from endoskarn to exoskarn. Endoskarns consist of grossular-andradite, clinopyroxene, and quartz in prograde associations, and magnetite, chalcopyrite, bornite, and native gold in retrograde associations (Figure 2). Exoskarns consist of wollastonite, clinopyroxene, potassium feldspar, quartz, epidote, and chromian muscovite ("fuchsite"; Figure 2).

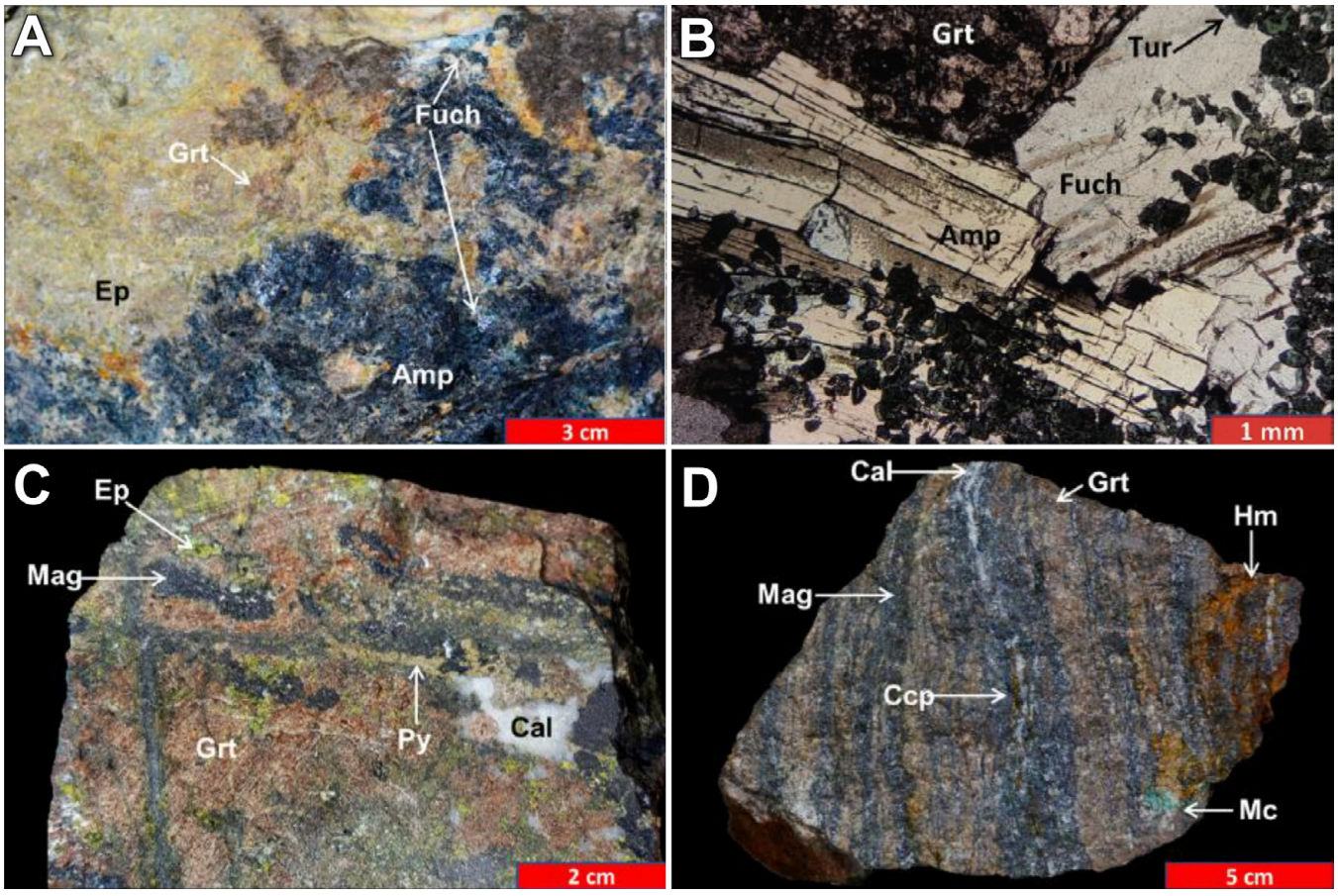

Figure 2 Selected aspects of the IOCG skarn mineralization at the Tatatila–Las Minas deposits showing both prograde (garnet and tourmaline) and retrograde (actinolite and fuchsite) associations. (A) Hand specimen showing a garnet-rich prograde association followed by an actinolite- and fuchsite-rich retrograde association in the Santa Cruz mine. (B) Photomicrography of a garnet and tourmaline prograde association followed by an actinolite and fuchsite retrograde association; transmitted light, crossed polars; same sample as in A. Fuchsite separates from A and B were dated by argon geochronometry in this study. (C) Hand specimen of prograde patchy to partially banded magnetite ore; El Dorado mine. (D) Hand specimen of banded exoskarn magnetite- and chalcopyrite-rich retrograde ore, with martitized magnetite; El Dorado mine. Key: Amp = amphibole-group minerals (actinolite), Cal = calcite, Ccp = chalcopyrite, Ep = epidote, Fuch = chromian muscovite or "fuchsite", Grt = garnet-group minerals (grossular-andradite), Hm = hematite, Mag = magnetite, Mc = malachite, Py = pyrite, Tur = tourmaline.

http://dx.doi.org/10.18268/BSGM2020v72n3a110520

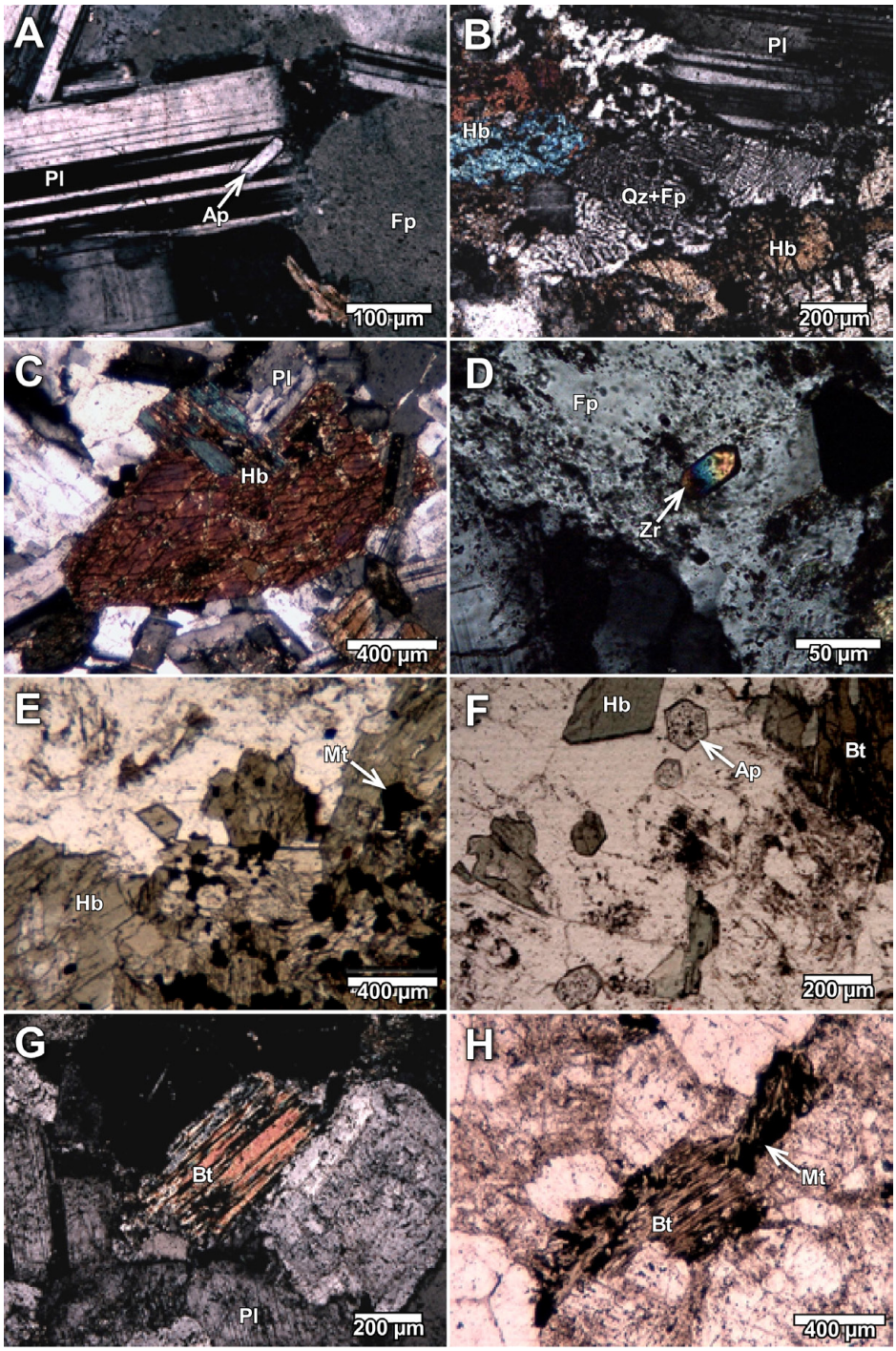

Figure 3 Photomicrographs of representative hypabyssal bodies, unaffected by hydrothermal alteration, associated with IOCG skarn mineralization in the Tatatila–Las Minas district. (A) Quartz-monzodiorite showing euhedral apatite crystals within plagioclase phenocrysts, Santa Cruz mine; transmitted light, crossed polars. (B) Quartz-monzodiorite showing myrmekitic intergrowths, surrounded by hornblende and plagioclase phenocrysts, La Virgen mine; transmitted light, crossed polars. (C) Quartz-monzodiorite showing hornblende phenocrysts, Santa Cruz mine; transmitted light, crossed polars. (D) Quartz-monzodiorite showing euhedral zircon crystals within potassium feldspar, Santa Cruz mine; transmitted light, crossed polars. (E) Monzodiorite showing hornblende intergrown with magnetite, Carbonera mine; plane-polarized transmitted light. (F) Monzodiorite showing euhedral hornblende, biotite and apatite crystals within a plagioclase-potassium feldspar assemblage, Carbonera mine; plane-polarized transmitted light. (G) Monzogranite showing rock-forming biotite crystals, same sample as in F, Rancho La Virgen; transmitted light, crossed polars. (H) Monzogranite showing late biotite crystals intergrown with magnetite, Rancho La Virgen; plane-polarized transmitted light. Key: Ap = apatite, Bt = biotite, Fp = potassium feldspar, Hb = hornblende, Mt = magnetite, Pl = plagioclase, Qz = quartz, Zr = zircon.

http://dx.doi.org/10.18268/BSGM2020v72n3a110520

Mining activity in the study area can be dated back to pre-colonial epochs, when the native population of Chiconquiaco obtained gold that was mainly destined to fulfill the contributions imposed upon them by their Aztec overlords. Formal mining by the Spaniards can be dated back to at least 1680, when the exploitation of large high-grade gold and silver bonazas has been documented (Castro-Mora *et al.*, 1994). Mining and exploration have remained intermittently active in the area ever since (Viniegra, 1965; Castro-Mora *et al.*, 1994; Servicio Geológico Mexicano, 2007). By 1996, the exploration endeavors carried out by International Northair, in association with Battle Mountain Gold Co., allowed location of relevant Au-Cu-Fe resources in a broad area. In 2006, Bell Resources Corp. took over the property in the Las Minas area and subsequently assigned the mining rights to Chesapeake Gold Corp.

The formation of this Au-Cu-Fe rich area is generally acknowledged to belong to an IOCG model with overimposed late epithermal veins (Servicio Geológico Mexicano, 2007; Camprubí, 2009, 2013; Dorantes-Castro, 2016; Castro-Mora *et al.*, 2016; Sarabia-Jacinto, 2017). The metal grades in the deposit range between 1 and 39.3 ppm Au, between 4.11 and 127 ppm Ag, and between 0.64 and 11.7% Cu; inferred reserves are 719000 Oz Au equiv., and indicated reserves are 304000 Oz Au equiv. (Castro-Mora *et al.*, 2016).

3. Methodology

Representative samples from the Neogene intrusive ensemble were collected in the Tatatila–Las Minas mineralized area (47 samples; purple circles in Figure 1) in order to characterize the petrologic affinity and age of skarn-generating intrusive bodies, as well as the age of hydrothermal activity itself. The ages of intrusions are considered as representative of the age of prograde mineralization in IOCG skarns, and hydrothermal assemblages correspond to retrograde stages of these deposits. The representativeness of such samples with regard to the formation (or postdating) of mineralized bodies was determined on the basis of their distribution, their possible association with mineralized bodies, and the types of rocks thereby represented, after thorough cartography and sampling. All the analyzed samples were examined by means of petrographic studies in order to ensure that no alteration would cause any disturbances to the geochemical or geochronological analyses.

Elemental analyses were carried out on 15 g aliquots from samples at a 200 mesh. The two dated samples from retrograde hydrothermal associations are chromian muscovite, which correspond to high-temperature phyllic assemblages from the Las Minas area, and zircon within pervasive potassic alteration assemblages from the Tatatila area.

Multi-elemental geochemical analyses of host rocks were carried out by means of X-ray fluorescence (XRF) with a Rigaku Primus II equipment available at the Laboratorio Nacional de Geoquímica y Mineralogía (LANGEM) in accordance with the procedure described by Lozano-Santa Cruz *et al.* (1995); results are presented in Table 1. Trace and rare-earth elements (REE) were analyzed by means of inductively coupled plasma quadrupole mass spectrometery (Q-ICP-MS) with a Termo ICap Qc equipment, coupled to a collision/reaction cell (He, N_2, NH_3 and O_2) in order to minimize spectral interference, the procedure described by Mori *et al.* (2007), at the Laboratorio de Estudios Isotópicos (LEI) of the Centro de Geociencias (CGeo-UNAM). The obtained data are presented in Table 2. For Sr, Nd and Pb isotopic analyses, a Thermo Fisher Neptune Plus mass spectrometer available at the CGeo-UNAM. Sample preparation and measurement procedures for Sr–Nd–Pb isotopic analyses are described in Gómez-Tuena *et al.* (2003) for LDEO. $^{87}Sr/^{86}Sr$ ratios obtained in both labs were normalized to $^{86}Sr/^{88}Sr = 0.1194$ and corrected to a NBS-987 standard ratio of $^{87}Sr/^{86}Sr = 0.710230$, and $^{143}Nd/^{144}Nd$ ratios were normalized to $^{146}Nd/^{144}Nd = 0.72190$ and corrected to a La Jolla standard value of $^{143}Nd/^{144}Nd=0.511860$. At LDEO, Sr and Nd were measured by dynamic multicollection, with each analysis consisting of ~120 isotopic

http://dx.doi.org/10.18268/BSGM2020v72n3a110520

Table 1. Major elements in host intrusive rocks to the Tatatila-Las Minas IOCG deposits. All values in wt.%. Asterisks (*) correspond to analyses in Dorantes-Castro (2016).

	UTM coordinates		Rock	SiO_2	TiO_2	Al_2O_3	$Fe_2O_3(t)$	MnO	MgO	CaO	Na_2O	K_2O	P_2O_5	LOI	Total
	E	N													
TMG-1	699173	2176551	Gabbro	43.89	0.81	17.94	13.66	0.22	8.92	13.02	1.30	0.19	0.04	1.12	99.60
TMG-2	698856	2176474	Diorite	61.33	0.75	17.09	5.32	0.07	2.31	4.78	3.95	4.20	0.20	0.75	99.58
TMG-3	698516	2176325	Quartz monzodiorite	62.14	0.71	17.06	5.41	0.07	2.49	4.53	4.10	3.30	0.19	1.79	99.56
TMG-4	697820	2176599	Quartz monzodiorite	58.22	0.78	17.87	6.81	0.11	3.23	5.85	3.93	2.96	0.23	0.71	99.60
TMG-5	697764	2176999	Monzodiorite	58.63	0.85	17.35	6.81	0.12	3.03	5.72	3.97	3.28	0.23	0.68	99.60
TMG-6	696871	2177577	Quartz monzodiorite	61.78	0.71	17.05	5.46	0.10	2.39	4.32	3.82	4.19	0.19	0.49	99.60
TMG-7	692733	2179299	Quartz diorite	59.29	0.60	16.53	6.15	0.13	4.40	7.10	3.68	1.92	0.19	0.71	99.58
TMG-8	692919	2179241	Diorite	48.99	0.73	15.64	9.98	0.17	9.21	12.27	2.24	0.64	0.13	1.17	99.60
TMG-9	692782	2178838	Diorite	52.39	0.85	19.26	9.48	0.15	4.07	8.50	3.93	1.02	0.35	0.95	99.50
TMG-10	701856	2183672	Diorite	55.09	1.47	17.04	7.86	0.14	3.87	7.57	4.13	2.42	0.41	0.19	99.50
TMG-11	701275	2182995	Monzodiorite	62.15	0.90	16.83	5.13	0.10	2.42	4.02	4.60	3.58	0.27	0.54	99.28
TMG-12	701201	2183034	Monzonite	63.44	0.88	16.16	4.60	0.11	2.03	3.50	4.51	4.55	0.22	0.03	99.59
TMG-13	700794	2183290	Quartz diorite	59.34	1.00	15.69	6.09	0.17	5.08	4.72	3.76	3.82	0.35	2.31	99.58
TMG-14	699639	2181985	Monzonite	55.79	1.05	14.15	5.82	0.10	4.60	10.97	3.47	3.46	0.60	0.46	99.55
TMG-15	699490	2180296	Sienite	59.34	0.61	20.94	4.23	0.05	1.69	4.52	4.92	3.36	0.33	1.29	99.60
TMG-16	698062	2181248	Quartz monzonite	55.76	1.18	17.36	8.87	0.17	4.14	7.11	3.10	2.00	0.31	0.04	99.58
TMG-17	698283	2181931	Monzodiorite	57.89	1.16	17.38	6.62	0.12	3.51	6.11	4.12	2.75	0.34	0.67	99.55
TMG-18	698504	2182345	Monzogranite	71.60	0.25	15.89	1.13	0.02	0.36	1.95	3.64	5.09	0.07	0.72	99.60
TMG-19	694715	2179684	Diorite	63.04	0.82	16.39	4.86	0.11	2.26	4.67	4.22	3.39	0.23	0.75	99.59
TMG-20	696828	2180239	Quartz monzonite	63.02	0.52	18.26	4.66	0.07	1.74	5.24	4.71	1.51	0.27	0.79	99.61
TMG-21	696325	2179917	Diorite	52.79	1.47	19.06	8.42	0.15	3.73	7.90	4.27	1.80	0.42	1.41	99.62
TMG-22	695717	2179384	Granite	77.60	0.09	14.83	0.42	0.00	0.31	1.02	2.78	2.91	0.04	1.63	99.61
TMG-23	694397	2177628	Diorite	60.88	0.54	15.82	6.07	0.13	4.41	6.16	3.97	1.88	0.13	0.95	99.59
TMG-24	694207	2177867	Quartz diorite	55.59	0.79	19.02	7.76	0.14	3.14	8.17	3.75	1.39	0.25	0.47	99.59
TMG-26	692818	2176784	Diorite	58.33	0.92	18.96	6.01	0.10	2.40	6.50	4.17	2.23	0.38	0.52	99.58
TMG-23 B	694397	2177628	Diorite	52.36	1.37	18.46	7.94	0.14	3.93	6.67	4.34	1.63	0.39	2.38	99.61
TMG-1 2a	699173	2176551	Gabbro	43.27	0.79	17.69	13.34	0.21	8.80	12.86	1.30	1.87	0.37	1.12	99.60
RV-2	694740	2179098	Granodiorite	66.55	0.44	17.38	2.95	0.03	0.89	4.22	4.88	1.83	0.16	0.57	99.90
RV-3	694688	2179102	Gabbro	47.00	0.95	15.66	10.86	0.14	10.61	9.47	1.89	2.35	0.20	0.84	99.97
BQ-1	694445	2178202	Granite	65.36	0.48	17.94	2.72	0.03	1.06	4.01	5.01	2.06	0.17	1.04	99.86
CR-1	6946662	2179718	Gabbro-diorite	52.00	0.85	16.65	8.79	0.15	6.67	8.44	3.17	1.19	0.25	1.04	99.96
SC-2 b 1	694317	2177448	Diorite	61.46	0.53	17.10	5.30	0.08	2.43	5.20	4.28	2.10	0.19	1.24	99.92
SC-2 b 2	694317	2177448	Diorite	61.78	0.52	16.79	5.12	0.09	2.32	5.30	4.17	2.25	0.19	0.19	99.91
SC-2 b 3	694317	2177448	Diorite	60.65	0.53	16.58	5.89	0.10	2.77	5.37	4.39	2.32	0.21	1.13	99.92
LS-6	696153	2179805	Gabbro-diorite	54.06	1.32	18.07	8.60	0.14	3.97	8.14	3.52	1.50	0.31	0.36	100.00
Es-3	698250	2181451	Gabbro-diorite	51.68	1.21	18.04	8.75	0.16	5.10	8.83	3.77	1.05	0.32	1.09	99.99
Ag-2	699636	2180877	Monzodiorite	59.70	0.76	16.78	6.43	0.09	2.94	5.34	3.72	3.45	0.22	0.58	99.99
LS-4	697074	2180612	Granodiorite	64.27	0.47	18.58	3.81	0.10	1.09	4.39	3.93	2.50	0.22	0.64	99.99
CR-6	693182	2179054	Gabbro-diorite	52.84	0.90	18.13	9.12	0.14	4.64	8.49	3.39	1.29	0.28	0.78	99.99
SC-3	694347	2177616	Diorite	57.52	0.76	18.06	7.40	0.12	2.55	7.43	3.61	1.60	0.26	0.70	99.99
LV-1	701870	2184419	Monzodiorite	56.29	1.15	18.15	7.23	0.13	3.29	6.70	4.03	2.31	0.35	0.15	100.00
CR-5	694325	2179704	Gabbro-diorite	53.49	0.92	17.21	8.28	0.15	4.73	8.12	3.48	1.97	0.24	1.42	100.00
LV-2	702091	2184527	Monzodiorite	56.67	1.16	17.64	7.38	0.13	3.38	6.76	3.80	2.55	0.34	0.19	100.00
LS-3	696389	2080049	Monzodiorite	56.88	1.09	18.09	7.37	0.13	2.94	6.33	3.76	2.39	0.34	0.68	100.00
Ag-5	699561	2181458	Gabbro	51.74	1.16	16.83	7.95	0.07	6.17	9.68	3.49	2.02	0.27	0.62	100.00
Es-2	698330	2181972	Monzodiorite	57.42	1.16	17.22	7.03	0.12	3.49	6.30	3.76	2.83	0.35	0.32	100.00
1TJBQ*			Diorite	58.74	0.38	16.96	6.61	0.14	2.81	8.09	5.08	0.38	0.15	0.61	99.22
538*			Gabbro	48.29	0.94	15.68	7.58	0.14	4.24	9.59	2.51	1.60	0.22	9.1	99.06
33*			Monzodiorite	54.57	1.14	16.14	6.59	0.14	5.21	9.57	3.72	2.13	0.34	0.34	99.17
529*			Granodiorite	66.94	0.42	16.95	2.60	0.029	1.22	3.89	4.66	2.00	0.17	0.96	99.55

Key: LOI = loss on ignition.

Table 2. Trace elements in host intrusive rocks to the Tatatila-Las Minas IOCG deposits. All values in ppm unless otherwide noted. Asterisks (*) correspond to analyses in Dorantes-Castro (2016).

Sample	Li	Be	P (wt.%)	Sc	Ti	V	Cr	Co	Ni	Cu	Zn	Ga	Rb	Sr	Y	Zr	Nb	Mo	Sn	Sb	Cs
TMG-1	10.41	0.48	0.04	19.77	0.85	336.71	109.71	46.43	63.59	9.98	94.35	20.53	5.25	731.84	10.70	32.39	1.16	0.34	0.53	0.05	2.63
TMG-2	18.39	2.01	0.20	10.62	0.72	106.68	24.75	12.03	13.19	25.61	31.25	18.77	116.18	368.41	29.54	408.71	15.69	2.60	1.39	0.15	5.60
TMG-3	14.42	2.06	0.19	9.67	0.65	102.97	32.98	10.81	15.39	17.67	31.95	19.07	84.49	383.55	27.00	299.28	12.43	0.83	1.67	0.18	3.78
TMG-4	20.78	1.80	0.23	10.68	0.75	145.40	46.61	17.02	24.86	65.46	54.42	19.80	73.54	485.78	24.52	235.53	11.03	1.02	1.29	0.14	3.39
TMG-5	15.65	1.96	0.24	12.40	0.80	143.79	25.73	16.48	15.02	57.07	53.66	19.97	102.15	412.51	28.50	237.00	14.78	2.35	1.81	0.15	4.02
TMG-6	21.71	2.22	0.19	8.82	0.70	106.15	27.58	14.17	15.98	59.79	54.00	18.99	149.19	344.29	49.66	304.06	18.62	0.58	1.87	0.24	8.77
TMG-7	4.66	1.09	0.18	14.39	0.57	144.73	147.41	17.73	45.05	16.30	45.61	17.25	30.52	524.35	16.86	110.45	5.36	0.91	0.81	0.05	0.29
TMG-8	2.85	0.73	0.12	35.53	0.69	222.77	438.99	40.15	125.95	44.98	62.08	16.53	13.63	513.94	17.18	82.24	2.73	1.12	0.62	0.10	2.61
TMG-9	2.80	1.04	0.34	12.12	0.78	210.81	29.58	19.41	13.33	12.13	51.50	21.53	18.84	761.65	20.99	102.43	5.77	0.36	0.79	0.10	0.49
TMG-10	12.25	2.06	0.43	19.45	1.47	175.30	38.49	20.68	19.64	72.53	80.69	21.06	44.03	626.13	30.65	246.34	22.97	1.63	1.87	0.05	2.44
TMG-11	21.63	2.69	0.27	12.46	0.83	106.97	22.99	11.77	12.35	25.98	56.51	20.58	82.95	419.99	25.43	371.97	20.68	0.68	1.85	0.33	5.09
TMG-12	10.97	2.63	0.22	12.29	0.79	100.45	25.74	9.92	10.76	42.84	62.44	19.65	108.00	351.48	24.65	425.83	20.55	0.82	1.83	0.13	4.20
TMG-13	24.95	2.64	0.35	18.79	0.89	139.84	160.33	20.25	66.75	39.44	83.06	19.23	95.24	727.70	23.69	263.88	11.23	0.40	1.52	0.38	1.07
TMG-14	9.64	3.20	0.59	17.16	0.96	171.71	131.04	19.67	32.34	94.74	64.38	20.52	54.81	1124.33	34.36	413.32	17.21	1.09	2.35	0.16	1.69
TMG-15	22.67	3.09	0.33	9.65	0.57	118.47	13.32	6.14	18.40	47.05	34.44	23.15	69.27	792.45	9.84	256.89	4.19	0.27	0.56	0.13	6.76
TMG-16	14.20	1.41	0.31	21.06	1.16	191.06	17.87	14.09	4.49	6.91	89.43	20.55	59.36	496.28	36.74	159.13	10.47	0.78	1.48	0.58	5.26
TMG-17	10.17	2.25	0.35	12.62	1.13	147.96	48.94	14.88	20.40	53.18	57.11	20.62	59.19	536.61	25.91	322.84	19.02	2.85	1.55	0.36	2.74
TMG-18	8.03	1.11	0.07	1.41	0.23	11.74	2.97	1.30	0.13	0.64	20.65	14.82	79.79	338.12	8.54	168.55	5.49	0.32	0.54	0.18	5.67
TMG-19	8.15	2.13	0.23	14.76	0.79	101.29	18.97	10.77	6.77	23.39	80.37	18.99	73.33	466.29	20.39	260.61	16.56	1.14	1.19	0.18	1.64
TMG-20	4.58	2.01	0.27	5.61	0.47	77.35	8.37	8.30	2.90	33.81	30.72	20.66	36.48	845.42	17.22	149.11	8.53	0.48	1.56	0.26	1.35
TMG-21	7.46	1.63	0.42	15.65	1.38	240.87	13.21	19.85	17.12	63.18	69.19	23.00	25.03	717.80	24.29	172.85	11.56	0.89	1.12	0.12	1.14
TMG-22	3.83	1.16	0.03	-	0.08	6.41	2.03	-	-	-	11.20	12.54	79.74	55.65	7.49	70.92	10.26	0.16	0.60	0.32	6.61
TMG-23	10.45	1.62	0.37	14.93	1.29	208.09	18.75	20.12	14.32	58.40	72.76	22.34	28.14	644.22	22.53	186.92	14.65	1.77	1.24	0.62	2.47
TMG-24	7.03	1.21	0.24	13.74	0.75	161.35	6.21	15.59	4.54	12.66	62.20	20.69	31.34	563.93	21.65	20.08	5.58	1.03	0.78	0.08	0.88
TMG-26	9.65	1.94	0.37	8.11	0.90	120.98	11.78	12.20	9.27	34.38	65.37	21.60	33.51	731.53	21.16	239.47	11.07	0.67	1.14	0.08	1.26
AG-2	13.67	2.05	0.22	12.99	0.73	122.80	133.60	14.60	27.98	38.45	43.63	18.83	107.72	395.48	27.55	207.93	13.89	4.23	1.80	0.17	5.10
AG-5	27.01	1.30	0.26	26.37	1.12	235.84	128.56	15.77	25.51	8.30	26.28	19.92	53.00	898.63	20.00	154.15	7.18	1.44	0.70	0.45	3.34
CR-6	2.94	1.07	0.27	19.11	0.86	220.45	108.01	18.67	26.28	11.84	51.30	19.33	20.19	633.39	20.93	130.93	6.98	1.03	0.85	0.28	0.28
ES-2	7.49	2.19	0.35	13.71	1.11	154.96	128.08	17.57	23.35	77.23	64.48	20.46	71.91	556.29	24.13	327.13	17.00	10.10	1.61	0.26	5.95
ES-3	9.20	1.43	0.32	21.69	1.21	223.94	110.03	24.50	30.73	42.77	80.77	21.46	19.70	620.53	23.53	153.09	9.46	1.34	1.04	0.23	1.03
LS-3	8.01	1.88	0.34	10.41	1.07	168.94	56.10	16.30	6.62	74.84	76.16	21.62	36.53	748.69	21.75	220.73	11.42	1.53	1.28	0.28	1.77
LS-4	12.80	1.97	0.22	5.13	0.46	44.52	100.47	4.73	6.29	9.20	57.71	19.12	75.95	416.90	20.22	266.60	8.92	3.72	1.30	0.11	4.22
LV-1	16.15	2.05	0.35	12.32	1.16	160.92	70.38	16.60	14.90	43.69	73.91	21.60	49.93	591.43	24.45	313.51	17.07	2.47	1.54	0.08	3.45
SC-2 b 1	10.28	1.55	0.20	8.80	0.53	106.97	178.66	13.91	22.59	34.97	37.89	18.21	57.47	468.02	16.89	251.57	7.71	3.12	0.78	0.24	2.28
SC-3	9.46	1.35	0.26	8.75	0.74	140.78	93.78	11.91	4.93	13.42	40.99	19.97	31.25	500.22	27.90	244.55	8.75	2.38	1.09	0.09	0.70
LS-6	5.00	1.60	0.31	17.23	1.32	226.21	78.98	21.84	19.60	45.06	78.92	21.08	29.30	504.79	22.88	116.97	10.54	1.23	1.26	0.16	3.12
LV-2	15.18	2.20	0.35	13.27	1.15	176.32	80.44	18.11	15.98	74.96	76.69	21.35	59.50	586.07	25.62	290.33	17.29	4.23	2.09	0.19	5.36
CR-5	13.47	2.75	0.06	1.61	0.23	15.90	6.91	2.02	2.50	1.88	31.60	15.14	77.21	123.28	9.67	114.46	18.26	0.24	2.22	0.12	1.36
RV-3			1.89										45.95	66.24	14.45	10.50	18.53	1.05	0.41	14.67	98.31
SC-2-B3			2.13										39.32	58.31	12.42	5.37	52.35	4.98	0.49	0.81	25.48
CR-1			2.59										18.63	101.88	16.56	10.97	30.82	1.41	0.34	0.97	4.31
SC-2-B1			1.84										23.48	49.83	7.80	3.74	43.12	3.23	0.33	1.60	12.41
SC-2-B2			2.15										12.27	93.14	6.37	4.59	48.28	4.40	0.42	-3.86	-26.90
AG-2			-										46.43	54.47	17.55	53.73	56.48	4.60	1.05	1.08	27.15
AG-5			-										22.85	123.78	12.74	39.83	29.19	1.57	0.41	2.81	17.75
CR-6			-										8.70	87.24	13.33	33.83	28.39	1.12	0.49	1.75	1.50
ES-2			-										31.00	76.62	15.37	84.53	69.11	10.98	0.93	1.65	31.66
ES-3			-										8.49	85.47	14.99	39.56	38.47	1.45	0.61	1.41	5.48
LS-3			-										15.75	103.13	13.86	57.04	46.43	1.66	0.74	1.77	9.40
LS-4			-										32.74	57.42	12.88	68.89	36.26	4.04	0.76	0.68	22.46
LV-1			-										21.52	81.46	15.57	81.01	69.38	2.69	0.89	0.48	18.34
SC-3			-										13.47	68.90	17.77	63.19	35.59	2.59	0.63	0.54	3.74
LS-6			-										12.63	69.53	14.57	30.22	42.85	1.34	0.73	1.01	16.58
LV-2			-										25.65	80.73	16.32	75.02	70.28	4.60	1.21	1.20	28.50
CR-5			-										33.28	16.98	6.16	29.58	74.23	0.26	1.29	0.74	7.25
33*			-											598.15	43.42	43.86	11.27	1.51	1.46	0.23	0.55
1TIJBQ*			-											615.63	1197.00	23.77	6.12	4.12	3.23	0.32	0.68
529*			-											734.40	3.86	5.93	5.67	2.14	0.63	0.16	1.41
538*			-											640.89	20.42	169.66	8.03	1.26	1.04	0.14	8.76

http://dx.doi.org/10.18268/BSGM2020v72n3a110520

Table 2. (Continuation) Trace elements in host intrusive rocks to the Tatatila-Las Minas IOCG deposits. All values in ppm unless otherwide noted. Asterisks (*) correspond to analyses in Dorantes-Castro (2016).

Sample	Ba	La	Ce	Pr	Nd	Sm	Eu	Tb	Gd	Dy	Ho	Er	Yb	Lu	Hf	Ta	W	Tl	Pb	Th	U	B	Tm
TMG-1	89.31	4.81	12.29	1.59	7.69	2.11	0.67	0.33	2.19	2.00	0.41	1.05	0.98	0.15	0.92	0.08	0.07	0.08	3.50	0.33	0.21		
TMG-2	692.36	28.50	59.17	7.69	29.47	6.18	1.29	0.85	5.66	4.98	1.02	2.91	3.02	0.46	10.02	0.99	0.66	0.70	8.36	21.60	4.68		
TMG-3	690.67	27.28	54.61	7.20	27.38	5.72	1.30	0.79	5.22	4.58	0.92	2.65	2.69	0.41	7.48	0.84	0.76	0.58	8.52	17.62	3.61		
TMG-4	628.10	29.72	59.39	7.27	26.77	5.32	1.30	0.71	4.85	4.06	0.82	2.34	2.33	0.35	5.87	0.71	0.37	0.48	13.26	11.62	2.62		
TMG-5	708.86	30.30	60.74	8.04	30.67	6.41	1.39	0.87	5.80	5.00	0.99	2.81	2.81	0.42	6.21	0.93	0.73	0.67	10.46	18.05	2.63		
TMG-6	735.52	32.27	56.30	8.40	32.99	7.68	1.58	1.31	8.17	8.73	1.89	5.66	6.65	1.13	7.77	1.28	0.76	0.86	12.14	20.65	4.45		
TMG-7	499.87	15.34	26.95	3.50	14.34	3.09	0.93	0.45	3.01	2.68	0.56	1.59	1.61	0.25	2.77	0.38	0.25	0.11	5.23	5.50	0.79		
TMG-8	205.84	10.92	21.44	2.97	13.40	3.35	1.05	0.51	3.36	3.12	0.62	1.67	1.54	0.23	2.08	0.16	0.14	0.11	3.00	1.23	0.38		
TMG-9	406.33	18.82	40.09	5.24	21.26	4.60	1.37	0.63	4.34	3.77	0.75	2.04	1.98	0.30	2.61	0.29	0.17	0.10	3.15	2.33	0.58		
TMG-10	689.26	35.72	77.57	10.03	39.54	8.29	2.03	1.03	7.21	5.66	1.08	2.97	2.72	0.40	5.47	1.34	0.34	0.30	11.20	9.12	2.53		
TMG-11	572.79	41.44	81.94	10.48	38.18	7.29	1.48	0.86	6.14	4.54	0.86	2.40	2.23	0.33	8.58	1.39	0.73	0.74	13.84	21.32	4.85		
TMG-12	701.13	40.56	82.50	10.28	37.47	7.10	1.43	0.84	5.92	4.48	0.86	2.44	2.33	0.35	10.07	1.36	0.42	0.76	20.51	21.48	6.26		
TMG-13	1067.10	51.04	103.69	12.69	51.18	10.01	2.38	0.99	7.77	4.62	0.82	2.23	1.92	0.28	6.57	0.73	0.34	1.25	10.11	19.85	5.31		
TMG-14	1351.37	91.44	198.89	23.31	89.81	20.16	4.18	1.77	14.79	7.46	1.21	3.21	2.47	0.35	10.19	1.10	0.32	0.35	16.60	35.51	8.67		
TMG-15	796.79	8.51	16.16	2.25	9.35	1.98	0.73	0.28	1.90	1.60	0.34	0.95	1.03	0.18	5.98	0.11	0.97	0.67	10.33	7.43	1.63		
TMG-16	546.99	24.49	56.34	7.66	31.59	7.22	1.66	1.07	7.03	6.63	1.29	3.67	3.46	0.51	4.06	0.65	0.72	0.60	12.16	7.38	1.39		
TMG-17	723.95	37.54	74.16	9.77	37.57	7.47	1.80	0.90	6.39	4.81	0.91	2.52	2.34	0.35	7.53	1.19	0.46	0.64	12.57	12.13	3.39		
TMG-18	2387.17	50.34	91.28	9.25	31.36	3.86	1.63	0.35	2.80	1.35	0.28	0.85	0.84	0.14	4.37	0.33	0.33	0.69	11.22	13.96	1.20		
TMG-19	734.89	33.82	61.68	7.92	29.11	5.49	1.40	0.68	4.75	3.73	0.72	2.06	2.03	0.31	6.25	1.15	1.54	0.63	24.12	16.54	3.89		
TMG-20	808.02	15.07	27.79	3.67	15.52	3.23	0.97	0.44	2.98	2.66	0.55	1.54	1.68	0.26	3.63	0.60	0.63	0.40	11.67	2.66	2.49		
TMG-21	583.71	30.74	63.69	8.85	35.68	7.37	2.05	0.87	6.33	4.58	0.87	2.39	2.12	0.31	4.13	0.68	0.22	0.25	8.05	6.24	1.75		
TMG-22	518.65	8.67	17.53	1.59	5.71	0.98	0.29	0.16	1.00	0.98	0.23	0.66	0.78	0.13	2.24	0.85	0.37	1.09	8.38	1.36	0.89		
TMG-23	503.48	24.25	46.53	7.27	29.82	6.49	1.82	0.80	5.70	4.28	0.81	2.23	2.00	0.29	4.44	0.85	0.36	0.36	6.26	4.82	1.36		
TMG-24	411.36	17.98	37.94	4.83	19.95	4.41	1.33	0.63	4.09	3.65	0.74	2.07	2.02	0.30	0.78	0.33	0.22	0.17	3.73	3.01	0.65		
TMG-26	660.10	33.47	59.21	8.71	32.97	6.22	1.72	0.73	5.25	3.83	0.75	2.11	2.07	0.31	5.66	0.68	0.23	0.33	10.92	9.26	2.37		
AG-2	649.99	25.50	53.23	7.10	27.56	5.99	1.25	0.82	5.46	4.80	0.95	2.69	2.65	0.40	5.31	0.86	0.74	0.75	10.09	17.07	4.49	8.19	
AG-5	471.36	15.67	32.39	4.54	20.42	5.08	1.29	0.66	4.67	3.73	0.71	1.91	1.74	0.26	3.89	0.40	0.12	0.56	4.54	5.54	1.13	3.66	
CR-6	391.33	16.96	36.80	4.86	20.16	4.47	1.28	0.62	4.20	3.72	0.75	2.08	2.05	0.31	3.20	0.39	0.35	0.14	3.95	2.31	0.57	3.00	
ES-2	725.30	36.21	72.89	9.25	35.10	7.02	1.79	0.83	5.96	4.47	0.85	2.35	2.20	0.33	7.45	1.04	1.23	0.64	15.55	13.67	3.97	4.85	
ES-3	317.06	20.11	44.17	5.91	24.61	5.52	1.60	0.74	5.07	4.28	0.84	2.32	2.18	0.32	3.53	0.53	0.24	0.25	15.02	3.18	0.99	5.04	
LS-3	545.55	29.06	60.47	8.04	31.67	6.55	1.74	0.77	5.55	4.08	0.77	2.11	1.93	0.29	5.30	0.69	0.30	0.34	11.87	9.44	2.83	3.56	
LS-4	606.24	13.09	25.42	3.18	12.70	2.96	1.35	0.51	2.97	3.38	0.71	2.06	2.24	0.34	6.00	0.86	0.71	0.71	20.19	3.97	2.40	6.27	
LV-1	670.19	34.38	63.88	9.11	35.11	7.10	1.79	0.85	6.08	4.55	0.87	2.38	2.18	0.33	6.73	0.97	0.34	0.46	11.44	9.34	2.91	3.70	
SC-2 b 1	732.89	21.54	37.86	4.57	16.95	3.33	0.99	0.46	3.10	2.67	0.55	1.55	1.62	0.26	5.58	0.53	6.59	0.32	11.05	8.07	1.65	2.65	
SC-3	434.39	19.65	40.63	5.87	24.07	5.40	1.40	0.78	5.12	4.72	0.96	2.73	2.76	0.42	5.63	0.52	0.42	0.16	4.40	5.33	1.24	3.51	
LS-6	337.69	17.97	40.82	5.59	23.56	5.40	1.57	0.76	5.09	4.51	0.90	2.48	2.36	0.35	2.56	0.65	0.31	0.28	8.99	3.98	2.03	4.58	
LV-2	558.92	33.04	66.95	9.03	35.12	7.23	1.70	0.88	6.18	4.76	0.91	2.50	2.33	0.35	6.86	1.06	0.73	0.49	13.19	11.78	3.77	4.14	
CR-5	368.05	19.71	35.73	3.96	13.47	2.42	0.48	0.30	2.04	1.60	0.32	0.91	1.01	0.16	3.47	1.96	0.19	0.49	12.93	9.68	3.53	5.07	
RV-3	111.82	61.83	51.00	49.19	43.86	32.71	25.17	20.47	23.47	17.31	15.63	14.50	12.20	12.08	17.06	35.08	42.02		2.08	82.13	87.64		12.79
SC-2-B3	297.65	125.42	67.37	59.23	44.73	29.71	21.89	17.88	22.13	14.85	13.73	13.40	12.82	13.31	9.79	92.44	146.71		4.25	471.59	230.20		12.60
CR-1	167.89	83.39	65.46	57.15	50.70	37.12	27.38	23.12	26.58	19.73	18.14	17.09	15.20	15.54	19.88	47.50	61.72		1.45	94.35	59.66		15.52
SC-2-B1	332.11	75.40	29.29	42.17	33.22	20.97	16.89	12.88	15.27	10.85	10.27	10.09	9.64	10.16	7.30	72.34	175.00		4.96	144.16	95.90		9.42
SC-2-B2	433.45	91.48	50.73	50.66	39.97	23.94	19.36	12.12	16.61	8.97	7.84	7.61	7.08	7.48	8.40	73.83	198.92		4.57	145.47	93.43		6.88
AG-2	269.71	107.61	86.98	74.79	59.01	39.16	21.53	21.82	26.56	18.90	16.87	16.23	15.57	15.56	49.85	61.08	7.82		4.09	588.76	561.31		0.00
AG-5	195.59	66.10	52.92	47.74	43.72	33.24	22.28	17.67	22.75	14.70	12.62	11.53	10.24	10.15	36.45	28.73	1.25		1.84	191.01	141.65		0.00
CR-6	162.38	71.57	60.13	51.17	43.16	29.19	21.99	16.67	20.43	14.65	13.23	12.58	12.08	12.30	30.04	27.89	3.68		1.60	79.51	71.77		0.00
ES-2	300.96	152.78	119.10	97.32	75.15	45.86	30.83	22.23	28.99	17.60	15.07	14.22	12.94	12.95	69.90	74.25	12.97		6.30	471.51	496.36		0.00
ES-3	131.56	84.85	72.18	62.21	52.70	36.09	27.53	19.71	24.69	16.83	14.88	14.00	12.84	12.73	33.11	37.79	2.50		6.08	109.66	123.83		0.00
LS-3	226.37	122.64	98.81	84.65	67.81	42.81	30.07	20.50	27.01	16.05	13.61	12.75	11.37	11.41	49.72	49.35	3.14		4.81	325.55	353.20		0.00
LS-4	251.55	55.25	41.54	33.45	27.21	19.33	23.33	13.61	14.45	13.31	12.56	12.46	13.16	13.23	56.27	61.08	7.48		8.17	136.96	300.36		0.00
LV-1	278.09	145.05	104.38	95.90	75.17	46.39	30.93	22.63	29.58	17.91	15.28	14.39	12.83	12.80	63.14	69.62	3.62		4.63	322.22	363.31		0.00
SC-3	180.25	82.92	66.40	61.77	51.54	35.31	24.22	20.89	24.94	18.59	17.02	16.48	16.21	16.56	52.82	37.05	4.43		1.78	183.76	155.20		0.00
LS-6	140.12	75.83	66.70	58.86	50.45	35.28	27.01	20.34	24.75	17.76	15.83	14.99	13.88	13.77	23.99	46.77	3.26		3.64	137.14	254.24		0.00
LV-2	231.92	139.42	109.40	95.09	75.21	47.28	29.28	23.45	30.09	18.74	16.06	15.10	13.69	13.68	64.36	75.98	7.72		5.34	406.10	470.73		0.00
CR-5	152.72	83.15	58.38	41.64	28.85	15.82	8.26	7.96	9.94	6.32	5.72	5.50	5.96	6.26	32.51	139.88	2.01		5.24	333.95	441.83		0.00
33*	516.80	22.64	52.37	7.70	34.64	8.66	2.05	1.26	8.38	7.73	1.52	4.49	3.74	0.53	1.84	0.56	0.72		7.22	3.26	1.05		
1TIJBQ*	115.52	12.66	28.65	3.94	15.47	2.91	0.97	0.37	2.62	2.12	0.42	1.15	1.08	0.16	0.69	0.30	0.38		8.86	2.10	1.83		
529*		17.70	33.25	4.13	15.58	2.81	0.92	0.25	2.20	0.94	0.14	0.30	0.18	0.02	0.01	0.31	0.48		6.80	3.43	0.59		
538*	533.23	20.62	54.11	5.99	24.33	5.28	1.42	0.66	4.69	3.74	0.73	1.98	1.86	0.27	4.09	0.49	0.22		7.75	6.82	2.41		

http://dx.doi.org/10.18268/BSGM2020v72n3a110520

http://dx.doi.org/10.18268/BSGM2020v72n3a110520

Table 3. Sr, Nd and Pb isotopic values of selected samples from intrusive rocks associated with IOCG skarn mineralization in the Tatatila–Las Minas area

Muestra	$^{87}Sr/^{86}Sr$	εSr	$^{143}Nd/^{144}Nd$	εNd	$^{206}Pb/^{204}Pb$	$^{207}Pb/^{204}Pb$	$^{208}Pb/^{204}Pb$
SC-2 b1	0.7044	-1.4	0.5127	1.2	18.75	15.6012	38.4921
SC-2 b2	0.7045	0	0.5127	1.2	18.70	15.6004	38.4490
SC-2 b3	0.7041	-5.7	0.5127	1.2	18.73	15.5966	38.4887
BQ-1	0.7059	19.9	0.5123	-6.6	18.68	15.6085	38.4041
RV-2	0.7059	19.9	0.5123	-6.6	18.65	15.6062	38.4562
RV-3	0.7040	-7.1	0.5128	3.2	18.69	15.5993	38.4149
CR-5	0.7042	-4.3	0.5126	-0.7	18.75	15.5994	38.4601
LV-2	0.7039	-8.5	0.5128	3.2	18.74	15.5947	38.4433
Es-3	0.7042	-4.3	0.5127	1.2	18.72	15.5982	38.5354
LS-3	0.7037	-11.4	0.5128	3.2	18.67	15.5800	38.3878
LS-6	0.7040	-7.1	0.5128	3.2	18.68	15.5928	38.4449

ratios. Sr ratios were measured using tungsten filaments and a $TaCl_4$ activator solution (Birck, 1986). Nd isotopes were measured as NdO+. During five separate analysis intervals the measured values of the NBS-987 standard were $^{87}Sr/^{86}Sr$ = 0.710245 ± 0.000016 (2σ, n = 4); 0.710271 ± 0.000014 (2σ, n = 6); 0.710274 ± 0.000016 (2σ, n=18); 0.710310 ± 0.000013 (2σ, n = 5); 0.710261 ± 0.000012 (2σ, n = 10). The measured $^{143}Nd/^{144}Nd$ ratio of the La Jolla standard at LDEO was 0.511836 ± 0.000013 (2σ, n = 15), as of Todt *et al.* (1996), according to the procedure described by Mori *et al.* (2007), obtained data are presented in Table 3.

The two dated samples from retrograde hydrothermal associations are chromian muscovite that corresponds to high-temperature phyllic assemblages from the Las Minas area, and zircon within pervasive potassic alteration assemblages from the Tatatila area, the $^{40}Ar/^{39}Ar$ analyses of samples from intrusive rocks were carried out at the Noble Gas Laboratory, Pacific Centre for Isotopic and Geochemical Research, University of British Columbia (Vancouver, British Columbia, Canada). The mineral separates were step-heated at incrementally higher powers in the defocused beam of a 10W CO_2 laser (New Wave Research MIR 10) until fused. The gas evolved from each step was analyzed by a VG5400 mass spectrometer equipped with an ion-counting electron multiplier. All measurements were corrected for total system blank, mass spectrometer sensitivity, mass discrimination, radioactive decay during and subsequent to irradiation, as well as interfering Ar from atmospheric contamination and the irradiation interferences of Ca, Cl and K. The plateau and correlation ages were calculated using the Isoplot 3.09 software (Ludwig, 2003). Errors are quoted at the 2-sigma (95% confidence) level and are propagated from all sources except mass spectrometer sensitivity and age of the flux monitor. The full results and spectra are reported in Appendices 1 and 2 and summarized in Figure 4.

The $^{40}Ar/^{39}Ar$ analysis were performed at the Geochronology Laboratory of the Departmento de Geología, Centro de Investigación Científica y Educación Superior de Ensenada (CICESE, Mexico). The argon isotope experiments were conducted on a few flakes of fuchsite, hornblende, K-feldspar and biotite. The mineral grains were heated with a Coherent Ar-ion Innova 370 laser. The extraction system is on line with a VG5400 mass spectrometer. The sample and irradiation monitors, were irradiated in the Uenriched research reactor of University of McMaster in Hamilton, Canada, at position 5C. To block thermal neutrons, the capsule was covered with a cadmium liner during irradiation of chromian muscovite ("fuchsite"; Figure 5A and 5B) from the skarn gangue association in IOCG mantos, Santa Cruz mine (sample SC-1). The mineral grains were heated with a Coherent Ar ion Innova 370 laser. The extraction system is on line with a VG5400 mass spectrometer. The sample and irradiation monitors were irradiated

http://dx.doi.org/10.18268/BSGM2020v72n3a110520

in the U-enriched research reactor of University of McMaster in Hamilton, Canada, at position 5C. To block thermal neutrons, the capsule was covered with a cadmium liner during irradiation. To determine the neutron flux variations, aliquots of the irradiation monitor FCT-2 sanidine (28.201 ± 0.046 Ma; Kuiper *et al.*, 2008) were irradiated alongside sample SC-1. Upon irradiation the monitors were fused in one step while the fuchsite sample was step-heated. The argon isotopes were corrected for blank, mass discrimination, radioactive decay of ^{37}Ar and ^{39}Ar, and atmospheric contamination. For the Ca neutron interference reactions, the factors given by Masliwec (1984) were used. The decay constants recommended by Steiger and Jäger (1977) were applied in the data processing. The equations reported by York *et al.* (2004) were used in all the straight line fitting routines of the argon data reduction. $^{40}Ar/^{39}Ar$ data are presented in Appendices 1 and 2, which includes the results of the individual steps, and the integrated, plateau and isochron ages, and their synthetic version in Figure 5. The analytical precision is reported as standard deviation (2σ). The error in the integrated, plateau and isochron ages includes the scatter in the irradiation monitors. With the exception of the first fraction, a well-defined straight line, with mean squared weighted deviations (MSWD) of 0.55 for n = 6, indicates an isochron age of 12.49 ± 0.09 Ma.

Zircon crystals were separated by means of panning from samples selected for U–Pb dating that are representative of various sets of rocks in the area: Au-Ag mineralized vein from Tatatila (sample TMG-5), and granodiorite to granite samples from the Santa Cruz (samples TMG-24 and SC-2), Carboneras (CR-5), Escalona (ES-3), Cinco Señores (5S-1), Boquillas (BQ-1), and Rancho Virgen (RV-2) areas. The sizes of the collected zircon crystals range between 20 and

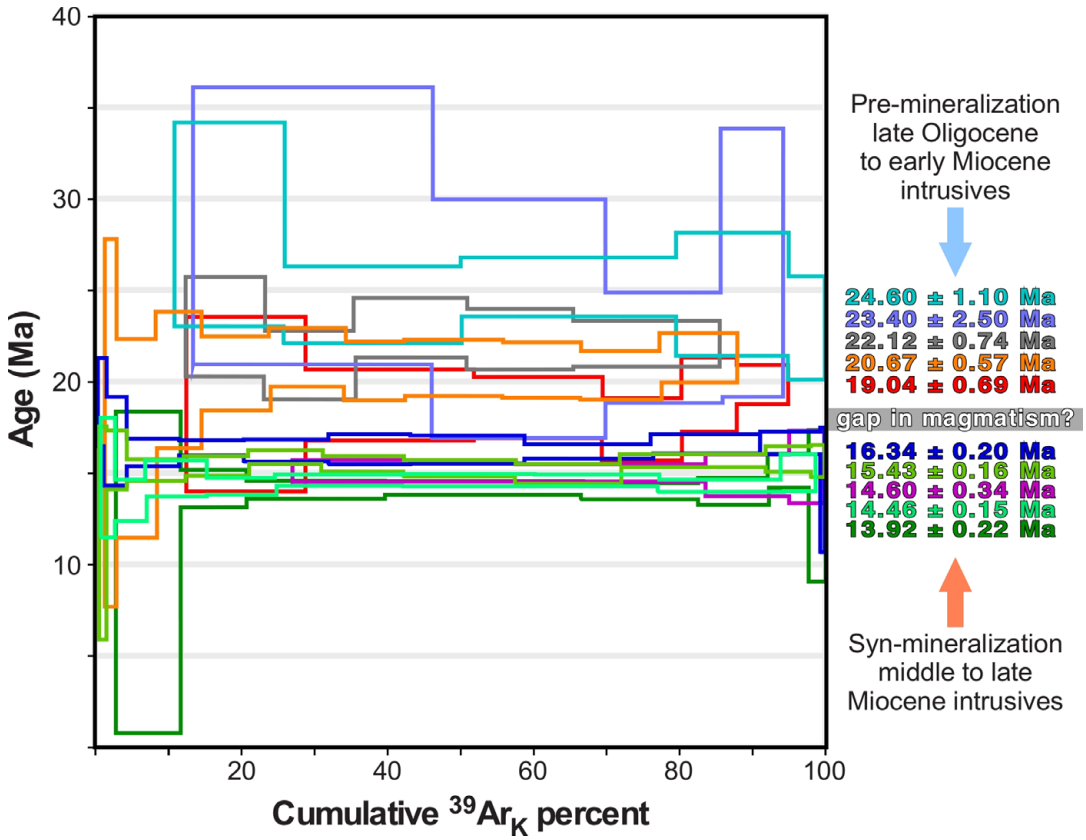

Figure 4 Outlines of $^{40}Ar/^{39}Ar$ age spectra (plateau ages) of intrusive host rocks to the IOCG skarn deposits in the Tatatila–Las Minas district, Veracruz.

http://dx.doi.org/10.18268/BSGM2020v72n3a110520

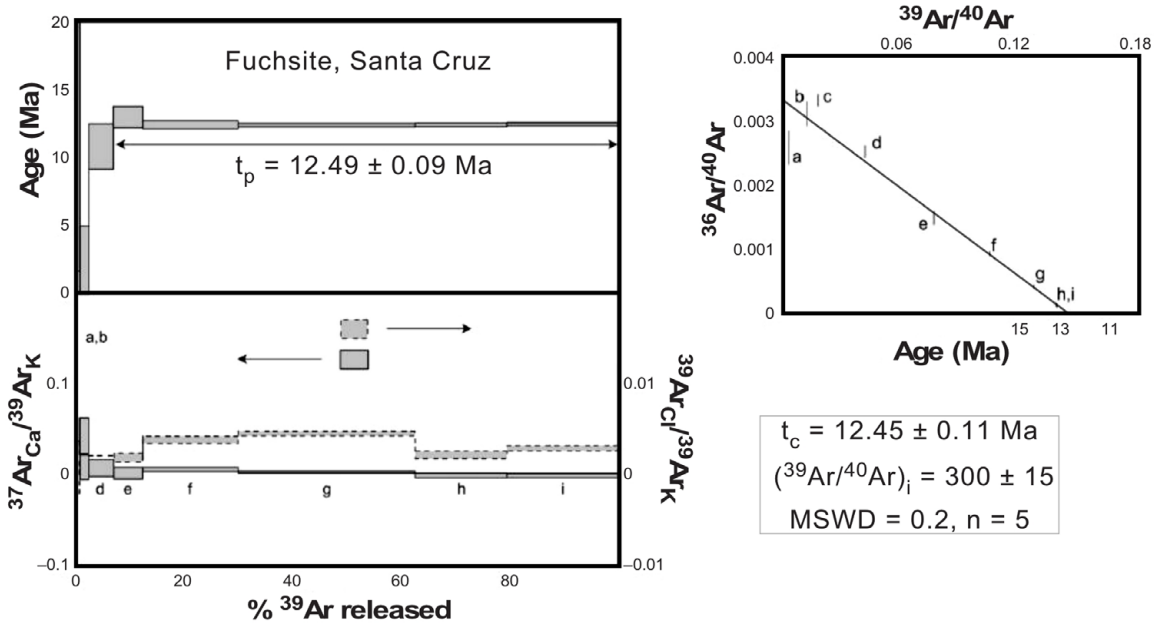

Figure 5 $^{40}Ar/^{39}Ar$ age spectra (plateau and isochron ages) of a chromian muscovite ("fuchsite") from the magmatic-hydrothermal retrograde assemblage of the IOCG skarn deposit in the Santa Cruz mine, Tatatila–Las Minas district, Veracruz.

90 µm in length. The U–Pb zircon analyses were performed with a quadrupole Thermo-X series ICP-MS with an Excimer (193 nm) laser ablation system by Resonetics, at the Isotopic Studies Laboratory (LEI), CGeo-UNAM, and following the procedure described by Solari *et al.* (2010). The data reduction was performed with the aid of the UPb.age in-house software (Solari and Tanner, 2011) and plotted with the Isoplot 3.0 software (Ludwig, 2003). See further technical aspects in González-León *et al.* (2017). U-Pb ages are displayed in Figures 6 and 7, Table 4 and Appendix 3.

4. Results

The U-Pb ages of zircon crystals from granite, granodiorite, quartz-monzonite and monzodiorite are displayed in Figures 6 and 7, in Table 4, and Appendices 3 and 4. The sample from Carboneras (CR-5) yielded a U-Pb concordia lower intercept at 15.05 ± 0.94 Ma (MSWD = 2.5, n = 19; Figure 7C). Two samples from the Santa Cruz mine were dated; sample TMG-24 yielded a U-Pb concordant age at 15.27 ± 0.36 Ma (MSWD = 2 n = 14; Figure 6A), and sample SC-2b a weighted mean U-Pb age at 14.33 ± 0.38 Ma (MSWD = 2.6, n = 9; Figure 7B). The sample from Cinco Señores (5S-1) yielded a U-Pb weighted mean age at 15.09 ± 0.48 Ma (MSWD = 4.0, n = 8; Figure 7D). $^{40}Ar/^{39}Ar$ determinations in host intrusive samples as granodiorite, granite, monzodiorite and quartz-monzonite yielded two groups of ages: (A) late Oligocene to early Miocene, between 22.12 ± 0.74 and 19.04 ± 0.69 Ma for a pre-mineralization suite of intrusive bodies, and (B) middle to late Miocene, between 16.34 ± 0.20 and 13.92 ± 0.22 Ma for a syn-mineralization suite of intrusive bodies, all reported ages correspond to plateau ages.

The samples for $^{40}Ar/^{39}Ar$ different minerals such as biotite, hornblende, K-feldspar and fuchsite, were separated from each sample for analysis.

The $^{40}Ar/^{39}Ar$ determination in hydrothermal chromian muscovite ("fuchsite") of the Santa Cruz mine yielded a plateau age of 12.49 ± 0.09 Ma (isochron age at 12.39 ± 0.1 Ma; Figure 5). The sample (TMG-5) from a potassic alteration assemblage that was pervasively developed on a granite-granodiorite intrusion in the village of Tatatila (thus corresponding to hydrothermal

http://dx.doi.org/10.18268/BSGM2020v72n3a110520

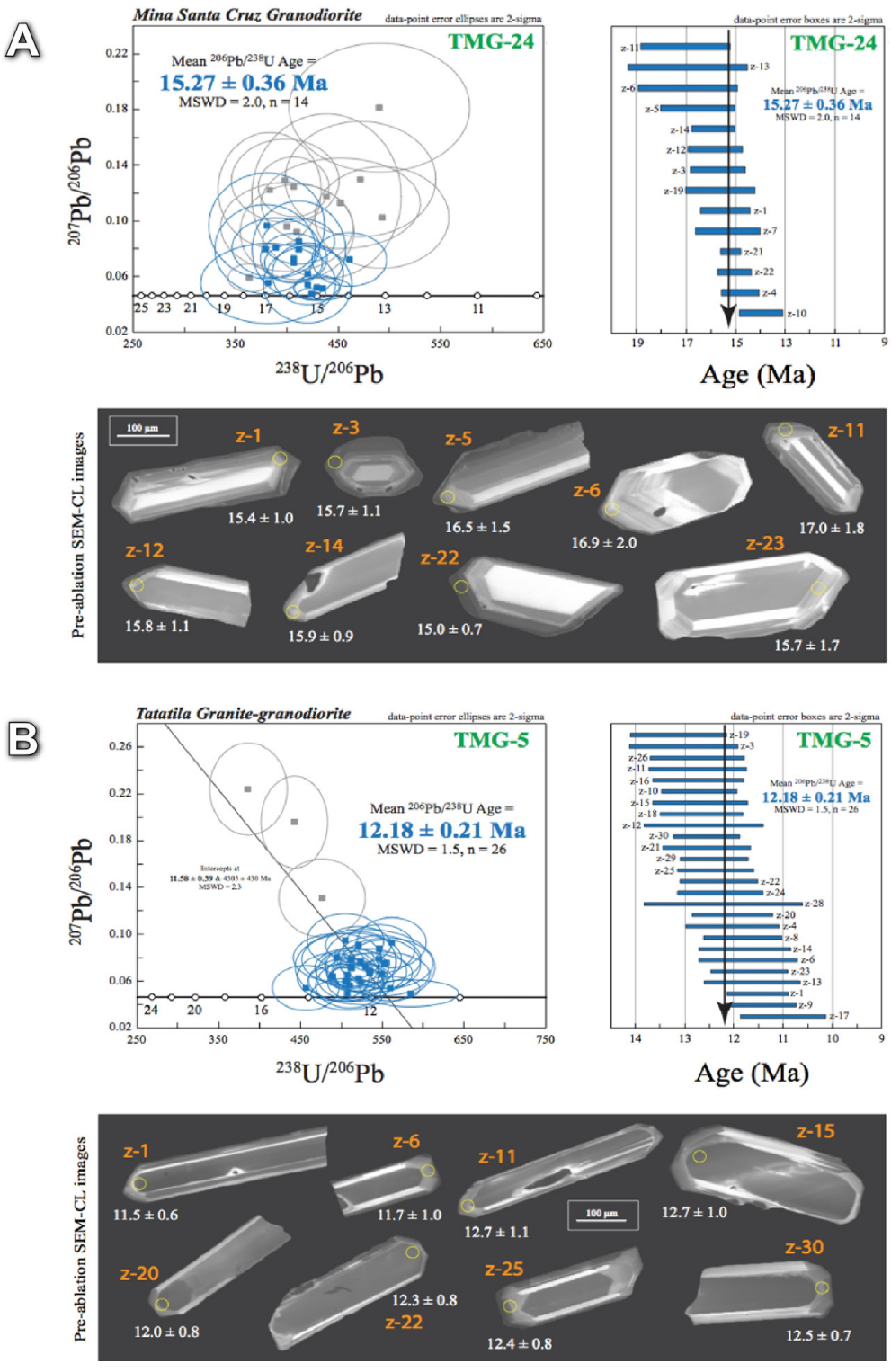

Figure 6 Tera-Wasserburg U-Pb concordia diagrams and plots of weighted averages of individual $^{206}Pb/^{238}U$ ages of analyzed zircons, and pre-ablation SEM-CL images of zircons from a granodiorite intrusive from the Santa Cruz Mine (A), and from a potassic alteration assemblage that was pervasively developed on a granite-granodiorite intrusion in the village of Tatatila (B), from the Tatatila–Las Minas district, Veracruz. Solid-line ellipses, with blue square centers, are data used for age calculations; gray-line ellipses are data excluded from age calculations due to different degrees of Pb-loss and/or zircon inheritance. All U–Pb data are plotted with 2-sigma errors and all calculated weighted mean ages are also listed at the 2-sigma level. Original U(Th)–Pb data can be found for inspection in Table 5.

Table 4. U-Th-Pb analytical data for LA-ICPMS spot analyses on zircon grains for granitic units in Tatatila de Las Minas, Veracruz, Mexico.

				CORRECTED ISOTOPIC RATIOS										CORRECTED AGES (Ma)								
Analisys/Zircon	U# (ppm)	Th# (ppm)	Th/U	$^{207}Pb/^{206}Pb^{\dagger}$	err %*	$^{207}Pb/^{235}U^{\dagger}$	err %*	$^{206}Pb/^{238}U^{\dagger}$	err %*	$^{208}Pb/^{232}Th^{\dagger}$	err %*	Rho**	% disc.***	$^{206}Pb/^{238}U$	±2σ*	$^{207}Pb/^{235}U$	±2σ*	$^{207}Pb/^{206}Pb$	±2σ*	Best Age (Ma)	±	2σ
Sample **TMG-5**	**Granite-granodiorite** (Tatatila de Las Minas, Veracruz) Mount ICGEO-100 (January 2017)																					
TMG-5-17	724	1273	1.76	0.04730	18.4	0.01170	20.5	0.00171	8.2	0.00057	14.4	0.399	7	11.0	0.9	11.8	2.4	690	330	**11.0**	±	**0.9**
TMG-5-9	226	180	0.80	0.08800	21.6	0.02280	19.7	0.00178	6.2	0.00068	20.6	0.313	50	11.5	0.7	22.8	4.5	1620	410	**11.5**	±	**0.7**
TMG-5-1	455	618	1.36	0.05180	18.0	0.01320	16.7	0.00179	5.4	0.00067	10.2	0.322	13	11.5	0.6	13.3	2.2	750	320	**11.5**	±	**0.6**
TMG-5-13	343	437	1.27	0.07800	23.1	0.01870	24.6	0.00180	8.3	0.00067	13.2	0.339	38	11.6	1.0	18.8	4.6	1100	510	**11.6**	±	**1.0**
TMG-5-23	345	367	1.06	0.07900	25.3	0.01860	23.7	0.00181	6.6	0.00065	14.7	0.280	37	11.7	0.8	18.6	4.4	1410	480	**11.7**	±	**0.8**
TMG-5-6	204	141	0.69	0.06400	26.6	0.01660	24.7	0.00182	8.8	0.00068	19.1	0.356	30	11.7	1.0	16.6	4.1	1460	450	**11.7**	±	**1.0**
TMG-5-14	232	155	0.67	0.07400	24.3	0.01990	22.1	0.00183	7.7	0.00072	15.3	0.346	41	11.8	0.9	19.9	4.4	1570	420	**11.8**	±	**0.9**
TMG-5-8	212	189	0.89	0.08900	21.3	0.02210	20.4	0.00183	6.6	0.00053	22.6	0.322	47	11.8	0.8	22.1	4.5	1440	370	**11.8**	±	**0.8**
TMG-5-4	268	240	0.89	0.07400	24.3	0.01720	22.1	0.00187	8.0	0.00060	20.0	0.363	31	12.0	1.0	17.3	3.8	1230	450	**12.0**	±	**1.0**
TMG-5-20	255	221	0.87	0.07100	23.9	0.01770	23.7	0.00187	7.0	0.00069	17.4	0.293	32	12.0	0.8	17.7	4.2	1220	440	**12.0**	±	**0.8**
TMG-5-28	167	157	0.94	0.08400	44.0	0.01880	38.8	0.00189	13.2	0.00068	22.1	0.341	35	12.2	1.6	18.8	7.2	1730	790	**12.2**	±	**1.6**
TMG-5-24	156	126	0.81	0.07200	29.2	0.02030	27.6	0.00191	6.8	0.00076	21.1	0.247	39	12.3	0.9	20.2	5.6	1540	520	**12.3**	±	**0.9**
TMG-5-22	313	324	1.04	0.05600	23.2	0.01560	23.1	0.00191	6.3	0.00063	17.5	0.272	22	12.3	0.8	15.7	3.6	840	470	**12.3**	±	**0.8**
TMG-5-25	311	188	0.60	0.08300	16.9	0.02410	15.4	0.00192	6.3	0.00070	20.0	0.407	49	12.4	0.8	24.1	3.6	1530	340	**12.4**	±	**0.8**
TMG-5-29	379	247	0.65	0.06500	16.9	0.01660	16.3	0.00192	5.7	0.00061	19.7	0.352	26	12.4	0.7	16.7	2.7	1090	330	**12.4**	±	**0.7**
TMG-5-21	274	283	1.03	0.07400	21.6	0.01910	20.9	0.00195	7.2	0.00078	19.2	0.343	34	12.5	0.9	19.1	4.0	1440	420	**12.5**	±	**0.9**
TMG-5-30	286	228	0.80	0.07100	22.5	0.01930	20.2	0.00195	5.1	0.00081	18.5	0.254	35	12.5	0.7	19.3	3.9	1590	410	**12.5**	±	**0.7**
TMG-5-12	258	238	0.92	0.07900	24.1	0.02110	25.6	0.00195	9.7	0.00047	57.4	0.381	40	12.6	1.2	21.1	5.3	1170	450	**12.6**	±	**1.2**
TMG-5-18	209	131	0.63	0.05200	30.8	0.01530	28.8	0.00196	6.6	0.00077	19.5	0.231	17	12.6	0.8	15.3	4.3	1130	520	**12.6**	±	**0.8**
TMG-5-15	176	152	0.86	0.06300	23.8	0.01650	25.5	0.00197	7.6	0.00076	22.4	0.299	23	12.7	1.0	16.5	4.2	1030	450	**12.7**	±	**1.0**
TMG-5-10	254	157	0.62	0.05800	27.6	0.01780	26.4	0.00197	6.1	0.00056	21.4	0.231	28	12.7	0.8	17.7	4.7	1310	480	**12.7**	±	**0.8**
TMG-5-16	278	242	0.87	0.05100	25.5	0.01330	23.3	0.00197	7.1	0.00066	16.7	0.305	5	12.7	0.9	13.4	3.1	1080	420	**12.7**	±	**0.9**
TMG-5-11	207	184	0.89	0.06300	23.8	0.01610	23.0	0.00198	7.6	0.00079	16.5	0.330	21	12.7	1.0	16.2	3.7	1280	460	**12.7**	±	**1.0**
TMG-5-26	203	189	0.93	0.09700	25.8	0.02580	21.3	0.00198	7.6	0.00062	21.0	0.355	50	12.7	1.0	25.6	5.4	1790	480	**12.7**	±	**1.0**
TMG-5-3	173	112	0.65	0.08100	23.5	0.02230	22.9	0.00202	8.9	0.00080	22.5	0.390	41	13.0	1.1	22.2	5.0	1620	460	**13.0**	±	**1.1**
TMG-5-19	213	206	0.97	0.05700	36.8	0.01790	26.8	0.00204	7.4	0.00060	20.0	0.274	27	13.1	1.0	17.9	4.8	1420	500	**13.1**	±	**1.0**
TMG-5-2	200	117	0.58	0.14100	23.4	0.03790	22.7	0.00210	9.0	0.00056	48.2	0.399	64	13.5	1.2	37.5	8.3	2350	410	13.5	±	1.2
TMG-5-7	194	170	0.88	0.05200	32.7	0.01640	29.9	0.00219	7.3	0.00077	18.2	0.245	14	14.1	1.0	16.4	4.9	1180	520	14.1	±	1.0
TMG-5-5	160	117	0.74	0.20500	17.6	0.06100	18.0	0.00226	7.5	0.00177	20.3	0.417	76	14.5	1.1	60.0	10.0	2950	410	14.5	±	1.1
TMG-5-27	221	193	0.87	0.24200	19.8	0.08000	17.5	0.00259	10.0	0.00118	53.4	0.574	79	16.7	1.7	78.0	13.0	3110	320	16.7	±	1.7

n = 30

Mean $^{206}Pb/^{238}U$ Age = 12.18 ± 0.21

(2 sigma, MSWD = 1.5; n = 26)

#U and Th concentrations (ppm) are calculated relative to analyses of trace-element glass standard NIST 610.
†Isotopic ratios are corrected relative to 91500 standard zircon for mass bias and down-hole fractionation (91500 with an age ~1065 Ma; Wiedenbeck *et al.*, 1995). Isotopic $^{207}Pb/^{206}Pb$ ratios, ages and errors are calculated following Paton *et al.* (2010).

*All errors in isotopic ratios are in percentage whereas ages are reported in absolute and given at the 2-sigma level. The weighted mean $^{206}Pb/^{238}U$ age is also reported in absolute values at the 2-sigma level. The uncertenties have been propagated following the methodology discussed by Paton *et al.* (2010).

**Rho is the error correlation value for the isotopic ratios $^{206}Pb/^{238}U$ and $^{207}Pb/^{235}U$ calculated by dividing these two percentage errors. The Rho value is required for plotting concordia diagrams.

***Percentage discordance values are obtained using the following equation (100*[(edad $^{207}Pb/^{235}U$)-(edad $^{206}Pb/^{238}U$)]/edad $^{207}Pb/^{235}U$) proposed by Ludwig (2001). Positive and negative values indicate normal and inverse discordance, respectively.

Individual zircon ages in bold were used to calculate the weighted mean $^{206}Pb/^{238}U$ age and MSWD (Mean Square of Weigthed Deviates) using the computacional program Isoplot (Ludwig , 2003).

http://dx.doi.org/10.18268/BSGM2020v72n3a110520

Table 4. (Continuation) U-Th-Pb analytical data for LA-ICPMS spot analyses on zircon grains for granitic units in Tatatila-Las Minas, Veracruz, Mexico.

Sample **TMG-24**	**Mina Santa Cruz granodiorite** (Tatatila de Las Minas, Veracruz) Mount ICGEO-100 (January 2017)																								
TMG-24-15	103	76	0.74		0.11900	31.9	0.02870	31.0	0.00203	10.8	0.00085	28.2		0.349	54		13.1	1.4	28.4	8.8	2270	620		13.1	±	1.4
TMG-24-24	57	32	0.57		0.19000	63.2	0.05100	25.5	0.00204	14.7	0.00181	26.5		0.577	73		13.2	1.9	49.0	13.0	2940	2400		13.2	±	1.9
TMG-24-20	63	34	0.54		0.14100	28.4	0.03800	28.9	0.00212	12.7	0.00091	50.5		0.440	63		13.7	1.7	37.0	11.0	2670	560		13.7	±	1.7
TMG-24-10	175	70	0.40		0.07000	22.9	0.02160	22.7	0.00217	6.5	0.00095	24.2		0.284	35		14.0	0.9	21.5	4.9	1280	390		**14.0**	**±**	**0.9**
TMG-24-8	110	93	0.85		0.14000	30.7	0.03430	27.4	0.00221	14.0	0.00083	28.9		0.512	58		14.2	2.0	33.9	9.2	2080	580		14.2	±	2.0
TMG-24-18	64	44	0.68		0.12200	44.3	0.03700	43.2	0.00228	13.6	0.00137	35.0		0.314	59		14.7	2.0	36.0	15.0	2790	910		14.7	±	2.0
TMG-24-4	574	534	0.93		0.05470	14.8	0.01630	14.1	0.00230	5.2	0.00077	10.5		0.370	10		14.8	0.8	16.4	2.3	700	280		**14.8**	**±**	**0.8**
TMG-24-22	760	560	0.74		0.05240	15.3	0.01670	15.0	0.00233	4.3	0.00084	11.3		0.287	11		15.0	0.7	16.8	2.5	660	280		**15.0**	**±**	**0.7**
TMG-24-21	2120	2370	1.12		0.04810	7.3	0.01540	7.8	0.00236	2.6	0.00074	6.6		0.338	2		15.2	0.4	15.5	1.2	333	140		**15.2**	**±**	**0.4**
TMG-24-7	110	62	0.56		0.06000	46.7	0.01780	42.1	0.00238	8.4	0.00123	25.2		0.199	19		15.3	1.3	18.9	7.8	1800	710		**15.3**	**±**	**1.3**
TMG-24-1	234	113	0.48		0.06900	30.4	0.02030	30.0	0.00238	6.7	0.00103	17.5		0.224	24		15.4	1.0	20.2	6.1	1150	550		**15.4**	**±**	**1.0**
TMG-24-19	77	65	0.84		0.07200	41.7	0.02660	36.8	0.00243	9.1	0.00088	25.0		0.246	40		15.6	1.4	26.0	9.7	2050	740		**15.6**	**±**	**1.4**
TMG-24-3	275	152	0.55		0.08300	16.9	0.02860	17.1	0.00243	7.0	0.00091	18.7		0.408	45		15.7	1.1	28.4	4.8	1580	350		**15.7**	**±**	**1.1**
TMG-24-23	64	32	0.51		0.11900	34.5	0.03100	32.3	0.00244	11.1	0.00073	57.5		0.343	47		15.7	1.7	29.9	9.9	2170	680		15.7	±	1.7
TMG-24-9	146	154	1.05		0.12800	16.4	0.04220	15.6	0.00246	6.9	0.00108	16.7		0.442	62		15.8	1.1	41.7	6.4	2160	320		15.8	±	1.1
TMG-24-12	248	150	0.60		0.08900	24.7	0.02480	21.0	0.00246	6.5	0.00075	24.0		0.310	36		15.8	1.1	24.7	5.2	1630	380		**15.8**	**±**	**1.1**
TMG-24-14	350	234	0.67		0.06800	17.6	0.02370	16.9	0.00246	5.7	0.00075	22.7		0.337	33		15.9	0.9	23.7	4.0	1280	370		**15.9**	**±**	**0.9**
TMG-24-17	65	34	0.52		0.12600	33.3	0.03300	30.3	0.00250	13.2	0.00113	30.1		0.436	51		16.1	2.1	33.0	10.0	2640	710		16.1	±	2.1
TMG-24-25	80	66	0.83		0.13800	51.4	0.04460	21.7	0.00251	10.8	0.00093	30.1		0.495	63		16.1	1.7	43.7	9.4	2300	2200		16.1	±	1.7
TMG-24-5	115	48	0.41		0.08100	24.7	0.02860	23.4	0.00257	8.9	0.00098	33.7		0.382	42		16.5	1.5	28.3	6.7	1610	450		**16.5**	**±**	**1.5**
TMG-24-16	65	31	0.47		0.19200	46.9	0.04400	29.5	0.00261	10.7	0.00123	43.9		0.363	60		16.8	1.8	42.0	13.0	2650	1000		16.8	±	1.8
TMG-24-6	67	31	0.46		0.10500	43.8	0.03500	34.3	0.00263	12.2	0.00141	30.5		0.355	50		16.9	2.0	34.0	12.0	2010	720		**16.9**	**±**	**2.0**
TMG-24-13	70	34	0.49		0.08100	54.3	0.01990	44.7	0.00262	14.1	0.00103	39.8		0.316	14		16.9	2.4	19.6	8.9	2430	880		**16.9**	**±**	**2.4**
TMG-24-11	120	54	0.45		0.09900	34.3	0.02900	34.5	0.00264	10.6	0.00082	48.8		0.308	40		17.0	1.8	28.2	9.9	1970	700		**17.0**	**±**	**1.8**
TMG-24-2	1550	930	0.60		0.05960	15.6	0.02240	14.7	0.00275	4.7	0.00065	44.6		0.321	21		17.7	0.9	22.5	3.3	640	310		17.7	±	0.9

n = 25

Mean $^{206}Pb/^{238}U$ Age = 15.27 ± 0.36

(2 sigma, MSWD = 2.0; n = 14)

#U and Th concentrations (ppm) are calculated relative to analyses of trace-element glass standard NIST 610.
†Isotopic ratios are corrected relative to 91500 standard zircon for mass bias and down-hole fractionation (91500 with an age ~1065 Ma; Wiedenbeck *et al*., 1995). Isotopic $^{207}Pb/^{206}Pb$ ratios, ages and errors are calculated following Paton *et al*. (2010).

*All errors in isotopic ratios are in percentage whereas ages are reported in absolute and given at the 2-sigma level. The weighted mean $^{206}Pb/^{238}U$ age is also reported in absolute values at the 2-sigma level. The uncertenties have been propagated following the methodology discussed by Paton *et al*. (2010).

**Rho is the error correlation value for the isotopic ratios $^{206}Pb/^{238}U$ and $^{207}Pb/^{235}U$ calculated by dividing these two percentage errors. The Rho value is required for plotting concordia diagrams.

***Percentage discordance values are obtained using the following equation (100*[(edad $^{207}Pb/^{235}U$)-(edad $^{206}Pb/^{238}U$)]/edad $^{207}Pb/^{235}U$) proposed by Ludwig (2001). Positive and negative values indicate normal and inverse discordance, respectively.

Individual zircon ages in bold were used to calculate the weighted mean $^{206}Pb/^{238}U$ age and MSWD (Mean Square of Weigthed Deviates) using the computacional program Isoplot (Ludwig , 2003).

http://dx.doi.org/10.18268/BSGM2020v72n3a110520

http://dx.doi.org/10.18268/BSGM2020v72n3a110520

associations) yielded a U-Pb age of 12.18 ± 0.21 Ma, (2σ, MSWD = 1.5; n = 26; Figure 6B).

The sample ES-3 from Escalona corresponds to a dyke that crosscuts the IOCG mineralization and yielded a U-Pb weighted mean age at 4.11 ± 0.11 Ma (MSWD = 0.53, n = 8; Figure 7A). A sample from Boquillas (BQ-1a, BQ-1b) yielded a U-Pb weighted mean age at 286 ± 2 Ma (MSWD = 1.02, n = 6; Artinskian, early Permian; Figure 7E).

The intrusive rocks associated with the formation of IOCG deposits in the Tatatila–Las Minas area span compositions between those of sub-alkaline gabbros and granodiorites, and mostly concentrate in the granite, diorite and monzodiorite fields (Figure 8A). The geochemical affinity of the rocks is essentially metaluminous (Figure 8B), calc-alkaline (Figure 8C), and they plot within the fields of volcanic-arc granites (VAG) (Figure 9A) and I- and S-type granites (Figure 9B). Some samples have adakitic signatures (Figure 9D), mostly of the high-silica type (Figure 9E), thus indicating that their compositional variation is controlled mainly by partial melting (Figure 9C). Light rare-earth and large-ion lithophile elements (LREE and LILE) are slightly enriched in such rocks (Figure 10) with respect to heavy rare-earth and high field strength elements (HREE and HFSE), as is characteristic for rocks associated with subduction, and conform with the results obtained by Dorantes-Castro (2016). Radiogenic isotope data range as follows: $^{87}Sr/^{86}Sr$ between 0.7040 and 0.7059, εSr between −11.4 and 19.9, $^{143}Nd/^{144}Nd$ between 0.5123 and 0.5128, εNd between −6.6 and 3.2, and $^{206}Pb/^{204}Pb$ between 18.65 and 18.75 (Table 3; Figure 11). The distribution of such data is in accordance with that determined by Gómez-Tuena *et al.* (2003) for rocks from the Trans-Mexican Volcanic Belt.

5. Discussion

5.1. AGE CONSTRAINTS

The ages (Figures 4 and 12; Table 5) of magmatic and hydrothermal episodes the Tatatila-Las Minas deposits range between 16.34 and 13.92 Ma for the associated intrusive bodies (all of them observed as direct contributors to prograde skarn formation), and between 12.49 and 12.18 Ma for hydrothermal minerals (retrograde skarn stages). It is important to emphasize that the analyzed rocks are not merely terms of an intrusive suite that included IOCG skarn generators, but IOCG skarn generators themselves, as the sampling strategy was directed to rocks spatially associated with such mineralization—whether prograde or retrograde. The discussion to follow relies on this fact. The maximum time gap between prograde and retrograde skarn associations thus determined spans ~1.5 My, which is similar to that defined for other skarn deposits (*i.e.*, Camprubí *et al.*, 2015). A late dyke that crosscuts the mineralization, in association with capping volcanic rocks of the Trans-Mexican Volcanic Belt, was dated at 4.11 Ma. The early Permian age obtained for intrusive rocks in the Las Minas area (286 ± 2 Ma) is likely to correspond to the Carboniferous-Permian arc (Ortega-Obregón *et al.*, 2013; Kirsch *et al.*, 2012), known as the Teziutlán massif, that constitutes the basement in the region and was dated at 269–252 Ma (K–Ar; López-Infanzón, 1991) and at 281–268 Ma ($^{40}Ar/^{39}Ar$; Iriondo *et al.*, 2003).

A consistent range of ages between 24.60 and 19.04 Ma (late Oligocene to early Miocene; Figures 4 and 12; Table 5) has been additionally obtained, which corresponds to intrusive rocks that predate the syn-mineralization suite. Such ages also predate the earliest stage of magmatism that is associated with the Trans-Mexican Volcanic Belt (Gómez-Tuena *et al.*, 2005, 2007) and are similar to those characteristic of the final stage of magmatic activity of the Sierra Madre Occidental (Ferrari *et al.*, 2005b, 2007).

5.2. PETROLOGIC AFFINITY

The multielemental and isotopic geochemical determinations of IOCG skarn-related intrusive rocks at Tatatila–Las Minas are sound and congruent indicators of mostly intermediate

http://dx.doi.org/10.18268/BSGM2020v72n3a110520

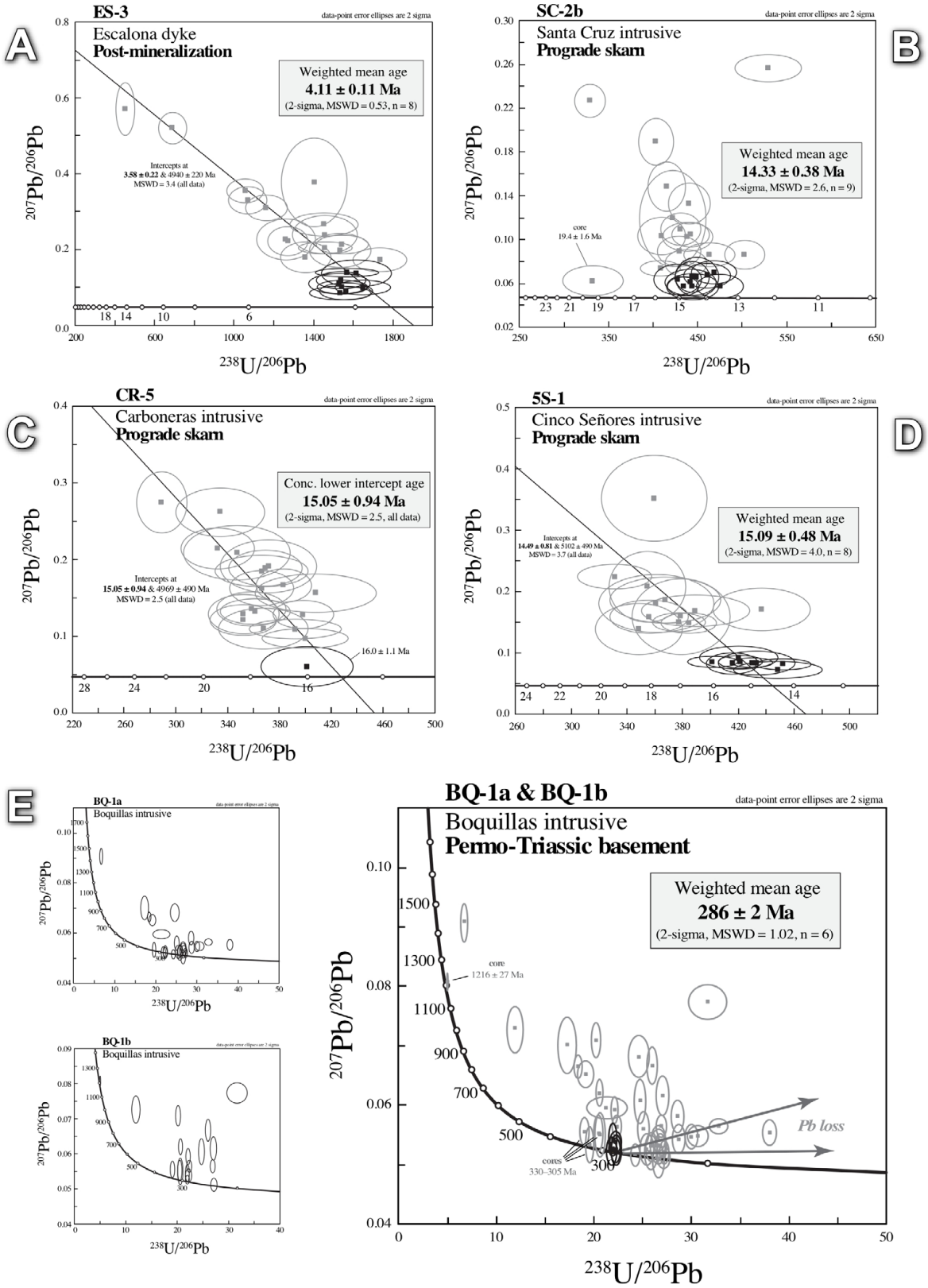

Figure 7 Tera-Wasserburg U-Pb concordia diagrams for zircons from various intrusive bodies in the Tatatila–Las Minas area. (A) Post-mineralization dyke. (B to D) Syn-mineralization hypabyssal bodies whose age can be attributed to the prograde skarn associations. (E) Granitic intrusive that corresponds to the Permo-Triassic basement. Solid-line ellipses, with black square centers, are data used for age calculations; gray-line ellipses are data excluded from age calculations due to different degrees of Pb-loss and/or zircon inheritance. All U–Pb data are plotted with 2-sigma errors. Original U(Th)–Pb data can be found for inspection in Appendix 3.

http://dx.doi.org/10.18268/BSGM2020v72n3a110520

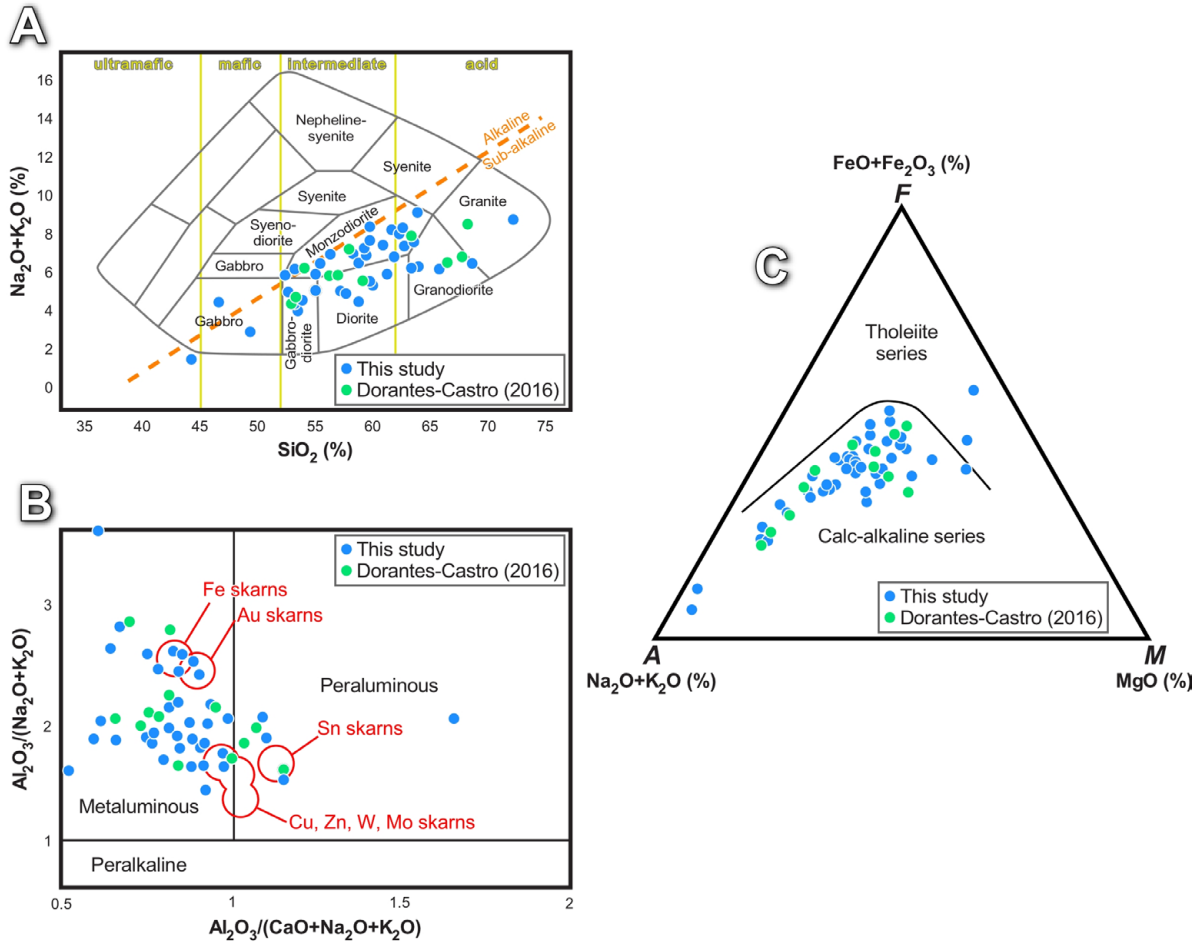

Figure 8 **Petrological discrimination diagrams from major elements in intrusions associated with IOCG skarn mineralization in the Tatatila–Las Minas district, Veracruz. (A) Silica vs. alkaline element bivariant diagram, adapted from Cox *et al.* (1979). (B) Alumina saturation diagram, adapted from Frost *et al.* (2001), with compositions of skarns from Meinert (1995). (C) AFM diagram, adapted from Irvine and Baragar (1971).**

to acid (Figure 8A), metaluminous (Figure 8B), and I- and S-type rocks (Figure 9B) that were emplaced in a subduction-related continental arc (Figure 9A), and high La/Yb ratios could also be obtained through high pressures in basaltic melt (Figure 9C; McPherson *et al.*, 2006), since the late Oligoce to Miocene. In addition, these rocks are part of the medium- to high-potassium (not shown) calc-alkaline series, with adakitic signatures and a compelling isotopic affinity with the Trans-Mexican Volcanic Belt (TMVB). A sound adakitic affinity of most analyzed samples in the study area is determined by a general geochemical behavior (Tables 1 to 3; Figure 9D, E) that meets most of the characteristics of such petrological association (Table 6). If anything, Y and Yb contents appear to be significantly higher than in adakitic (Tables 3 and 6), a characteristic that will be addressed later on. Despite the possible occurrence of alkaline magmatism in the Palma Sola region in association with the Eastern Mexico Alkaline Province (EMAP; Demand and Robin, 1975; Negendank *et al.*, 1985; Ferrari *et al.*, 2005a), the formation of IOCG skarn deposits in the Tatatila–Las Minas district can be solely attributed to the TMVB, as no adakitic affinity has been consistently reported for the magmatism associated with the EMAP (see references in Camprubí, 2013). However, some ages of alkaline rocks in Palma Sola are much younger than syn-mineralization ages, with no associated mineralization. Then, the adakitic signatures

http://dx.doi.org/10.18268/BSGM2020v72n3a110520

Table 5. Summary of geochronometric data obtained for host intrusive rocks and IOCG mineralization at the Tatatila–Las Minas area.

Sample / location	Association	Method / mineral	Age ± 2σ (Ma)	Comments
Tatatila–Las Minas district				
BQ-1a, BQ-1b / Boquillas	Granite	U-Pb / zircon	286 ± 2	Early Permian granitoids in the Permo-Triassic basement
CR-1 / Carboneras	Granodiorite	$^{40}Ar/^{39}Ar$ / biotite	24.60 ± 1.10	Pre-mineralization intrusive suite (late Oligocene to early Miocene)
CR-1 / Carboneras	Granodiorite	$^{40}Ar/^{39}Ar$ / HB	23.40 ± 2.50	
BQ-1c / Boquillas	Granite	$^{40}Ar/^{39}Ar$ / KF	22.12 ± 0.74	Transition between the Sierra Madre Occidental and the Trans-Mexican Volcanic Belt?
RV-2 / Vaquería	Granite	$^{40}Ar/^{39}Ar$ / KF	20.67 ± 0.57	
CR-1 / Carboneras	Granodiorite	$^{40}Ar/^{39}Ar$ / KF	19.04 ± 0.69	
SC-2-b1 / Santa Cruz	Granodiorite	$^{40}Ar/^{39}Ar$ / biotite	16.34 ± 0.20	
SC-2a / Santa Cruz	Granodiorite	$^{40}Ar/^{39}Ar$ / biotite	15.43 ± 0.16	Syn-mineralization intrusive suite (middle to late Miocene)
TMG-24 / Santa Cruz	Qz-monzonite	U-Pb / zircon	15.27 ± 0.36	
5S-1 / Cinco Señores	Granite	U-Pb / zircon	15.09 ± 0.48	
CR-5 / Carboneras	Granodiorite	U-Pb / zircon	15.05 ± 0.94	Matches with the middle to late Miocene age range of intrusive bodies of gabbroic to dioritic composition defined by Ferrari *et al.* (2005a) at the Palma Sola massif, east of the Tatatila–Las Minas area
BQ-1b / Boquillas	Granite	$^{40}Ar/^{39}Ar$ / biotite	14.60 ± 0.34	
SC-2b / Santa Cruz	Granodiorite	$^{40}Ar/^{39}Ar$ / biotite	14.46 ± 0.15	
SC-2b / Santa Cruz	Granodiorite	U-Pb / zircon	14.33 ± 0.38	
BQ-1b / Boquillas	Granite	$^{40}Ar/^{39}Ar$ / biotite	13.92 ± 0.22	
FSC-1 / Santa Cruz	mineralization	$^{40}Ar/^{39}Ar$ / CM	12.49 ± 0.09	
TMG-5 / Tatatila	mineralization	U-Pb / zircon	12.18 ± 0.21	
Es-3 / Escalona	Granodiorite	U-Pb / zircon	4.11 ± 0.11	Post-mineralization intrusives
Regional intrusive ages				
Laguna Verde	microdiorite		17	Cantagrel and Robin (1979), deemed as unreliable by Ferrari *et al.* (2005a)
Junique	gabbro	$^{40}Ar/^{39}Ar$	15.62 ± 0.5	Ferrari *et al.* (2005a)
Plan de las Hayas	hypabyssal rock	$^{40}Ar/^{39}Ar$	14.65 ± 0.32	Ferrari *et al.* (2005a)
Tenochtitlan to Junique	granitic plutons		13.0 ± 1.0	López-Infanzón (1991)
			9.0 ± 0.7	
			6.2 ± 0.6	
Candelaria	gabbro		12.3 and 12.9	Negendank *et al.* (1985)
		$^{40}Ar/^{39}Ar$ / PL	10.9 ± 0.8	Ferrari *et al.* (2005a)
El Limón	hypabyssal rock	$^{40}Ar/^{39}Ar$	11.07 ± 0.2	Ferrari *et al.* (2005a)
Whole range of ages of magmatism in the Palma Sola massif			15.6 to 10.9	Ferrari *et al.* (2005a)
			17 to 7.5	Camprubí (2009, 2013)

found in the Palma Sola region are more likely to correspond to the volcanism of the TMVB rather than that of the EMAP. This is the first instance in which adakites are directly associated with the formation of any ore deposits in the TMVB—in this case, IOCG skarn deposits.

However, anomalously high Y and Yb contents (with respect to typical adakitic signatures) similar to those found in the Tatatila–Las Minas host rocks have been explained in adakites as to reflect some degree of interaction with alkaline or ultrapotassic rocks (Lu *et al.*, 2013; Liu *et al.*, 2017)—hence the high-potassium character of many of the studied rocks (?)—or due to crustal contamination (Zhang *et al.*, 2017). Therefore, despite the likely dominant affinity of these rocks with the TMVB, some degree of interaction between their parental TMVB magmas and EMAP magmas cannot be ruled out at this

http://dx.doi.org/10.18268/BSGM2020v72n3a110520

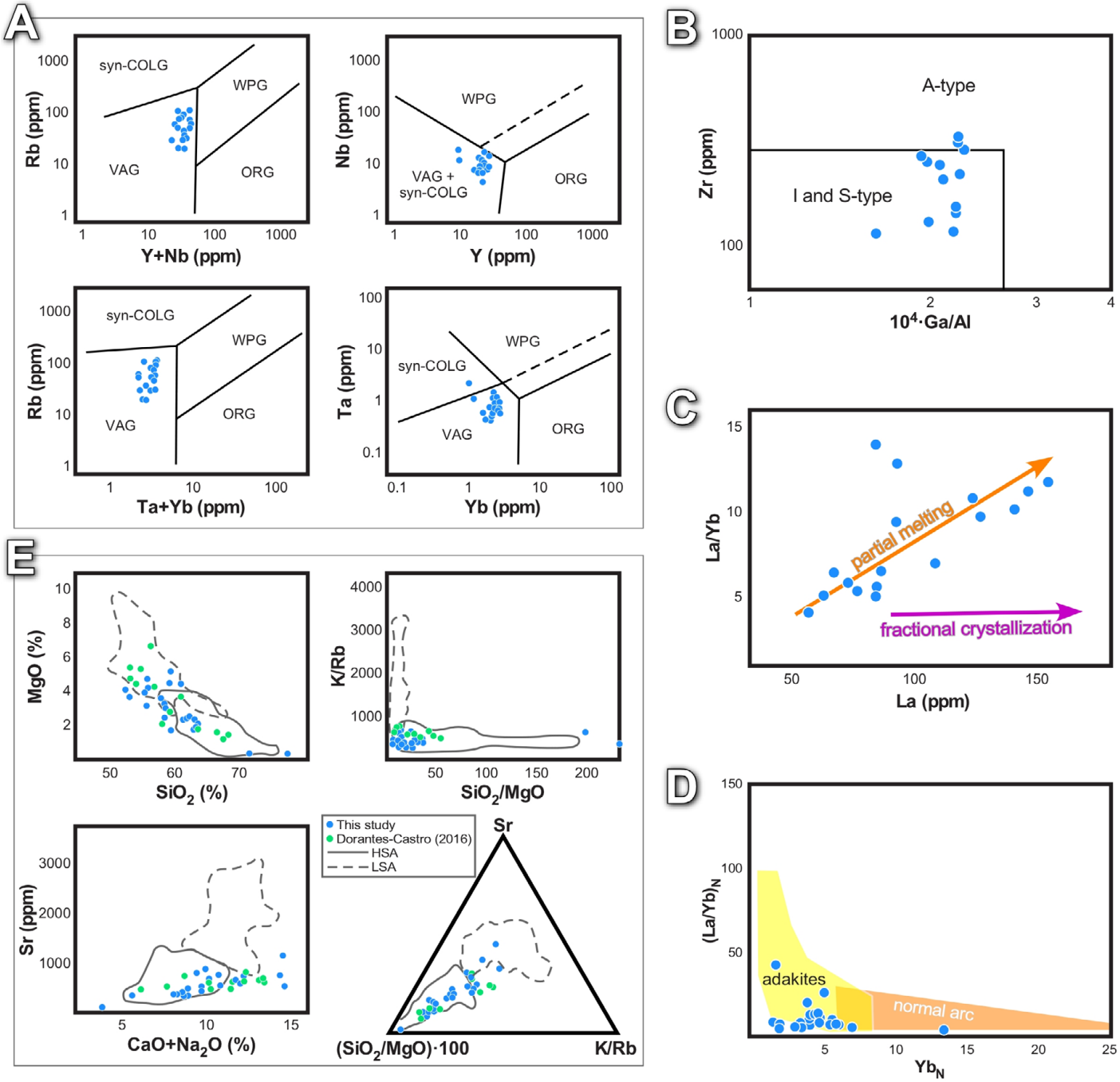

Figure 9 Petrological discrimination diagrams from trace elements in intrusive rocks associated with IOCG skarn mineralization in the Tatatila–Las Minas district, Veracruz. (A) Y+Nb *vs.* Rb, Y *vs.* Nb, Ta+Yb *vs.* Rb, and Yb *vs.* Ta diagrams for discriminating tectonic settings, adapted from Pearce *et al.* (1984). (B) Discrimination diagram for different granite sources, adapted from Whalen *et al.* (1987). (C) Discrimination diagram for the generation of magmas by fractional crystallization *vs.* variable degree of partial melting, adapted from Thirlwall *et al.* (1994). (D) Discrimination diagram for adakitic affinity, adapted from Martin (1986) with chondrite-normalized values Sun and McDonough (1989). (E) Discrimination diagrams for high-silica (HSA) and low-silica adakites (LSA), adapted from Martin and Moyen (2002, 2003) and Martin *et al.* (2005). Key: HSA = high-silica adakites (>60% SiO_2), LSA = low-silica adakites (<60% SiO_2), ORG = ocean ridge granites, VAG = volcanic arc granites, syn-COLG = syn-collision granites, WPG = within plate granites.

http://dx.doi.org/10.18268/BSGM2020v72n3a110520

Table 6. Comparative table between the general geochemical composition of adakites (as of Mori *et al.*, 2007; Richards and Kerrich, 2007) and of intrusive rocks at the Tatatila–Las Minas area.

	"Normal" adakites	Tatatila–Las Minas	
SiO_2 (wt.%)	≥56	~44 to 68	
Al_2O_3 (wt.%)	≥15	~14 to 21	
MgO (wt.%)	~<3	<1 to ~11	Mostly <6.7 wt.%
Na_2O (wt.%)	3.5 to 7.5	~3 to 5	
K_2O/Na_2O	~0.42	0.1 to 1.2	Mostly 0.4 to 0.6
HREE	depleted	depleted	
Sr (ppm)	≥400	~16 to 734	
Y (ppm)	≤18	~3 to 50	Mostly between 20 and 40 ppm
Yb (ppm)	≤1.9	~0 to 16	Mostly <3 ppm
Cr (ppm)	≥30	~2 to 439	9 out of 25 values are ≥30 ppm
Sr/Y	≥20	~7 to 190	
La/Yb	≥20	~5 to 13	
$^{87}Sr/^{86}Sr$	≤0.7045	0.7037 to 0.7059	
εNd	-0.1 to 1.7	-6.6 to 3.2	
εSr		-11.4 to 19.9	

stage of research. As a matter of fact, magmas with either affinity coexisted in the region, as evidenced by the formation of the Tatatila–Las Minas deposits (Negendank *et al.*, 1985; Ferrari *et al.*, 2005a; see also Figure 7 in Camprubí, 2009). Also, the occurrence of A-type granites (alkaline) is hinted at in some of the analyzed samples despite mostly belonging to I- and S-types (Figure 9B), but no affinity with within-plate granites was found (Figure 9A).

In addition, the data in this paper stand for the idea of a metallogeny of the TMVB in its own right, as established by Camprubí (2013). The ages of Miocene IOCG skarn-related magmatism in the Tatatila-Las Minas area (16.34 to 13.92 Ma) fit well within the ~19 to 10 Ma bracket defined by Gómez-Tuena *et al.* (2005, 2007) for the early stages of the TMVB, particularly in its eastern region, in which the adakitic signature of volcanism is conspicuous. Such continental magmatism display geochemical signatures that strongly evoke those of adakites, with the inherent likeliness that it may be associated with melting of the flattened subducted slab (Gómez-Tuena *et al.*, 2005, 2007; Mori *et al.*, 2007). Adakite is the common term that refers to magmas produced by melting of subducted oceanic crust under high pressures and in the presence of water (due to dehydration of the subducted slab). However, other processes for magma generation are possible in the generation of magmas with adakitic geochemical signatures (Defant *et al.*, 2002; Richards and Kerrich, 2007; Rodríguez *et al.*, 2007; Richards, 2011; Ma *et al.*, 2015; Ribeiro *et al.*, 2016; Deng *et al.*, 2017; Keevil *et al.*, 2019). The adakitic signatures at a regional scale in the TMVB are the very high Sr/Y ratios, depletion in Y and HREE, and Sr, Nd and Pb isotopic compositions that approximate to those of mid-ocean ridge basalts in the East Pacific Rise (Gómez-Tuena *et al.*, 2005, 2007; Mori *et al.*, 2007). Nonetheless, adakitic affinities do not necessarily imply that these magmas are derived from the melting of the subducted slab alone, and other geological mechanisms are also plausible for their inception or as relevant contributors to adakitic signatures, as discussed below.

5.3. ORIGIN OF ADAKITIC COMPOSITIONS AND LINKAGE WITH ORE DEPOSITS

The linkage between adakitic magmas and the variety of tectonomagmatic settings that the generation of such magmas entails is suggestive of a significant potential for the formation of associated ore deposits (González-Partida *et al.*, 2003a, 2003b; Chiaradia *et al.*, 2004; Sun *et al.*, 2011;

http://dx.doi.org/10.18268/BSGM2020v72n3a110520

Deng *et al.*, 2017; Keevil *et al.*, 2019). Although the association between "adakites" and ore deposits normally refers to the classic definition of adakite magmas, the generation of such magma through melting of a subducted slab has been questioned (Richards and Kerrich, 2007; Richards, 2011). In the case of Tatatila-Las Minas, however, the intrusive rocks of adakitic-affinity associated with IOCG skarn mineralization have dominantly high-silica compositions (Figure 9E). This denotes that melting of basalt from the subducted slab would have effectively occurred, with subsequent reaction of the resulting melts with peridotites during their ascent through the mantle wedge (Defant and Drummond, 1990; Drummond and Defant, 1990; Martin *et al.*, 2005). Also, the distribution of Nd and Sr isotopic compositions in the Tatatila–Las Minas intrusions point to magma fractionation as per their distribution (Figure 11A). εNd values in the analyzed rocks (between −6.6 and 3.2; Table 3) point to contributions of both relatively isotopically enriched and depleted magma sources for Nd, and represent mantle derived melts that were contaminated by continental crust lithologies, especially when correlated with εSr values (Figure 11D). As already highlighted by Gómez-Tuena *et al.* (2003), Pb isotopic compositions lie between those expected for subducted sediments and MORB (Figure 11B, 11C and Table 3), thus requiring an isotopically depleted source.

An association between adakites and the formation of IOCG skarn deposits was earlier established in Mexico for the late Cretaceous–early Paleocene Mezcala deposits in the Sierra Madre del Sur (Camprubí and González-Partida, 2017, and references therein). The formation of adakites in that locality has been linked to early stages of a subduction-related continental arc (González-Partida *et al.*, 2003b), a feature that is explained by the switch from subduction-related oceanic arcs to continental arcs in southern Mexico during the Late Cretaceous (Camprubí, 2013, 2017). Besides the particular case of Mezcala, in these and the Tatatila-Las Minas deposits the formation of associated adakitic magmas can be explained by slab rollback or flattening subduction as younger portions of the subducted slab were being consumed (Morán-Zenteno *et al.*, 1999; Ferrari and Rosas-Elguera, 1999; Gutscher *et al.*, 2000; Gómez-Tuena *et al.* 2003; Keppie and Morán-Zenteno, 2005). Also, in both regions similar associations of different magmatic-hydrothermal types of deposits (*i.e.*, IOCG, sulfide skarns, metalliferous porphyries, epithermal deposits; Camprubí, 2013, 2017) were produced. Such flattening of the subducted slab has been extensively documented along the entire Western Cordillera of North America and the Andes and explains the historical distribution of metallogenic provinces within them (Camprubí, 2017, and references within).

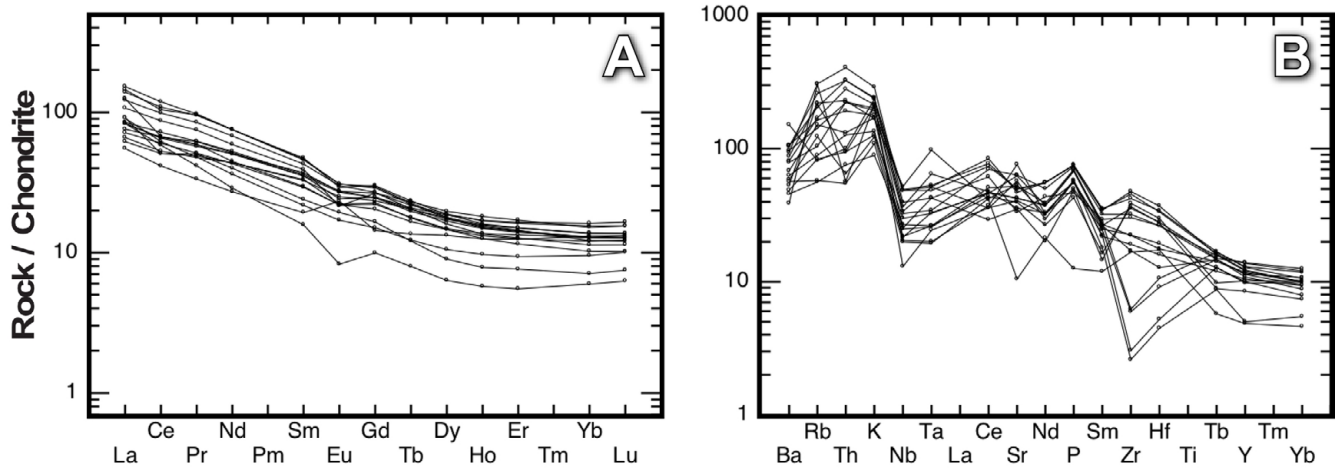

Figure 10 Spider diagrams of REE (A) and trace element contents (B) normalized to chondrite (Sun and McDonough, 1989).

http://dx.doi.org/10.18268/BSGM2020v72n3a110520

However, magmatic processes such as assimilation and fractional crystallization (AFC) or those occurring in melting-assimilation-storage-homogenization (MASH) zones in "normal" continental arc magmas may also account for adakitic compositions of intrusions in association with the subsequent formation of magmatic-hydrothermal ore deposits (Richards and Kerrich, 2007; Richards, 2011; Gatzoubaros *et al.*, 2014; Lohmeier *et al.*, 2019). fact, these processes can generate andesitic to dacitic differentiates with HREE-depleted normalized REE patterns, and high La/Yb and Sr/Y ratios (Feeley and Davison, 1994; Kay *et al.*, 1999; Klepeis *et al.*, 2003; Richards, 2011). However, AFC processes can be virtually ruled out as important contributors to the adakitic signal because Eu anomalies in this case are weak (Figure 10; see Chen *et al.*, 2014). The absence of Eu anomalies would support the model by Richards (2011), as high water contents in typical adakitic rocks are characteristic of MASH zones. MASH interactions may involve partial melts of lower crustal rocks that may imprint high La/Yb and Sr/Y. Such signature is derived from high pressure fractionation in MASH zones with amphibole and garnet, which would produce high La/Yb ratios, and from the suppression of plagioclase fractionation due to high water content in the magmas, thus resulting in high Sr/Y ratios (see references in Richards, 2011). In low $f\ S_2$ and high $f\ O_2$ conditions underneath "normal" continental arcs, MASH processes may induce the formation of IOCG deposits in intra-arc settings (Richards and Mumin, 2013), thus producing an alternative scenario for the association between adakite-like and IOCG deposits. With regard to slab flattening underneath a continental arc due to steep subduction, Richards and Mumin (2013) argued about scarce to nil associated magmatic activity or the migration of magmatism toward back-arc settings. Interestingly, slab flattening would cause the dehydration of the slab and the subsequent hydration of the lithosphere, which would be too cold to melt. However, once the slab re-steepened, the temperature of the hydrated lithosphere would rise in contact with the asthenosphere, generating the partial melting of sub-continental mantle and subsequent vigorous volcanic flare-ups, thus reactivating the formation of magmatic-hydrothermal ore deposits—among them, IOCG deposits (see Figure 1 in Richards and Mumin, 2013). The formation of adakites in such specific settings and in association with magmatic-hydrothermal ore deposits has not been reported. However, the involvement of MASH-type processes in metallogeny has actually been invoked in the formation of continental-arc related magmatic-hydrothermal ore deposits nonetheless (Sun *et al.*, 2011). The possibility of magma generation by MASH-type processes that followed re-steepening of the subducted slab with which the formation of IOCG deposits would be linked is particularly significant for the Tatatila–Las Minas case. Indeed, the formation of these deposits occurred during the late Miocene, once the subducted slab underneath the Trans-Mexican Volcanic Belt, in fact, re-steepened (see Figure 13 in Gómez-Tuena *et al.*, 2003).

In summary, the most likely settings for the formation of parental adakitic magmas to the IOCG skarn deposits at Tatatila–Las Minas would be (1) a "normal adakitic" slab-melt setting with some crustal contamination, or (2) MASH-related adakitic compositions. However, these settings do not necessarily have to be considered as mutually exclusive in the generation of adakites with associated magmatic-hydrothermal ore deposits (Chen *et al.*, 2014; Sun *et al.*, 2018). To our reckoning, these settings cannot be effectively discriminated given the current wealth of data from the Tatatila–Las Minas district. In addition, it is possible that TMVB calc-alkaline and EMAP alkaline magmas underwent some kind of interaction that produced the intrusive bodies with which the studied IOCG skarn deposits are associated. Interestingly, despite the common tectonomagmatic affinity of all the Cenozoic magmatic rocks, the only samples that show high Y and Yb contents are those whose ages correspond entirely to the initial stages of the TMVB (not those older than 19 Ma). This, again, stands for different magmatic processes—albeit slightly—between TMVB and pre-TMVB rocks.

http://dx.doi.org/10.18268/BSGM2020v72n3a110520

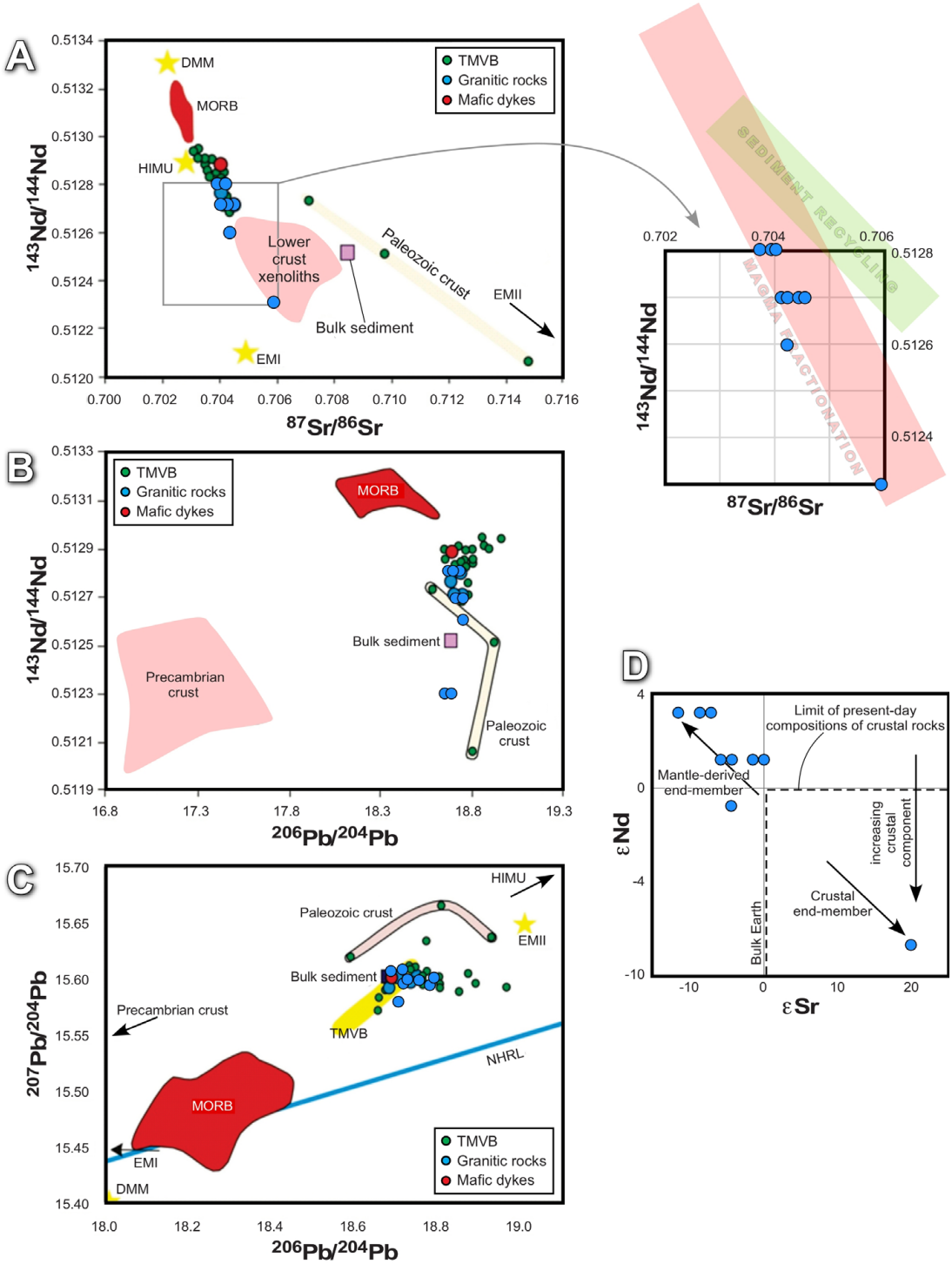

Figure 11 Isotope variation diagrams for the Tatatila–Las Minas Miocene intrusive bodies associated with IOCG skarn mineralization. (A) Sr-Nd isotopes variation diagram. (B) Pb-Nd isotopes variation diagram. (C) Pb isotopes variation diagram. (D) εNd vs. εSr diagram that illustrates possible end-member sources for magmas, after DePaolo and Wasserburg (1979a, 1979b). Key = DMM = depleted MORB-mantle, EMI = enriched mantle I, EMII = enriched mantle II, HIMU = mantle component, MORB = 5°-15° NE Pacific Rise mid-ocean ridge basalts, NHRL = northern hemisphere reference line, TMVB = current volcanic front of the Trans-Mexican Volcanic Belt. See sources for all reference values in Gómez-Tuena *et al.* (2003), which is also the source of values represented as green dots in diagrams A to C that correspond to volcanic rocks from the Palma Sola area in the eastern TMVB. The magmatic fractionation and sediment recycling trends in the zoomed view of A are simplified after Hoffman and White (1982).

http://dx.doi.org/10.18268/BSGM2020v72n3a110520

6. Conclusions

The iron oxide-Cu-Au deposits at the Tatatila–Las Minas district (central Veracruz) are skarn-related deposits that belong to the IOCG family, and associated Au-rich epithermal deposits also occur in the area. U-Pb and $^{40}Ar/^{39}Ar$ dating of these IOCG skarns yielded early to middle Miocene ages for prograde (16.34 to 13.92 Ma for the associated intrusive bodies) and retrograde (12.44 to 12.18 Ma for hydrothermal minerals) associations. Such ages and the geochemical affinity of host intrusive rocks (calc-alkaline to adakitic) that are directly involved in the formation of IOCG skarns match well with those previously established for the early stages of evolution of the Trans-Mexican Volcanic Belt (TMVB). A set of pre-TMVB Cenozoic rocks has been also dated between ~24.6 and 19 Ma.

The multi-elemental and isotopic geochemical study of IOCG skarn-related intrusive rocks determined that these are intermediate to acid, metaluminous, I- and S-type, medium- to high-potassium, typical calc-alkaline to adakitic rocks that are compatible with those expected for a continental volcanic arc such as the TMVB. Therefore, the studied deposits are likely to be ascribed to the metallogeny of the TMVB, which can be rightfully spoken of as an actual metallogenic province. Such a fact broadens the economic expectations of a province that has traditionally been overlooked by mineral exploration.

The prominent adakitic signal as found in the IOCG skarn-generating intrusive rocks has been regionally attributed to adakitic melts associated with flat subduction and the subsequent resteepening of the subducted slab—with independent

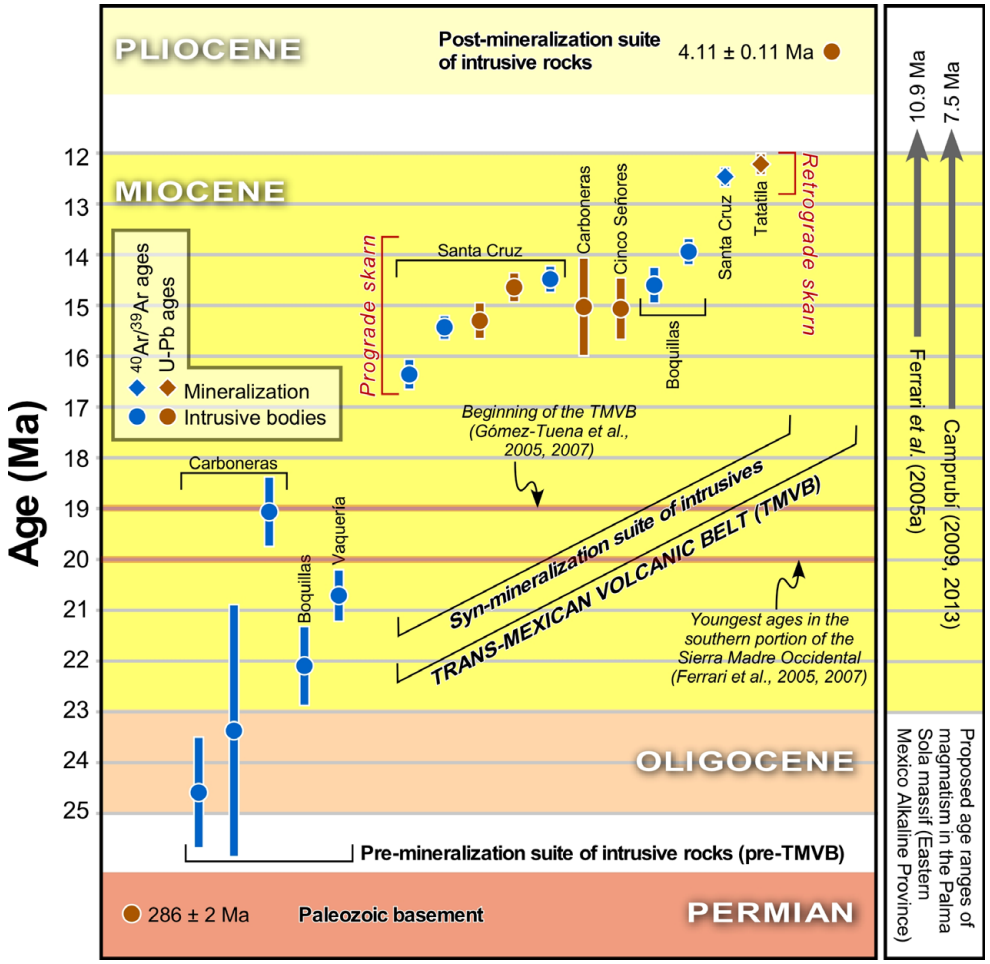

Figure 12 Summary of the U-Pb and $^{39}Ar/^{40}Ar$ ages obtained in this study for the intrusive rocks and IOCG skarn mineralization at the Tatatila–Las Minas area, Veracruz.

http://dx.doi.org/10.18268/BSGM2020v72n3a110520

evidence for crustal contamination. The results in this paper concur with such an interpretation. The general geochemical characteristics of these rocks, however, do not rule out the possibility that melting-assimilation-storage-homogenization (MASH) processes were involved in the generation of parental magmas. There are also hints that these magmas interacted with alkaline melts, which would likely be associated with the nearly contemporaneous EMAP. Only TMVB rocks display Y and Yb contents that would suggest such interaction—all other petrologic indicators suggest common characteristics for TMVB and pre-TMVB Cenozoic rocks. In both a adakitic and MASH scenarios, the most plausible stage at which the formation of IOCG skarn-associated magmas occurred would be once the flattened subducted slab re-steepened, thus allowing melting of either (or both) slab material or the hydrated lower lithosphere.

Acknowledgements

This paper constitutes a part of the dissertations of E.F.G. and G.H.A., who acknowledge the support of CONACyT through PhD and MSc grants, respectively. The Instituto de Geología UNAM is acknowledged for authorizing E.F.G. to carry on her PhD research along with her academic duties. Funding for this work was provided by CONACyT through the research grants 155662 to A.C. and "*GEMex: Cooperación México-Europa para la investigación de sistemas geotérmicos mejorados y sistemas geotérmicos supercalientes*" (within the 4.1 and 8.2 research sections: *Determinación de propiedades petrológicas, de alteración hidrotermal, microtermométricas, geoquímicas, de isótopos estables y geocronológicos de afloramientos basamentales de áreas aledañas a Los Humeros y Acoculco, Pue.*" to GEOMINCO S.A. de C.V. Additional funding was provided by the Instituto de Geología UNAM and the Centro de Geociencias UNAM through personal allocations. The radiogenic isotope determinations were carried out at the Centro de Geociencias UNAM with the assistance of Ofelia Pérez Arvizu and Carlos Ortega Obregón. The thin sections were elaborated by Juan Tomás Vázquez Ramírez of the Centro de Geociencias UNAM. FRX determinations were carried out at the Laboratorio Nacional de Geoquímica y Mineralogía–Instituto de Geología UNAM with the assistance of Rufino Lozano Santacruz. The separation of zircon crystals was carried out with the assistance of Teodoro Hernández Treviño of the Instituto de Geofísica UNAM. Assistance during field work was provided by Jesús Castro and Dunia Figueroa. Also, Figure 1 was drawn with the assistance of Rodrigo Delgado Sánchez. The authors are also grateful to Carl Nelson, Lisard Torró and Joaquín Proenza, the guest editors of the present special issue, and to three anonymous referees, whose comments helped to significantly improve this manuscript.

References

Besch, T., Negendank, J., Emmermann, R., 1988, Geochemical constraints on the origin of the calc-alkaline and alkaline magmas of the eastern Trans-Mexican Volcanic Belt: Geofísica Internacional, 27, 641–663.

Birck, J. L.,1986, Precision K-Rb-Sr isotopic analysis: application to Rb-Sr chronology: Chemical geology, 56(1-2), 73-83. https://doi.org/10.1016/0009-2541(86)90111-7

Camprubí, A., 2009, Major metallogenic provinces and epochs of Mexico: SGA News, 25, 1-21. https://e-sga.org/fileadmin/sga/newsletter/news25/SGANews25.pdf

Camprubí, A., 2013, Tectonic and metallogenic history of Mexico, in Colpron, M., Bissig, T., Rusk, B.G., Thompson, J.F.H., (eds.), Tectonics, metallogeny, and discovery: the North American Cordillera and similar accretionary settings: Littleton, Colorado, USA, Society of Economic Geologists. Society of Economic Geologists Special Publication, 17, 201-243. https://doi.org/10.5382/SP.17.06

Camprubí, A., 2017, The metallogenic evolution in Mexico during the Mesozoic, and its

bearing in the Cordillera of Western North America. Ore Geology Reviews, 81, 1193-1214. https://doi.org/10.1016/j.oregeorev.2015.11.007

Camprubí, A., González-Partida, E., 2017, Mesozoic magmatic-hydrothermal iron oxide deposits (IOCG 'clan') in Mexico: Ore Geology Reviews, 81, 1084-1095. https://doi.org/10.1016/j.oregeorev.2015.11.025

Camprubí, A., González-Partida, E., Valencia, V.A., Barra, F., 2015, Geochronology of Mexican mineral deposits. I: the San Martín polymetallic skarn, Zacatecas: Boletín de la Sociedad Geológica Mexicana, 67, 119-122. http://dx.doi.org/10.18268/BSGM2015v67n1a10

Camprubí, A., Albinson, T., Iriondo, A., 2016a, Geochronology of Mexican mineral deposits. V: the Peñón Blanco epithermal deposit, Durango: Boletín de la Sociedad Geológica Mexicana, 68, 365-370. http://dx.doi.org/10.18268/BSGM2016v68n2a13

Camprubí, A., Iriondo, A., Martínez-López, M., Ramos-Rosique, A., 2016b, Geochronology of Mexican mineral deposits. IV: the Cinco Minas epithermal deposit, Jalisco: Boletín de la Sociedad Geológica Mexicana, 68, 357-364. http://dx.doi.org/10.18268/BSGM2016v68n2a12

Camprubí, A., González-Partida, E., Alfonso, P., López-Martínez, M., Iriondo, A., Cienfuegos-Alvarado, E., Gutiérrez-Armendáriz, E., Morales-Puente, P., Canet, C., González-Ruiz, L., 2017, The Late Cretaceous Guaynopa IOCG and Guaynopita porphyry copper deposits, Chihuahua, Mexico. Ore Geology Reviews, 81, 1096-1112. https://doi.org/10.1016/j.oregeorev.2016.01.006

Camprubí, A., Centeno-García, E., Tolson, G., Iriondo, A., Ortega, B., Bolaños, D., Abdullin, F., Portugal-Reyna, J.L., Ramos-Arias, M.A., 2018, Geochronology of Mexican mineral deposits. VII: the Peña Colorada magmatic-hydrothermal iron oxide deposit (IOCG "clan"), Colima: Boletín de la Sociedad Geológica Mexicana, 70, 633-674. http://dx.doi.org/10.18268/BSGM2018v70n3a4

Camprubí, A., Cabrera-Roa, M.A., González-Partida, E., Martínez-López, M., 2019, Geochronology of Mexican mineral deposits. VIII: the Zacatepec polymetallic skarn, Oaxaca: Boletín de la Sociedad Geológica Mexicana, 71, 207-218. http://dx.doi.org/10.18268/BSGM2019v71n1a11

Camprubí, A., Fuentes-Guzmán, E., Gabites, J., Ortega-Larrocea, P., Colín-García, M., González-Partida, E., 2020, The Pliocene Ixtacamaxtitlán low sulfidation epithermal deposit (Puebla, Mexico): A case of fossil fungi consortia in a steam-heated environment: Boletín de la Sociedad Geológica Mexicana, 72(3), A140420. http://dx.doi.org/10.18268/BSGM2020v72n3a140420

Cantagrel, J.M., Robin, C., 1979, K–Ar dating on eastern Mexican volcanic rocks—relations between the andesitic and the alkaline provinces: Journal of Volcanology and Geothermal Research, 5, 99-114. https://doi.org/10.1016/0377-0273(79)90035-0

Carrasco-Nuñez, G., Bernal, J.P., Dávila, P., Jicha, B., Giordano, G., Hernández, J., 2018. Reappraisal of Los Humeros volcanic complex by new U/Th zircon and $^{40}Ar/^{39}Ar$ dating: Implications for greater geothermal potential: Geochemistry, Geophysics, Geosystems, 19, 132-149. https://doi.org/10.1002/2017GC007044

Castro-Mora, J., Hernández-Pérez, I., Vélez-López, J., Baca-Carreón, J. C., 1994, Monografía Geológico-Minera del estado de Veracruz: Pachuca, Hidalgo, Consejo de Recursos Minerales.

Castro-Mora, J., Ortíz-Hernández, L.E., Escamilla-Casas, J.C., Cruz-Chávez, E., Dorantes-Castro, C.G., 2016, Metalogénesis de la mineralización tipo IOCG relacionada al skarn del Distrito Minero Las Minas, Estado de Veracruz: Tópicos de Investigación en Ciencias de la Tierra y Materiales, 3, 128-143.

http://dx.doi.org/10.18268/BSGM2020v72n3a110520

Centeno-García, E., 2017, Mesozoic tectono-magmatic evolution of Mexico: An overview: Ore Geology Reviews, 81, 1035-1052. https://doi.org/10.1016/j.oregeorev.2016.10.010

Chen, J.-L., Xu, J.-F., Ren, J.-B., Huang, X.-X., Wang, B.-D., 2014, Geochronology and geochemical characteristics of Late Triassic porphyritic rocks from the Zhongdian arc, eastern Tibet, and their tectonic and metallogenic implications: Gondwana Research, 26, 492-504. https://doi.org/10.1016/j.gr.2013.07.022

Chiaradia, M., Fontboté, L., Beate, B., 2004, Cenozoic continental arc magmatism and associated mineralization in Ecuador: Mineralium Deposita, 39, 204-222. https://doi.org/10.1007/s00126-003-0397-5

Clark, K.F., Fitch, D.C., 2009, Evolución de depósitos metálicos en tiempo y espacio en Mexico, *in* Clark, K.F., Salas-Pizá, G., Cubillas-Estrada, R., eds., Geología Económica de México, II Edición: Pachuca, Hidalgo, Servicio Geológico Mexicano, 62-133.

Cox, K.G., Bell, J.D., Pankhurst, R.J., 1979, The interpretation of igneous rocks: Boston, USA, George Allen and Unwin, 459 p.

Defant, M.J., Drummond, M.S., 1990, Derivation of some modern arc magmas by melting of young subducted lithosphere: Nature, 347, 662-665. https://doi.org/10.1038/347662a0

Defant, M.J., Xu, J.F., Kepezhinskas, P., Wang, Q., Zhang, Q., Xiao, L., 2002, Adakites: Some variations on a theme: Acta Petrologica Sinica, 18, 129-142.

Demant, A., and Robin, C., 1975, Las fases del volcanismo en Mexico; una sintesis en relacion con la evolucion geodinamica desde el Cretacico: Revista - Instituto de Geologia UNAM, Mexico, D.F., Mexico, v. I, p. 70-82.

Deng, J., Wang, Q., Li, G., 2017, Tectonic evolution, superimposed orogeny, and composite metallogenic system in China: Gondwana Research, 50, 216-266. https://doi.org/10.1016/j.gr.2017.02.005

DePaolo, D.J., Wasserburg, G.J., 1979a, Petrogenetic mixing models and Nd-Sr isotopic patterns: Geochimica et Cosmochimica Acta, 43, 615-627. https://doi.org/10.1016/0016-7037(79)90169-8

DePaolo, D.J., Wasserburg, G.J., 1979b, Sm-Nd age of the Stillwater complex and the mantle evolution curve for neodymium: Geochimica et Cosmochimica Acta, 43, 999-1008. https://doi.org/10.1016/0016-7037(79)90089-9

Dorantes-Castro, C.G., 2016, Características petrológicas y geoquímicas de los intrusivos relacionados a la mineralización y paragénesis del skarn tipo IOCG en la zona minera de Las Minas, estado de Veracruz: Instituto Politécnico Nacional, unpublished BSc thesis, 120 p.

Drummond, M.S., Defant, M.J., 1990, A model for trondhjemite–tonalite–dacite genesis and crustal growth via slab melting: Archaean to modern comparisons: Journal of Geophysical Research, 95, 21503-21521. https://doi.org/10.1029/JB095iB13p21503

Enríquez, E., Iriondo, A., Camprubí, A., 2018, Geochronology of Mexican mineral deposits. VI: the Tayoltita low-sulfidation epithermal district, Durango and Sinaloa: Boletín de la Sociedad Geológica Mexicana, 70, 531-547. http://dx.doi.org/10.18268/BSGM2018v70n2a13

Farfán-Panamá, J.L., Camprubí, A., González-Partida, E., Iriondo, A., González-Torres, E.A., 2015, Geochronology of Mexican mineral deposits. III: the Taxco epithermal deposit, Guerrero: Boletín de la Sociedad Geológica Mexicana, 67, 357-366. http://dx.doi.org/10.18268/BSGM2015v67n2a16

Feeley, T.C., Davidson, J.P., 1994, Petrology of calc-alkaline lavas at Volcán Ollagüe and the origin of compositional diversity at Central Andean stratovolcanoes: Journal of Petrology, 35, 1295-1340. https://doi.org/10.1093/petrology/35.5.1295

Ferrari, L., Rosas-Elguera, J., 1999, Late Miocene to Quaternary extension at the northern

boundary of the Jalisco block, western Mexico: the Tepic-Zacoalco rift revised, in Delgado-Granados, H., Stock, J., Aguirre-Díaz, G.J. (eds.), Cenozoic tectonics and volcanism of Mexico. Geological Society of America Special Paper, 334, 42-64. https://doi.org/10.1130/0-8137-2334-5.41

Ferrari, L., Tagami, T., Eguchi, M., Orozco-Esquivel, M.T., Petrone, C.M., Jacobo-Albarrán, J., López-Martínez, M., 2005a, Geology, geochronology and tectonic setting of late Cenozoic volcanism along the southwestern Gulf of Mexico: The Eastern Alkaline Province revisited: Journal of Volcanology and Geothermal Research, 146, 284-306. https://doi.org/10.1016/j.jvolgeores.2005.02.004

Ferrari, L., Valencia-Moreno, M., Bryan, S., 2005b, Magmatismo y tectónica en la Sierra Madre Occidental y su relación con la evolución de la margen occidental de Norteamérica: Boletín de la Sociedad Geológica Mexicana, 57, 343-378. http://dx.doi.org/10.18268/BSGM2005v57n3a5

Ferrari, L., Valencia-Moreno, M., Bryan, S., 2007, Magmatism and tectonics of the Sierra Madre Occidental and its relation with the evolution of the western margin of North America, in Alaniz-Álvarez, S.A., Nieto-Samaniego, Á.F. (eds.), Geology of México: Celebrating the Centenary of the Geological Society of México: Geological Society of America Special Paper, 422, 1-39. https://doi.org/10.1130/2007.2422(01)

Fitz-Díaz, E., Lawton, T.F., Juárez-Arriaga, E., Chávez-Cabello, G., 2018, The Cretaceous-Paleogene Mexican orogen: Structure, basin development, magmatism and tectonics: Earth-Science Reviews, 183, 56-84. https://doi.org/10.1016/j.earscirev.2017.03.002

Frost, B.R., Barnes, C.G., Collins, W.J., Arculus, R.J., Ellis, D.J., Frost, C.D., 2001, A geochemical classification for granitic rocks: Journal of Petrology, 42 (11), 2033-2048. https://doi.org/10.1093/petrology/42.11.2033

Fuentes-Guzmán, E., Camprubí, A., Gabites, J., González-Partida, E., 2020, The Pliocene Xoconostle high sulfidation epithermal deposit in the Trans-Mexican Volcanic Belt:Preliminary study: Boletín de la Sociedad Geológica Mexicana, 72(3), A260520. http://dx.doi.org/10.18268/BSGM2020v72n3a260520

Gatzoubaros, M., von Quadt, A., Gallhofer, D., Rey, R., 2014, Magmatic evolution of pre-ore volcanics and porphyry intrusives associated with the Altar Cu-porphyry prospect, Argentina: Journal of South American Earth Sciences, 55, 58-82. https://doi.org/10.1016/j.jsames.2014.06.005

Gómez-Tuena, A., La Gatta, A., Langmuir, C., Goldstein, S., Ortega-Gutiérrez, F., Carrasco-Núñez, G., 2003, Temporal control of subduction magmatism in the Eastern Trans-Mexican Volcanic Belt: mantle sources, slab contributions and crustal contamination: Geochemistry, Geophysics, Geosystems, 4 (8), 8912. https://doi.org/10.1029/2003GC000524

Gómez-Tuena, A., Orozco-Esquivel, M.T., Ferrari, L., 2005, Petrogénesis ígnea de la Faja Volcánica Transmexicana: Boletín de la Sociedad Geológica Mexicana, 57, 227-283. http://dx.doi.org/10.18268/BSGM2005v57n3a2

Gómez-Tuena, A., Orozco-Esquivel, M.T., Ferrari, L., 2007, Igneous petrogenesis of the Trans-Mexican Volcanic Belt, in Alaniz-Álvarez, S.A., Nieto-Samaniego, Á.F., eds., Geology of México: Celebrating the centenary of the Geological Society of México: Boulder, Colorado, USA, The Geological Society of America. Geological Society of America Special Paper, 422, 129-182. https://doi.org/10.1130/2007.2422(05)

González-Jiménez, J.M., Camprubí, A., Colás, V., Griffin, W.L., Proenza, J.A., Belousova, E., Centeno-García E., O'Reilly, S.Y., Talavera, C., Farré-de-Pablo, J., Satsukawa, T., 2017a, The recycling of chromitites in ophiolites

from southwestern North America: Lithos, 294-295, 53-72. https://doi.org/10.1016/j.lithos.2017.09.020

González-Jiménez, J.M., Proenza, J.A., Martini, M., Camprubí, A., Griffin, W.L., O'Reilly, S.Y., Pearson, N.J., 2017b, Deposits associated with ultramafic-mafic complexes in Mexico: the Loma Baya case: Ore Geology Reviews, 81, 1053-1065. https://doi.org/10.1016/j.oregeorev.2015.05.014

González-León, C.M., Solari, L., Valencia-Moreno, M., Rascon Heimpel, M.A., Solé, J., González Becuar, E., Lozano Santacruz, R., Pérez Arvizu, O., 2017, Late Cretaceous to early Eocene magmatic evolution of the Laramide arc in the Nacozari quadrangle, northeastern Sonora, Mexico and its regional implications: Ore Geology Reviews, 81, 1137-1157. https://doi.org/10.1016/j.oregeorev.2016.07.020

González-Partida, E., Levresse, G., Carrillo-Chávez, A., Cheilletz, A., Gasquet, D., Jones, D., 2003a, Paleocene adakite Au-Fe bearing rocks, Mezcala, Mexico: Evidence from geochemical characteristics: Journal of Geochemical Exploration, 80, 25-40. https://doi.org/10.1016/S0375-6742(03)00180-8

González-Partida, E., Levresse, G., Carrillo-Chávez, A., Cheilletz, A., Gasquet, D., Solorio-Munguía, J., 2003b, (Au-Fe) skarn deposits of the Mezcala district, South-Central Mexico: Adakite association of the mineralizing fluids: International Geology Review, 45, 79-93. https://doi.org/10.2747/0020-6814.45.1.79

Gutscher, M.A., Maury, R., Eissen, J.P., Bourdon, E., 2000, Can slab melting be caused by flat subduction?: Geology, 28 (6), 535-538. https://doi.org/10.1130/0091-7613(2000)28<535:CSMBCB>2.0.CO;2

Hoffman, A.W., White, W.M., 1982, Mantle plumes from ancient oceanic crust: Earth and Planetary Science Letters, 57, 421-436. https://doi.org/10.1016/0012-821X(82)90161-3

Iriondo, A., Kunk, M.J., Winick, J.A., CRM, 2003, $^{40}Ar/^{39}Ar$ dating studies of minerals and rocks in various areas in Mexico: USGS/CRM Scientific Collaboration: Part I: USGS Open File Report 03-020, online edition, 79 p. https://doi.org/10.3133/ofr0320

Irvine, T., Baragar, W., 1971, A guide to the chemical classification of the common volcanic rocks: Canadian Journal of Earth Sciences, 8, 523-548. https://doi.org/10.1139/e71-055

Jansen, N.H., Gemmell, J.B., Chang, Z., Cooke, D.R., Jourdan, F., Creaser, R.A., Hollings, P., 2017, Geology and genesis of the Cerro la Mina porphyry-high sulfidation Au (Cu-Mo) prospect, Mexico: Economic Geology, 112, 799-827. http://dx.doi.org/10.2113/econgeo.112.4.799

Kay, S.M., Mpodozis, C., Coira, B., 1999, Neogene magmatism, tectonism, and mineral deposits of the Central Andes (22° to 33°S latitude): Society of Economic Geologists, Special Publication, 7, 27-59. https://doi.org/10.5382/SP.07.02

Keevil, H.A., Monecke, T., Goldfarb, R.J., Möller, A., Kelly, N.M., 2019, Geochronology and geochemistry of Mesozoic igneous rocks of the Hunjiang basin, Jilin Province, NE China: Constraints on regional tectonic processes and lithospheric delamination of the eastern North China block: Gondwana Research, 68, 127-157. https://doi.org/10.1016/j.gr.2018.11.010

Keppie, J.D., Morán-Zenteno, D.J., 2005, Tectonic implications of alternative Cenozoic reconstructions for southern Mexico and the Chortis Block: International Geology Review, 47, 473-491. https://doi.org/10.2747/0020-6814.47.5.473

Kirsch, M, Keppie, J.D., Murphy, J.B., Solari, L., 2012, Permian–Carboniferous arc magmatism basin evolution along the western margin of Pangea: geochemical and geochronological evidence from the eastern Acatlán Complex, southern Mexico: Geological Society of America Bulletin, 124, 1607-1628. https://doi.org/10.1130/B30649.1

Klepeis, K.A., Clarke, G.L., Rushmer, T., 2003, Magma transport and coupling between deformation and magmatism in the continental lithosphere: GSA Today, 13, 4-11. https://www.geosociety.org/gsatoday/archive/13/1/pdf/i1052-5173-13-1-4.pdf

Kuiper, K.F., Deino, A., Hilgen, F.J., Krijgsman, W., Renne, P.R., Wijbrans, J.R., 2008, Synchronizing rock clocks of Earth history: Science, 320, 500-504. https://doi.org/10.1126/science.1154339

Liu, D., Zhao, Z., DePaolo, D.J., Zhu, D.-C., Meng, F.-Y., Shi, Q., Wang, Q., 2017, Potassic volcanic rocks and adakitic intrusions in southern Tibet: Insights into mantle–crust interaction and mass transfer from Indian plate: Lithos, 268-271, 48-64. https://doi.org/10.1016/j.lithos.2016.10.034

Lohmeier, S., Schneider, A., Belyatsky, B., Lehmann, B., 2019, Magmatic evolution of the Cerro Maricunga gold porphyry-epithermal system, Maricunga belt, N-Chile: Journal of South American Earth Sciences, 92, 374-399. https://doi.org/10.1016/j.jsames.2019.03.003

Lozano-Santa Cruz, R., Verma, S.P., Girón, P., Velasco-Tapia, F., Morán-Zenteno, D.J., Viera, F., Chávez, G., 1995, Calibración preliminar de fluorescencia de rayos X para análisis cuantitativo de elementos mayores en rocas ígneas: Actas INAGEQ, 1, 203-208.

López-Infanzón, M., 1991, Petrologic study of volcanic rocks from the Chiconquiaco–Palma Sola area, Central Veracruz, Mexico: unpublished MSc thesis, Tulane University, New Orleans, Louisiana, USA, 140 p.

Lu, Y.-J., Kerrich, R., Mccuaig, T.C., Li, Z.-X., Hart, C.J.R., Cawood, P.A., Hou, Z.-Q., Bagas, L., Cliff, J., Belousova, E.A., Tang, S.-H., 2013, Geochemical, Sr-Nd-Pb, and zircon Hf-O isotopic compositions of eocene-oligocene shoshonitic and potassic adakite-like felsic intrusions in western Yunnan, SW China: Petrogenesis and tectonic implications: Journal of Petrology, 54, 1309-1348. https://doi.org/10.1093/petrology/egt013

Ludwig, K.R., 2003, ISOPLOT, a geochronological toolkit for Microsoft Excel, Version 3.00: Berkeley Geochronology Center Special Publication, 4, 70 p.

Macpherson, C.G., Dreher, S.T., Thirlwall, M.F., 2006, Adakites without slab melting: High pressure differentiation of island arc magma, Mindanao, the Philippines: Earth and Planetary Science Letters, 243, 581-593. https://doi.org/10.1016/j.epsl.2005.12.034

Ma, Q., Zheng, J.P., Xu, Y.-G., Griffin, W.L., Zhang, R.-S., 2015, Are continental "adakites" derived from thickened or foundered lower crust?: Earth and Planetary Science Letters, 419, 125-133. https://doi.org/10.1016/j.epsl.2015.02.036

Martin, H., 1986, Effect of steeper Archaean geothermal gradient on geochemistry of subduction zone magmas: Geology, 14, 753-756. https://doi.org/10.1130/0091-7613(1986)14<753:EOSAGG>2.0.CO;2

Martin, H., Moyen, J.-F., 2002, Secular changes in TTG composition as markers of the progressive cooling of the Earth: Geology, 30 (4), 319-322. https://doi.org/10.1130/0091-7613(2002)030<0319:SCITTG>2.0.CO;2

Martin, H., Moyen, J.-F., 2003, Secular changes in TTG composition: comparison with modern adakites: EGS-AGU-EUG Joint Meeting, Nice, April, VGP7-1FR2O–001, abstract 2673. http://adsabs.harvard.edu/abs/2003EAEJA.....2673M

Martin, H., Smithies, R.H., Rapp, R., Moyen, J.-F., Champion, D., 2005, An overview of adakite, tonalite–trondhjemite–granodiorite (TTG), and sanukitoid: relationships and some implications for crustal evolution: Lithos, 79 (1-2), 1-24. https://doi.org/10.1016/j.lithos.2004.04.048

Martínez-Reyes, J.J., Camprubí, A., Uysal, I.T., Iriondo, A., González-Partida, E., 2015,

Geochronology of Mexican mineral deposits. II: Veta Madre and Sierra epithermal vein systems, Guanajuato district: Boletín de la Sociedad Geológica Mexicana, 67, 349-355. http://dx.doi.org/10.18268/BSGM2015v67n2a15

Martini, M., Ortega-Gutiérrez, F., 2018, Tectono-stratigraphic evolution of eastern Mexico during the break-up of Pangea: A review: Earth-Science Reviews, 183, 38-55. https://doi.org/10.1016/j.earscirev.2016.06.013

Masliwec, A., 1984, Applicability of the $^{40}Ar/^{39}Ar$ method to the dating of ore bodies: Unpublished PhD Dissertation. University of Toronto, Toronto, Ontario, Canada.

Meinert, L.D., 1995, Compositional variations of igneous rocks associated with skarn deposits chemical evidence for genetic connections between petrogenesis and mineralization, in Thompson, J.F.H. (ed.), Magmas, Fluids, and Ore Deposits: Mineralogical Association of Canada, Short Course Series, 23, 401-419.

Morán-Zenteno, D.J., Tolson, G., Martínez-Serrano, R.G., Martiny, B., Schaaf, P., Silva-Romo, G., Macías-Romo, C., Alba-Aldave, L., Hernández-Bernal, M.S., Solís-Pichardo, G.N., 1999, Tertiary arc-magmatism of the Sierra Madre del Sur, Mexico, and its transition to the volcanic activity of the Trans-Mexican Volcanic Belt: Journal of South American Earth Sciences, 12, 513-535. https://doi.org/10.1016/S0895-9811(99)00036-X

Mori, L., Gómez-Tuena, A., Cai, Y., Goldstein, S., 2007, Effects of prolonged flat subduction on the Miocene magmatic record of the central Trans-Mexican Volcanic Belt: Chemical Geology, 244, 452-473. https://doi.org/10.1016/j.chemgeo.2007.07.002

Murillo-Muñetón, G., Torres-Vargas, R., 1987, Mapa petrogenético y radiométrico de la República Mexicana: Mexico City, Instituto Mexicano del Petróleo, Subdirección de Tecnología de Exploración, informe del proyecto C-2010, 78 p.

Negendank, J.F.W., Emmermann, R., Krawczyk, R., Mooser, F., Tobschall, H., Werle, D., 1985, Geological and geochemical investigations on the eastern Trans Mexican Volcanic Belt: Geofísica Internacional, 24, 477-575.

Ortega-Obregón, C., Solari, L., Gómez-Tuena, A., Elías-Herrera, M., Ortega-Gutiérrez, F., Macías-Romo, C., 2013, Permian-Carboniferous arc magmatism in southern Mexico: U-Pb dating, trace element and Hf isotopic evidence on zircons of earliest subduction beneath the western margin of Gondwana: International Journal of Earth Sciences, 103, 1287-1300. https://doi.org/0.1007/s00531-013-0933-1.

Ortuño-Arzate, S., Ferket, H., Cacas, M.-C., Swennen, R., Roure, F., 2005, Late Cretaceous carbonate reservoirs in the Cordoba platform and Veracruz basin, eastern Mexico, in Bartolini, C., Buffler, R.T., Blickwede, J.F. (eds.), The circum-Gulf of Mexico and the Caribbean: Hydrocarbon habitats, basin formation and plate tectonics: AAPG Memoir, 79, 87-92. https://doi.org/10.1306/M79877C22

Orozco-Esquivel, M., Petrone, C., Ferrari, L., Tagami, T., Manetti, P., 2007, Geochemical and isotopic variability controlled by slab detachment in a subduction zone with varying dip: The eastern Trans-Mexican Volcanic Belt: Lithos, 93(1–2),149–174. https://doi.org/10.1016/j.lithos.2006.06.006

Pearce, J.A., Harris, N.B.W., Tindle, A.G., 1984, Trace element discrimination diagrams for the tectonic interpretation of granitic rocks: Journal of Petrology, 25, 956-983. https://doi.org/10.1093/petrology/25.4.956

Poliquin, M.J., 2009, Geology, geochemistry and age of intrusion-related mineralisation in Eastern Mexico: Exeter, U.K., University of Exeter, unpublished PhD dissertation, 398 p.

Ribeiro, J., Maury, R.C., Grégoire, M., 2016, Are adakites slab melts or high-pressure fractionated mantle melts?: Journal of Petrology, 57, 1-24. https://doi.org/10.1093/petrology/egw023

Richards, J.P., 2011, High Sr/Y arc magmas and porphyry Cu ± Mo ± Au deposits: just add water: Economic Geology, 106,

1075-1081. https://doi.org/10.2113/econgeo.106.7.1075

Richards, J.P., Kerrich, R., 2007, Adakite-like rocks: Their diverse origins and questionable role in metallogenesis: Economic Geology, 102, 537-576. http://dx.doi.org/10.2113/gsecongeo.102.4.537

Richards, J.P., Mumin, A.H., 2013, Lithospheric Fertilization and Mineralization by Arc Magmas: Genetic Links and Secular Differences Between Porphyry Copper ± Molybdenum ± Gold and Magmatic-Hydrothermal Iron Oxide Copper-Gold Deposits, in Colpron, M., Bissig, T., Rusk, B.G., Thompson, J.F.H., (eds.), Tectonics, metallogeny, and discovery: the North American Cordillera and similar accretionary settings: Littleton, Colorado, USA, Society of Economic Geologists. Society of Economic Geologists Special Publication, 17, 277-299. https://doi.org/10.5382/SP.17.09

Rodríguez, C., Sellés, D., Dungan, M., Langmuir, C., Leeman, W., 2007, Adakitic dacites formed by intracrustal crystal fractionation of water-rich parent magmas at Nevado de Longavi volcano (36 ·2 S; Andean Southern Volcanic Zone, Central Chile): Journal of Petrology, 48, 2033-2061. https://doi.org/10.1093/petrology/egm049

Sarabia-Jacinto, L.O., 2017, Caracterización termo-barométrica de los fluidos mineralizantes de la mina El Dorado, del Distrito Minero de Tatatila-Las Minas, Veracruz: Universidad de Guanajuato, unpublished BSc thesis, 126 p.

Servicio Geológico Mexicano, 2007, Carta geológico-minera Perote E14-B26, Veracruz y Puebla, 1:50,000: Pachuca, Hidalgo, Mexico, Servicio Geológico Mexicano.

Servicio Geológico Mexicano, 2010, Carta geológico-minera Altotonga E14-B16, Veracruz y Puebla, 1:50,000: Pachuca, Hidalgo, Mexico, Servicio Geológico Mexicano.

Solari, L.A., Tanner, M., 2011, UPb.age, a fast data reduction script for LA-ICP-MS U–Pb geochronology: Revista Mexicana de Ciencias Geológicas, 28, 83-91. http://satori.geociencias.unam.mx/28-1/(06)Solari.pdf

Solari, L.A., Gómez-Tuena, A., Bernal, J.P., Pérez-Arvizu, O., Tanner, M., 2010, U–Pb zircon geochronology by an integrated LA-ICPMS microanalytical workstation: achievements in precision and accuracy: Geostandard and Geoanalytical Research, 34, 5-18. https://doi.org/10.1111/j.1751-908X.2009.00027.x

Sun, S.-S., McDonough, W.E., 1989, Chemical and isotopic systematics of oceanic basalts: implications for mantle composition and processes: Geological Society, London, Special Publication, 42, 313-345. https://doi.org/10.1144/GSL.SP.1989.042.01.19

Steiger, R.H., Jäger, E., 1977, Subcommission on Geochronology: Convention on the use of decay constants in Geo and Cosmochronology: Earth and Planetary Science Letters, 36, 359-362. https://doi.org/10.1016/0012-821X(77)90060-7

Sun, W., Zhang, H., Ling, M.-X., Ding, X., Chung, S.-L., Zhou, J., Yang, X.-Y., Fan, W., 2011, The genetic association of adakites and Cu-Au ore deposits: International Geology Review, 53, 691-703. https://doi.org/10.1080/00206814.2010.507362

Sun, X., Lu, Y.-J., McCuaig, T.C., Zheng, Y.-Y., Chang, H.-F., Guo, F., Xu, L.-J., 2018, Miocene ultrapotassic, high-Mg dioritic, and adakite-like rocks from Zhunuo in Southern Tibet: Implications for mantle metasomatism and porphyry copper mineralization in collisional orogens: Journal of Petrology, 59, 341-386. https://doi.org/10.1093/petrology/egy028

Thirlwall, M.F., Smith, T.E., Graham, A.M., Theodorou, N., Hollings, P., Davidson, J.P., Arculus, R.D., 1994, High field strength element anomalies in arc lavas: Source or processes?: Journal of Petrology, 35, 819-838. https://doi.org/10.1093/petrology/35.3.819

Todt, W., Cliff, R., Hanser A., Hofmann A.W., 1996, Evaluation of a ^{202}pb _ ^{205}pb Double Spike

http://dx.doi.org/10.18268/BSGM2020v72n3a110520

for High-Precision Lead Isotope Analysis. A. Basu, S. Hart (Eds.): Earth Processes: Reading the Isotopic Code, Geophys. Monogr., vol. 95, AGU, Washington D.C., pp. 429-437.

Viniegra, F., 1965, Geología del Macizo de Teziutlán y de la cuenca cenozoica de Veracruz: Boletín de la Asociación Mexicana de Geólogos Petroleros, 17, 7-12.

Whalen, J.B., Currie, K.J., Chappell, B.W., 1987, A-type granites: geochemical characteristics, discrimination and petrogenesis: Contributions to Mineralogy and Petrology, 95, 407-419. https://doi.org/10.1007/BF00402202

York, D., Evensen, N.M., López-Martínez, M., De Basabe-Delgado, J., 2004, Unified equations for the slope, intercept, and standard errors of the best straight line: American Journal of Physics, 73 (3), 367-375. https://doi.org/10.1119/1.1632486

Zhang, L., Hu, Y., Liang, J., Ireland, T., Chen, Y., Zhang, R., Sun, S., Sun, W., 2017, Adakitic rocks associated with the Shilu copper–molybdenum deposit in the Yangchun Basin, South China, and their tectonic implications: Acta Geochimica, 36, 132-150. https://doi.org/10.1007/s11631-017-0146-6

Appendix

Appendix 1. Ar/Ar determinations dataset for intrusive rocks associated with the IOCG skarn deposits at the Tatatila–Las Minas district, Veracruz.

SC-2b biotite

Laser	Isotope Ratios														
Power(%)	40Ar/39Ar	2σ	36Ar/39Ar	2σ	39Ar/40Ar	2σ	36Ar/40Ar	2σ	Rho	K/Ca	%40Ar rad	f 39Ar		40Ar*/39ArK	Age	2 σ
2.30	80.48	5.38	0.25	0.03	0.01	0.001	0.00308	0.00030	0.041	0.82	8.07	0.07		6.502	44.84	± 49.84
2.80	18.12	0.61	0.0603	0.0072	0.06	0.002	0.00331	0.00039	0.127	0.85	1.12	0.68		0.204	1.42	± 14.86
3.20	6.76	0.29	0.0160	0.0013	0.15	0.006	0.00230	0.00021	0.392	0.61	31.25	1.92		2.115	14.71	± 3.27
3.60	3.63	0.09	0.0059	0.0005	0.28	0.007	0.00156	0.00014	0.177	1.75	53.25	4.37		1.935	13.46	± 1.13
4.00	2.59	0.12	0.0017	0.0003	0.39	0.019	0.00062	0.00010	0.266	11.07	81.43	8.20		2.108	14.66	± 0.99
4.40	2.53	0.05	0.0018	0.0001	0.40	0.009	0.00064	0.00005	0.131	3.57	80.88	9.33		2.047	14.24	± 0.45
4.90	2.22	0.03	0.00064	0.00011	0.45	0.007	0.00018	0.00005	0.002	2.26	94.31	17.55		2.095	14.57	± 0.30
5.40	2.23	0.03	0.00061	0.00012	0.45	0.007	0.00020	0.00005	0.007	6.13	93.74	18.12		2.095	14.57	± 0.33
6.00	2.16	0.03	0.00036	0.00011	0.46	0.007	0.00010	0.00005	0.006	11.46	96.74	17.02		2.093	14.55	± 0.31
6.80	2.23	0.04	0.00076	0.00011	0.45	0.007	0.00027	0.00005	0.012	5.59	91.88	16.69		2.050	14.26	± 0.33
7.80	2.31	0.03	0.00065	0.00048	0.43	0.006	0.00023	0.00021	0.002	11.76	93.05	4.86		2.154	14.98	± 1.01
9.00	2.38	0.10	0.0039	0.0017	0.42	0.017	0.00160	0.00072	0.081	7.50	52.16	1.20		1.244	8.66	± 3.59

J = 0.00381413 ± 0.00000572 Volume 39ArK = 1.073 x E-13 cm3 NPT

Integrated Date = 14.45 ± 0.15 Ma

Plateau age = 14.46 ± 0.15 Ma (2s, including J-error of .2%) MSWD = 1.3, probability=0.24 Includes 98.8% of the 39Ar steps 1 through 12

Inverse isochron (correlation age) results, plateau steps: Model 1 Solution (±95%-conf.) on 9 points

Age = 14.32 ± 0.17 Ma Initial 40Ar/36Ar =285 ± 20 MSWD = 0.89 Probability = 0.51

SC-2a biotite

Laser	Isotope Ratios														
Power(%)	40Ar/39Ar	2σ	36Ar/39Ar	2σ	39Ar/40Ar	2σ	36Ar/40Ar	2σ	Rho	K/Ca	%40Ar rad	f 39Ar		40Ar*/39ArK	Age	2 σ
2.30	69.56	2.97	0.23	0.02	0.01	0.001	0.00329	0.00028	0.034	16.20	1.67	0.07		1.164	8.15	± 40.12
2.70	16.92	0.31	0.04089	0.00413	0.06	0.001	0.00240	0.00024	0.050	1.49	28.21	0.35		4.776	33.21	± 8.48
3.10	9.92	0.15	0.02785	0.00281	0.10	0.002	0.00279	0.00028	0.016	2.09	16.75	1.02		1.662	11.63	± 5.81
3.50	4.92	0.08	0.00914	0.00077	0.20	0.004	0.00183	0.00015	0.066	3.54	45.46	2.87		2.236	15.62	± 1.62
3.90	3.05	0.07	0.00310	0.00017	0.33	0.008	0.00097	0.00006	0.282	23.59	70.78	8.02		2.158	15.08	± 0.57
4.30	2.54	0.05	0.00126	0.00021	0.40	0.007	0.00045	0.00008	0.015	50.64	86.51	8.72		2.193	15.33	± 0.52
4.70	2.41	0.05	0.00061	0.00010	0.42	0.008	0.00020	0.00004	0.037	36.10	93.89	10.16		2.263	15.81	± 0.37
5.10	2.42	0.06	0.00082	0.00011	0.41	0.010	0.00028	0.00005	0.043	56.91	91.32	11.08		2.206	15.41	± 0.44
5.50	2.34	0.06	0.00066	0.00011	0.43	0.010	0.00023	0.00005	0.076	34.03	93.04	15.34		2.174	15.20	± 0.44
6.00	2.36	0.07	0.00090	0.00015	0.42	0.012	0.00032	0.00006	0.106	29.55	90.20	14.48		2.131	14.90	± 0.54
7.00	2.43	0.04	0.00078	0.00012	0.41	0.007	0.00026	0.00005	0.002	21.57	91.95	19.82		2.230	15.59	± 0.35
8.00	2.46	0.06	0.00087	0.00029	0.41	0.009	0.00029	0.00012	0.034	9.55	91.15	6.13		2.246	15.70	± 0.71
9.00	2.49	0.08	0.00099	0.00034	0.40	0.012	0.00034	0.00014	0.056	7.68	89.80	1.93		2.234	15.61	± 0.88

J = 0.00383360 ± 0.00000575 Volume 39ArK = 1.146 x E-13 cm3 NPT

Integrated Date = 15.44 ± 0.16 Ma

Plateau age = 15.43 ± 0.16 Ma (2s, including J-error of .2%) MSWD = 1.4, probability=0.16 Includes 99.58% of the 39Ar steps 3 through 13

Inverse isochron (correlation age) results, plateau steps: Model 1 Solution (±95%-conf.) on 11 points

Age = 15.30 ± 0.19 Ma Initial 40Ar/36Ar =287 ± 17 MSWD = 1.4 Probability = 0.19

http://dx.doi.org/10.18268/BSGM2020v72n3a110520

Appendix 1. (continuation) Ar/Ar determinations dataset for intrusive rocks associated with the IOCG skarn deposits at the Tatatila–Las Minas district, Veracruz.

SC-2-b1 biotite

Laser	Isotope Ratios														
Power(%)	40Ar/39Ar	2σ	36Ar/39Ar	2σ	39Ar/40Ar	2σ	36Ar/40Ar	2σ	Rho	K/Ca	%40Ar rad	f 39Ar	40Ar*/39ArK	Age	2 σ
2.30	84.01	12.49	0.25	0.05	0.01	0.002	0.0030	0.0003	0.017	1.16	9.49	0.03	7.973	55.48	± 57.63
2.70	26.65	0.80	0.080	0.006	0.04	0.001	0.0030	0.0002	0.033	1.41	10.24	0.35	2.730	19.18	± 12.66
3.10	8.91	0.15	0.0211	0.0012	0.11	0.002	0.0023	0.0001	0.058	1.71	30.11	1.16	2.684	18.86	± 2.41
3.50	6.33	0.09	0.0134	0.0012	0.16	0.002	0.0021	0.0002	0.024	2.34	37.59	2.74	2.380	16.74	± 2.42
3.90	3.56	0.07	0.0044	0.0003	0.28	0.005	0.0012	0.0001	0.080	12.29	64.39	7.24	2.291	16.11	± 0.75
4.30	2.77	0.06	0.0016	0.0001	0.36	0.007	0.0005	0.0000	0.134	14.08	83.92	8.88	2.325	16.36	± 0.43
4.70	2.72	0.05	0.0015	0.0003	0.37	0.007	0.0005	0.0001	0.043	14.88	84.62	11.60	2.305	16.21	± 0.63
5.10	2.64	0.04	0.0012	0.0004	0.38	0.006	0.0004	0.0001	0.023	19.94	87.79	11.13	2.316	16.29	± 0.81
5.70	2.66	0.06	0.0013	0.0003	0.38	0.009	0.0004	0.0001	0.042	12.00	86.87	15.75	2.313	16.27	± 0.78
6.30	2.47	0.05	0.0007	0.0001	0.40	0.008	0.0002	0.0000	0.031	22.81	92.79	17.23	2.296	16.15	± 0.41
7.00	2.62	0.05	0.0010	0.0002	0.38	0.008	0.0003	0.0001	0.028	19.58	89.91	15.08	2.357	16.57	± 0.51
8.00	2.68	0.06	0.0012	0.0002	0.37	0.009	0.0004	0.0001	0.032	12.04	88.18	8.18	2.365	16.63	± 0.61
9.00	5.26	0.32	0.0111	0.0013	0.19	0.012	0.0021	0.0003	0.440	2.75	37.91	0.63	1.993	14.02	± 3.41

J = 0.00385940 ± 0.00000579 Volume 39ArK = 1.775 x E-13 cm3 NPT

Integrated Date = 16.34 ± 0.20 Ma

Plateau age = 16.34 ± 0.20 Ma (2s, including J-error of .2%) MSWD = 0.89, probability=0.55 Includes 99.97% of the 39Ar steps 2 through 13

Inverse isochron (correlation age) results, plateau steps: Model 1 Solution (±95%-conf.) on 13 points

Age = 16.01 ± 0.22 Ma Initial 40Ar/36Ar = 308 ± 11 MSWD = 0.76 Probability = 0.68

RV-2 feldspar

Laser	Isotope Ratios														
Power(%)	40Ar/39Ar	2σ	36Ar/39Ar	2σ	39Ar/40Ar	2σ	36Ar/40Ar	2σ	Rho	K/Ca	%40Ar rad	f 39Ar	40Ar*/39ArK	Age	2 σ
2.70	138.70	2.29	0.48	0.02	0.01	0.000	0.0035	0.0002	0.062	0.61	-3.02	1.27	4.191	-30.25	± 48.11
2.90	33.11	0.61	0.103	0.005	0.03	0.001	0.0031	0.0001	0.020	0.61	7.50	1.62	2.485	17.70	± 10.08
3.20	18.27	0.41	0.054	0.003	0.05	0.001	0.0029	0.0001	0.022	0.63	12.94	5.42	2.367	16.87	± 5.45
3.50	14.25	0.27	0.039	0.002	0.07	0.001	0.0027	0.0001	0.026	0.62	19.73	6.32	2.814	20.04	± 3.74
3.80	8.72	0.19	0.020	0.001	0.11	0.002	0.0022	0.0001	0.011	0.60	32.84	9.32	2.866	20.40	± 2.01
4.10	7.75	0.11	0.016	0.001	0.13	0.002	0.0021	0.0001	0.088	0.55	38.51	10.38	2.987	21.26	± 1.63
4.40	7.45	0.10	0.016	0.001	0.13	0.002	0.0021	0.0001	0.055	0.55	38.68	8.01	2.886	20.54	± 1.60
5.00	7.46	0.10	0.016	0.001	0.13	0.002	0.0020	0.0001	0.009	0.52	38.98	13.46	2.910	20.71	± 1.56
5.40	7.32	0.10	0.015	0.001	0.14	0.002	0.0020	0.0001	0.018	0.62	39.52	10.73	2.893	20.60	± 1.53
6.00	6.79	0.09	0.014	0.001	0.15	0.002	0.0019	0.0001	0.023	0.55	41.95	10.95	2.850	20.29	± 1.33
7.00	6.98	0.09	0.014	0.001	0.14	0.002	0.0019	0.0001	0.032	0.48	42.79	10.43	2.988	21.27	± 1.35
8.40	6.40	0.08	0.010	0.001	0.16	0.002	0.0016	0.0001	0.032	0.51	53.03	7.23	3.395	24.15	± 1.09
10.00	5.87	0.08	0.009	0.000	0.17	0.002	0.0014	0.0001	0.054	0.51	58.66	4.87	3.447	24.51	± 0.95

J = 0.00391100 ± 0.00000587 Volume 39ArK = 1.264 x E-13 cm3 NPT

Integrated Date = 22.10 ± 0.45 Ma

Plateau age = 20.67 ± 0.57 Ma (2s, including J-error of .2%) MSWD = 0.46, probability=0.90 Includes 86.6% of the 39Ar steps 2 through 11

Inverse isochron (correlation age) results: Model 1 Solution (±95%-conf.) on 11 points

Age = 21.5 ± 1.1 Ma Initial 40Ar/36Ar = 288.5 ± 8.2 MSWD = 0.37 Probability = 0.95

http://dx.doi.org/10.18268/BSGM2020v72n3a110520

CR-1 biotite

Laser	Isotope Ratios													
Power(%)	40Ar/39Ar	2σ	36Ar/39Ar	2σ	39Ar/40Ar	2σ	36Ar/40Ar	2σ	Rho	K/Ca	%40Ar rad	f 39Ar	40Ar*/39ArK	Age 2 σ
2.30	843.11	44.89	2.40	0.17	0.00	0.000	0.0028	0.0001	0.024	0.29	14.99	0.18	126.590	740.17 ± 164.17
2.70	62.40	1.87	0.18	0.01	0.02	0.000	0.0029	0.0001	0.142	0.41	13.41	3.99	8.376	59.39 ± 19.08
3.10	31.24	0.68	0.084	0.004	0.03	0.001	0.0027	0.0001	0.166	0.49	20.31	6.67	6.350	45.20 ± 8.51
3.60	18.97	0.37	0.050	0.003	0.05	0.001	0.0026	0.0001	0.136	0.67	21.03	15.14	3.992	28.55 ± 5.60
4.20	8.41	0.13	0.019	0.001	0.12	0.002	0.0020	0.0001	0.084	0.14	40.02	24.21	3.378	24.18 ± 2.09
5.00	6.36	0.10	0.012	0.001	0.16	0.002	0.0015	0.0001	0.053	0.11	54.96	29.43	3.511	25.13 ± 1.61
6.00	6.79	0.44	0.014	0.001	0.15	0.009	0.0017	0.0001	0.689	0.10	50.64	15.38	3.454	24.72 ± 3.37
7.00	5.37	0.30	0.010	0.001	0.19	0.010	0.0014	0.0002	0.400	0.11	59.22	5.01	3.193	22.86 ± 2.83

J = 0.00393680 ± 0.00000591 Volume 39ArK = 0.369 x E-13 cm3 NPT

Integrated Date = 25.10 ± 1.07 Ma

Plateau age = 24.6 ± 1.1 Ma (2s, including J-error of .2%) MSWD = 1.02, probability=0.39 Includes 89.2% of the 39Ar steps 4 through 8

Inverse isochron (correlation age) results: Model 1 Solution (±95%-conf.) on 8 points

Age = 21.0 ± 2.5 Ma Initial 40Ar/36Ar = 335 ± 16 MSWD = 2.0 Probability = 0.06

CR-1 hornblende

Laser	Isotope Ratios													
Power(%)	40Ar/39Ar	2σ	36Ar/39Ar	2σ	39Ar/40Ar	2σ	36Ar/40Ar	2σ	Rho	K/Ca	%40Ar rad	f 39Ar	40Ar*/39ArK	Age 2 σ
2.30	357.33	104.57	1.17	0.38	0.00	0.001	0.0033	0.0004	0.005	0.16	2.29	0.11	8.217	58.28 ± 330.12
2.80	34.72	1.15	0.10	0.008	0.03	0.001	0.0027	0.0002	0.158	0.22	18.39	3.50	6.401	45.56 ± 17.77
3.20	17.36	1.66	0.040	0.007	0.06	0.006	0.0023	0.0004	0.318	0.52	31.13	9.87	5.411	38.58 ± 15.93
3.80	8.16	1.00	0.018	0.002	0.12	0.015	0.0017	0.0003	0.710	0.07	48.86	32.59	4.019	28.73 ± 7.73
4.30	5.91	0.75	0.012	0.002	0.17	0.022	0.0015	0.0004	0.519	0.07	55.41	23.80	3.296	23.60 ± 6.59
5.00	3.84	0.11	0.005	0.001	0.26	0.007	0.0007	0.0004	0.040	0.09	79.38	15.79	3.068	21.98 ± 3.07
6.00	5.87	0.40	0.009	0.003	0.17	0.012	0.0012	0.0006	0.142	0.10	63.35	8.51	3.737	26.73 ± 7.42
7.50	7.37	0.26	0.006	0.003	0.14	0.005	0.0006	0.0005	0.018	0.15	82.26	5.82	6.082	43.31 ± 7.32

J = 0.00393680 ± 0.00000591 Volume 39ArK = 0.079 x E-13 cm3 NPT

Integrated Date = 26.06 ± 2.30 Ma

Plateau age = 23.4 ± 2.5 Ma (2s, including J-error of .2%) MSWD = 1.19, probability=0.31 Includes 80.7% of the 39Ar steps 4 through 7

Inverse isochron (correlation age) results, plateau steps: Model 1 Solution (±95%-conf.) on 7 points

Age = 22.1 ± 2.8 Ma Initial 40Ar/36Ar = 332 ± 23 MSWD = 0.76 Probability = 0.958

http://dx.doi.org/10.18268/BSGM2020v72n3a110520

Appendix 1. (continuation) Ar/Ar determinations dataset for intrusive rocks associated with the IOCG skarn deposits at the Tatatila–Las Minas district, Veracruz.

CR-1 feldspar

Laser	Isotope Ratios														
Power(%)	40Ar/39Ar	2σ	36Ar/39Ar	2σ	39Ar/40Ar	2σ	36Ar/40Ar	2σ	Rho	K/Ca	%40Ar rad	f 39Ar		40Ar*/39ArK	Age	2 σ
2.30	211.15	3.20	0.71	0.03	0.005	0.0001	0.0033	0.0002	0.015	0.78	0.17	1.73		0.355		2.55 ± 69.27
2.50	50.66	0.81	0.16	0.01	0.020	0.0003	0.0031	0.0001	0.098	0.58	6.78	2.61		3.436		24.60 ± 15.70
2.80	35.74	1.22	0.11	0.01	0.03	0.001	0.0031	0.0002	0.040	0.27	6.51	8.26		2.331		16.72 ± 11.56
3.10	14.13	0.44	0.039	0.002	0.07	0.002	0.0027	0.0002	0.037	0.29	18.52	16.26		2.622		18.80 ± 4.80
3.40	6.89	0.21	0.015	0.001	0.15	0.005	0.0021	0.0001	0.013	0.44	37.98	23.01		2.619		18.77 ± 1.95
3.80	7.05	0.14	0.016	0.001	0.14	0.003	0.0021	0.0001	0.053	0.30	36.76	17.69		2.596		18.62 ± 1.69
4.40	7.18	0.12	0.017	0.001	0.14	0.002	0.0022	0.0001	0.020	0.28	33.74	10.92		2.428		17.41 ± 1.71
5.20	7.04	0.11	0.015	0.001	0.14	0.002	0.0021	0.0001	0.006	0.22	38.20	7.66		2.695		19.32 ± 2.03
6.50	5.22	0.07	0.009	0.000	0.19	0.003	0.0016	0.0001	0.016	0.20	52.95	7.00		2.772		19.87 ± 1.08
8.50	5.99	0.08	0.010	0.001	0.17	0.002	0.0015	0.0001	0.017	0.20	54.58	4.86		3.277		23.47 ± 1.23

J = 0.00393680 ± 0.00000591 Volume 39ArK = 0.565 x E-13 cm3 NPT

Integrated Date = 20.10 ± 0.60 Ma

Plateau age = 19.04 ± 0.69 Ma (2s, including J-error of .2%) MSWD = 0.91, probability=0.50 Includes 95.1% of the 39Ar steps 1 through 9

Inverse isochron (correlation age) results: Model 1 Solution (±95%-conf.) on 9 points

Age = 19.01 ± 0.98 Ma Initial 40Ar/36Ar = 296.0 ± 7.7 MSWD = 0.98 Probability = 0.44

BQ-1c feldspar

Laser	Isotope Ratios														
Power(%)	40Ar/39Ar	2σ	36Ar/39Ar	2σ	39Ar/40Ar	2σ	36Ar/40Ar	2σ	Rho	K/Ca	%40Ar rad	f 39Ar		40Ar*/39ArK	Age	2 σ
2.30	347.07	25.34	0.64	0.07	0.00	0.000	0.0018	0.0001	0.011	1.13	45.01	0.13		156.297		891.40 ± 86.60
2.70	164.62	4.48	0.39	0.02	0.01	0.000	0.0024	0.0001	0.004	0.54	29.20	1.06		48.110		323.22 ± 35.67
3.10	42.43	0.74	0.11	0.01	0.02	0.000	0.0026	0.0001	0.044	0.28	23.73	4.44		10.087		72.66 ± 11.14
3.50	18.10	0.28	0.042	0.002	0.06	0.001	0.0023	0.0001	0.075	0.29	32.17	6.71		5.833		42.37 ± 4.32
3.90	9.07	0.16	0.020	0.001	0.11	0.002	0.0022	0.0001	0.044	0.37	34.57	10.93		3.140		22.93 ± 2.72
4.30	6.80	0.12	0.014	0.001	0.15	0.003	0.0019	0.0001	0.030	0.40	41.86	12.11		2.850		20.82 ± 1.87
4.90	6.45	0.09	0.012	0.001	0.15	0.002	0.0017	0.0001	0.007	0.39	48.52	15.54		3.133		22.87 ± 1.62
5.60	6.04	0.09	0.011	0.001	0.17	0.003	0.0017	0.0001	0.018	0.38	50.36	14.55		3.046		22.25 ± 1.64
6.50	5.66	0.08	0.009	0.001	0.18	0.002	0.0016	0.0001	0.004	0.41	53.12	20.05		3.012		22.00 ± 1.23
7.50	6.21	0.09	0.007	0.001	0.16	0.002	0.0011	0.0001	0.016	0.32	67.83	14.50		4.218		30.74 ± 1.81

J = 0.00401420 ± 0.00000602 Volume 39ArK = 0.272 x E-13 cm3 NPT

Integrated Date = 24.15 ± 0.67 Ma

Plateau age = 22.12 ± 0.74 Ma (2s, including J-error of .2%) MSWD = 0.80, probability=0.52 Includes 73.2% of the 39Ar steps 5 through 9

Inverse isochron (correlation age) results, plateau steps: Model 1 Solution (±95%-conf.) on 5 points

Age = 21.4 ± 2.9 Ma Initial 40Ar/36Ar = 304 ± 35 MSWD = 1.03 Probability = 0.36

http://dx.doi.org/10.18268/BSGM2020v72n3a110520

BQ-1b biotite

Laser	Isotope Ratios														
Power(%)	40Ar/39Ar	2σ	36Ar/39Ar	2σ	39Ar/40Ar	2σ	36Ar/40Ar	2σ	Rho	K/Ca	%40Ar rad	f 39Ar		40Ar*/39ArK	Age	2 σ
2.30	409.99	15.09	1.42	0.086	0.00	0.000	0.0035	0.0002	0.006	0.94	-3.56	0.29		14.611		-110.64 ± 159.72
2.80	46.61	0.76	0.15	0.008	0.02	0.000	0.0033	0.0002	0.018	0.51	1.03	2.59		0.478		3.51 ± 16.43
3.10	23.90	0.44	0.08	0.004	0.04	0.001	0.0032	0.0002	0.132	0.65	5.39	8.90		1.289		9.45 ± 8.61
3.70	4.31	0.07	0.008	0.0004	0.23	0.004	0.0019	0.0001	0.115	1.68	44.20	8.94		1.904		13.94 ± 1.01
4.20	2.95	0.04	0.004	0.0002	0.34	0.005	0.0012	0.0001	0.030	2.02	64.12	18.93		1.893		13.86 ± 0.48
4.80	2.34	0.03	0.002	0.0001	0.43	0.006	0.0006	0.0001	0.011	1.65	81.49	26.94		1.907		13.96 ± 0.36
5.50	2.34	0.03	0.002	0.0002	0.43	0.005	0.0006	0.0001	0.011	1.34	80.42	15.97		1.882		13.78 ± 0.43
6.40	2.68	0.04	0.003	0.0003	0.37	0.005	0.0010	0.0001	0.035	0.77	70.14	9.51		1.882		13.78 ± 0.71
7.60	3.53	0.05	0.006	0.0004	0.28	0.004	0.0014	0.0001	0.057	0.49	57.57	5.60		2.033		14.87 ± 0.93
9.00	4.39	0.08	0.009	0.002	0.23	0.004	0.0020	0.0004	0.030	0.48	40.37	2.33		1.775		13.00 ± 4.07

J = 0.00401420 ± 0.00000602 Volume 39ArK = 0.483 x E-13 cm3 NPT

Integrated Date = 13.92 ± 0.22 Ma

Plateau age = 13.92 ± 0.22 Ma (2s, including J-error of .2%) MSWD = 1.14, probability=0.33 Includes 100% of the 39Ar steps 1 through 10

Inverse isochron (correlation age) results, plateau steps: Model 1 Solution (±95%-conf.) on 10 points

Age = 14.39 ± 0.26 Ma Initial 40Ar/36Ar =292.0 ± 7.5 MSWD = 0.96 Probability = 0.46

BQ-1b Biotite

Laser	Isotope Ratios														
Power(%)	40Ar/39Ar	2σ	36Ar/39Ar	2σ	39Ar/40Ar	2σ	36Ar/40Ar	2σ	Rho	K/Ca	%40Ar rad	f 39Ar		40Ar*/39ArK	Age	2 σ
3.40	5.62	0.56	0.0428	0.0034	0.18	0.02	0.00760	0.00093	0.753	2.90	-126.85	3.03		7.126		-53.12 ± 8.51
3.80	5.27	0.37	0.0256	0.0020	0.19	0.01	0.00485	0.00049	0.630	3.30	-44.84	8.95		2.362		-17.44 ± 4.97
4.30	2.11	0.15	0.0053	0.0010	0.47	0.03	0.00246	0.00048	0.334	8.64	26.36	15.06		0.557		4.09 ± 2.32
5.10	2.26	0.03	0.0010	0.0002	0.44	0.01	0.00038	0.00011	0.011	5.89	88.57	30.67		2.006		14.68 ± 0.58
5.90	2.18	0.03	0.0008	0.0002	0.46	0.01	0.00028	0.00009	0.005	6.01	91.34	25.88		1.989		14.56 ± 0.46
6.80	2.44	0.05	0.0018	0.0005	0.41	0.01	0.00063	0.00020	0.031	2.05	80.91	11.54		1.971		14.42 ± 1.10
8.00	2.67	0.05	0.0024	0.0009	0.38	0.01	0.00080	0.00033	0.012	2.12	76.10	4.86		2.032		14.87 ± 1.95

J = 0.00401420 ± 0.00000602 Volume 39ArK = 0.264 x E-13 cm3 NPT

Integrated Date = 14.13 ± 0.33 Ma

Plateau age = 14.60 ± 0.34 Ma (2s, including J-error of .2%) MSWD = 0.099, probability=0.96 Includes 73% of the 39Ar steps 4 through 7

Inverse isochron (correlation age) results, plateau steps: Model 1 Solution (±95%-conf.) on 4 points

Age = 14.33 ± 0.87 Ma Initial 40Ar/36Ar =307 ± 130 MSWD = 0.14 Probability = 0.87

http://dx.doi.org/10.18268/BSGM2020v72n3a110520

http://dx.doi.org/10.18268/BSGM2020v72n3a110520

Appendix 1. (continuation) Ar/Ar determinations dataset for intrusive rocks associated with the IOCG skarn deposits at the Tatatila–Las Minas district, Veracruz.

FSC-1 Fuchsita

Pwr	$^{39}Ar \times 10^{-6}$	% ^{39}Ar	$^{40}Ar^*/^{39}Ar_K$	1σ	Age in Ma	1σ		% $^{40}Ar^*$	$^{40}Ar/^{36}Ar$	$^{37}Ar_{Ca}/^{39}Ar_K$
0.6	0.668	0.08	33.6	12.03	140.99	48.56	a	23.27	385.11	0.003
1.5	4.769	0.57	2.57	2.18	11.18	9.47	b	7.65	319.96	1.58
2.2	14.443	1.74	0.39	0.76	1.71	3.3	c	1.68	300.54	0.044
2.7	38.246	4.61	2.5	0.39	10.88	1.67	d	25.18	394.94	0.008
3.4	43.922	5.3	3	0.18	13.04	0.77	e	55.38	662.25	0.003
4	145.819	17.59	2.87	0.06	12.47	0.26	f	72.32	1067.62	0.006
5	270.778	32.67	2.86	0.03	12.43	0.11	g	87.63	2388.74	0.004
6	140.591	16.96	2.87	0.03	12.46	0.12	h	95.72	6898.02	< 0.001
8	169.7	20.47	2.88	0.03	12.51	0.13	i	96.36	8120.85	< 0.001

Integrated results

$^{39}Ar \times 10^{-6}$	$^{40}Ar^*/^{39}Ar_K$	1σ	Age in Ma	1σ	% $^{40}Ar^*$	$^{40}Ar/^{36}Ar$	$^{37}Ar_{Ca}/^{39}Ar_K$
828.9	2.84	0.04	12.33	0.16	65.29	851.36	0.013

J = 0.002419 ± 0.000010

Plateau age $t_p = 12.49 \pm 0.09$ Ma

Weighted mean of fractions e to i, representing 92.99% of ^{39}Ar released in 5 consecutive fractions, MSWD = 0.18

Isochron age $t_c = 12.45 \pm 0.11$ Ma; $(^{40}Ar/^{36}Ar)_i = 300 \pm 15$, MSWD = 0.2 for n = 5 (e to i)

http://dx.doi.org/10.18268/BSGM2020v72n3a110520

Appendix 2. Plateau age spectra and normal isochron diagrams in host intrusive bodies to the IOCG skam deposits at the Tatatila-Las Minas district, Veracruz.

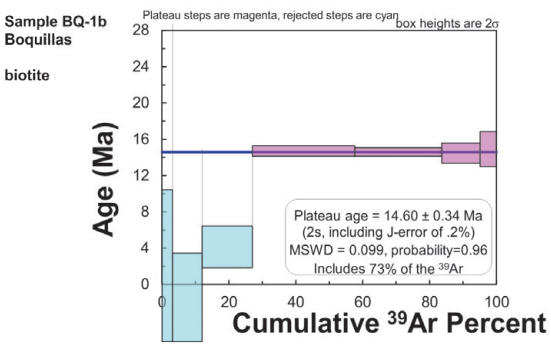

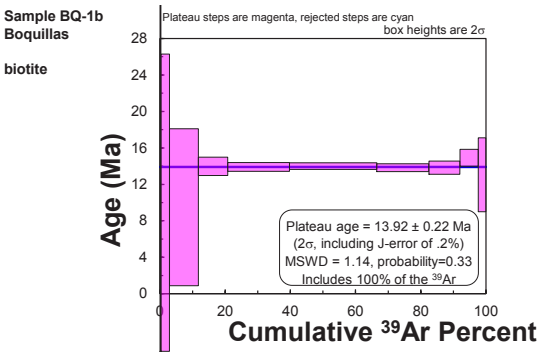

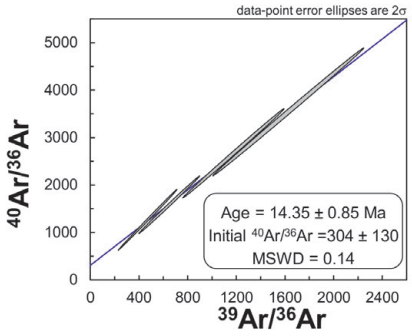

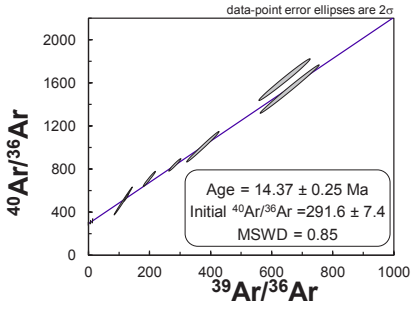

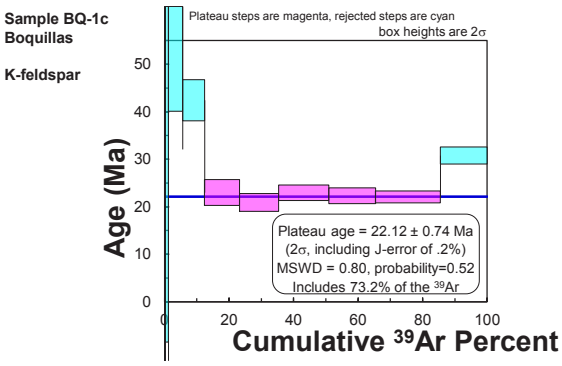

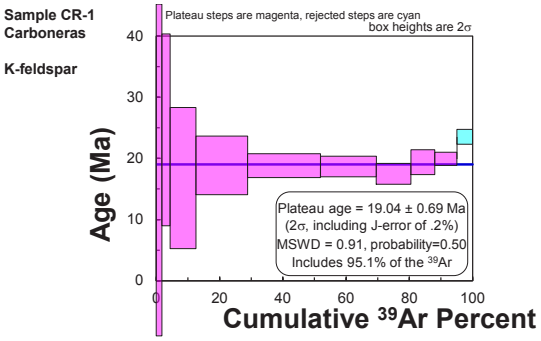

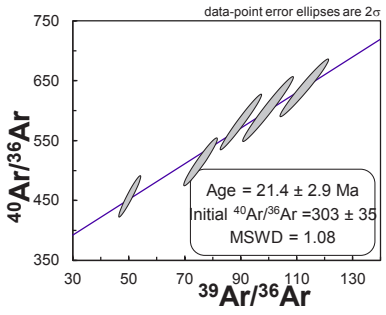

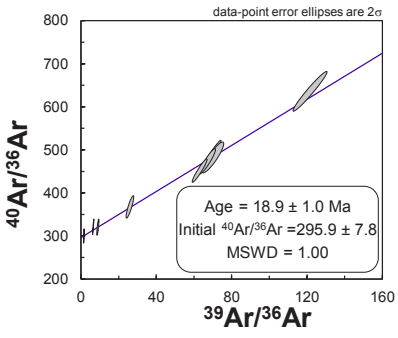

http://dx.doi.org/10.18268/BSGM2020v72n3a110520

Appendix 2. (Continuation) Plateau age spectra and normal isochron diagrams in host intrusive bodies to the IOCG skam deposits at the Tatatila-Las Minas district, Veracruz.

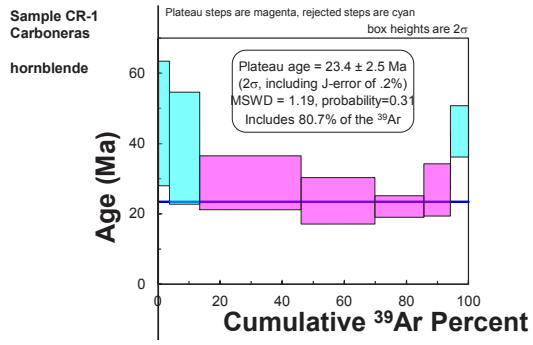

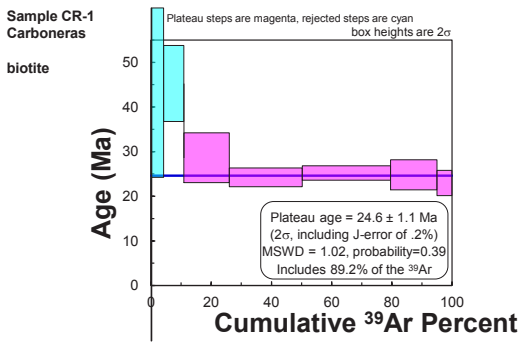

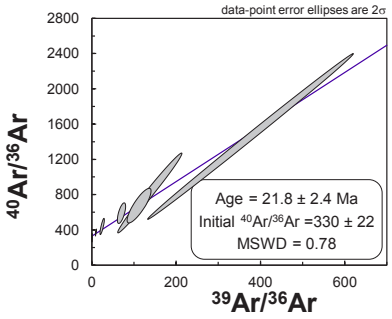

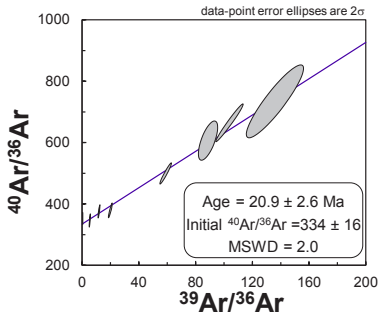

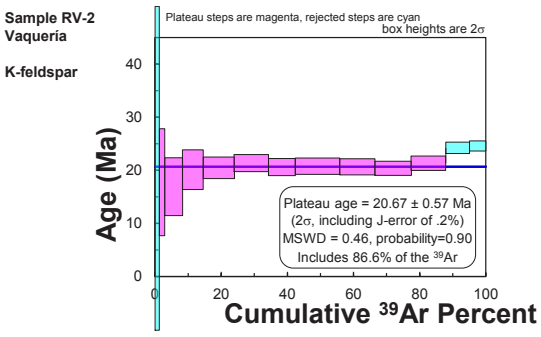

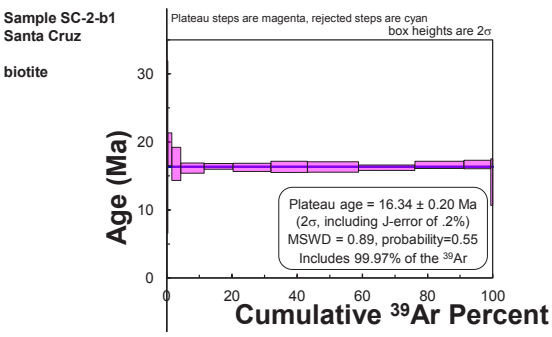

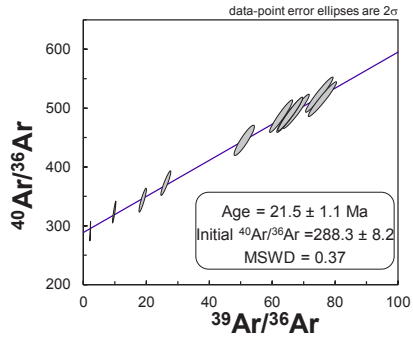

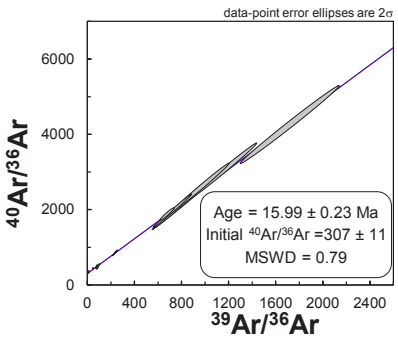

http://dx.doi.org/10.18268/BSGM2020v72n3a110520

Appendix 2. (Continuation) Plateau age spectra and normal isochron diagrams in host intrusive bodies to the IOCG skam deposits at the Tatatila-Las Minas district, Veracruz.

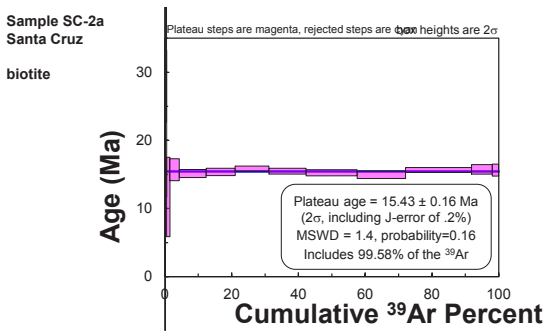

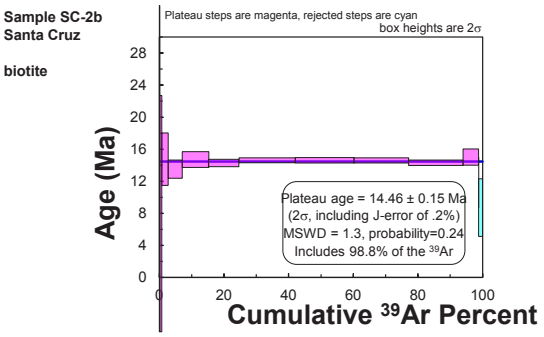

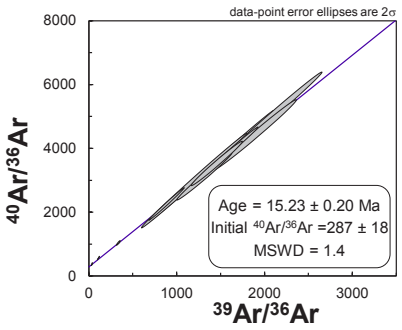

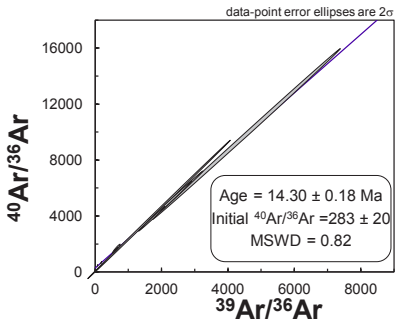

Appendix 3. U-Pb isotope data from zircons in the intrusive rocks associated with IOCG skarns in the Tatatila-Las Minas area.

Analisys/Zircon	U# (ppm)	Th# (ppm)	Th/U	CORRECTED ISOTOPIC RATIOS 207Pb/206Pb†	err %*	207Pb/235U†	err %*	206Pb/238U†	err %*	208Pb/232Th†	err %*	Rho**	% disc.***	CORRECTED AGES (Ma) 206Pb/238U ±2s*	207Pb/235U ±2s*	207Pb/206Pb ±2s*	Best Age (Ma) ± 2s
Sample ES-3 Escalona dyke (Tatatila de Las Minas, Veracruz)																	
ES-3-3	772	282	0.37	0.16900	16.0	0.01370	16.1	0.00058	6.4	0.00076	12.2	0.400	73	3.7	0.2	13.8	2.2	2520	190	3.7 ± 0.2
ES-3-11	1045	1075	1.03	0.09700	18.6	0.00830	16.9	0.00061	6.9	0.00024	10.0	0.411	53	3.9	0.3	8.4	1.4	1710	230	**3.9 ± 0.3**
ES-3-4	472	374	0.79	0.14000	24.3	0.01160	23.3	0.00062	8.9	0.00036	20.5	0.382	66	4.0	0.4	11.7	2.7	2400	180	**4.0 ± 0.4**
ES-3-13	1031	1276	1.24	0.14900	14.1	0.01220	10.7	0.00064	8.3	0.00030	10.2	0.781	67	4.1	0.3	12.3	1.3	2340	130	**4.1 ± 0.3**
ES-3-5	730	893	1.22	0.08900	24.7	0.00790	21.5	0.00064	7.0	0.00029	10.3	0.327	48	4.1	0.3	7.9	1.7	1270	310	**4.1 ± 0.3**
ES-3-14	761	827	1.09	0.10200	15.7	0.00900	15.6	0.00065	6.6	0.00026	12.0	0.427	54	4.2	0.3	9.1	1.4	1740	130	**4.2 ± 0.3**
ES3-18	830	762	0.92	0.21000	13.8	0.01900	11.6	0.00065	7.0	0.00040	7.8	0.601	78	4.2	0.3	19.1	2.2	2870	120	4.2 ± 0.3
ES-3-12	250	255	1.02	0.19800	22.2	0.01780	20.2	0.00065	8.3	0.00035	22.6	0.410	77	4.2	0.4	17.9	3.6	2930	160	4.2 ± 0.4
ES3-21	818	946	1.16	0.12200	18.9	0.01060	17.0	0.00065	6.6	0.00026	10.5	0.390	61	4.2	0.3	10.7	1.8	1930	220	**4.2 ± 0.3**
ES-3-23	839	1113	1.33	0.08600	22.1	0.00760	19.7	0.00065	8.3	0.00025	13.8	0.420	46	4.2	0.4	7.7	1.6	1320	290	**4.2 ± 0.4**
ES-3-20	602	343	0.57	0.10500	23.8	0.00990	21.2	0.00065	8.3	0.00032	20.5	0.390	58	4.2	0.4	10.0	2.1	1750	260	**4.2 ± 0.4**
ES-3-15	717	798	1.11	0.20600	11.2	0.01920	9.9	0.00069	7.6	0.00045	9.3	0.767	77	4.4	0.3	19.3	1.9	2882	91	4.4 ± 0.3
ES-3-19	300	276	0.92	0.25600	19.1	0.02260	19.5	0.00069	9.2	0.00042	16.4	0.472	80	4.4	0.4	22.6	4.3	3230	210	4.4 ± 0.4
ES3-1	384	497	1.29	0.25100	17.9	0.02530	13.4	0.00069	9.6	0.00045	12.5	0.714	83	4.4	0.4	25.4	3.4	3210	220	4.4 ± 0.4
ES-3-22	575	573	1.00	0.41000	29.3	0.03700	27.0	0.00071	9.6	0.00068	14.5	0.353	88	4.6	0.4	37.0	10.0	3920	280	4.6 ± 0.4
ES-3-2	425	357	0.84	0.19000	20.5	0.01820	19.8	0.00074	7.6	0.00049	15.7	0.385	74	4.7	0.4	18.2	3.6	2770	190	4.7 ± 0.4
ES-3-10	502	616	1.23	0.22000	15.9	0.02410	15.4	0.00079	6.5	0.00043	14.0	0.423	79	5.1	0.3	24.1	3.6	3050	130	5.1 ± 0.3
ES-3-16	583	839	1.44	0.21700	19.4	0.02480	21.8	0.00079	9.6	0.00055	18.1	0.440	80	5.1	0.5	26.0	5.6	3070	220	5.1 ± 0.5
ES-3-9	272	135	0.50	0.32000	12.8	0.03670	11.7	0.00086	7.4	0.00150	12.7	0.635	85	5.5	0.4	36.5	4.2	3570	140	5.5 ± 0.4
ES-3-8	342	140	0.41	0.35000	14.0	0.04250	11.5	0.00094	7.5	0.00184	14.1	0.649	86	6.0	0.5	42.2	4.8	3742	98	6.0 ± 0.5
ES-3-17	454	512	1.13	0.35400	13.0	0.04640	10.1	0.00095	7.1	0.00086	10.2	0.698	87	6.1	0.4	46.0	4.6	3730	130	6.1 ± 0.4
ES-3-7	468	622	1.33	0.52200	8.8	0.10400	10.6	0.00145	8.3	0.00157	7.6	0.782	91	9.3	0.8	100.2	9.9	4347	78	9.3 ± 0.8
ES-3-6	204	204	1.00	0.56900	15.3	0.17400	13.2	0.00221	8.6	0.00363	12.7	0.650	91	14.2	1.2	162.0	20.0	4390	160	14.2 ± 1.2
n = 23																			Mean $^{206}Pb/^{238}U$ Age =	**4,11 ± 0,11**
(2 sigma, MSWD = 0.53; n = 8)																				
Sample CR-5 Carbonera intrusive (Tatatila de Las Minas, Veracruz)																				
CR-5-4	264	341	1.29	0.16500	19.4	0.05290	16.1	0.00245	9.4	0.00128	10.2	0.584	70	15.7	1.5	52.2	8.1	2600	210	15.7 ± 1.5
CR-5-3	178	242	1.36	0.07600	34.2	0.02080	36.1	0.00249	7.2	0.00088	14.8	0.200	23	16.0	1.1	20.7	7.6	1490	180	**16.0 ± 1.1**
CR-5-15	188	321	1.71	0.10300	15.5	0.03350	12.8	0.00250	6.8	0.00092	7.4	0.530	52	16.1	1.1	33.4	4.3	1740	180	16.1 ± 1.1
CR-5-10	368	524	1.42	0.13500	14.8	0.04430	12.6	0.00251	4.8	0.00106	6.0	0.378	64	16.2	0.8	44.9	5.7	2110	140	16.2 ± 0.8
CR-5-7	503	889	1.77	0.10500	11.4	0.03850	11.9	0.00255	7.5	0.00104	7.5	0.624	57	16.4	1.2	38.3	4.5	1820	140	16.4 ± 1.2
CR-5-8	535	1006	1.88	0.17200	12.2	0.05990	11.7	0.00261	4.6	0.00115	6.1	0.393	71	16.8	0.7	58.9	6.7	2540	150	16.8 ± 0.7
CR-5-1	114	162	1.42	0.20400	21.1	0.07100	16.9	0.00269	8.2	0.00126	11.1	0.484	75	17.3	1.4	70.0	12.0	2800	180	17.3 ± 1.4
CR-5-2	179	238	1.33	0.10900	24.8	0.04140	21.3	0.00272	7.7	0.00119	11.8	0.363	57	17.5	1.4	41.0	8.5	1910	260	17.5 ± 1.4
CR-5-13	158	235	1.49	0.18800	13.8	0.07060	11.9	0.00271	6.3	0.00127	7.9	0.527	75	17.5	1.1	69.0	7.9	2800	170	17.5 ± 1.1
CR-5-12	283	438	1.55	0.16600	14.5	0.06130	12.7	0.00273	5.5	0.00135	9.6	0.432	71	17.6	1.0	60.2	7.5	2520	180	17.6 ± 1.0
CR-5-18	270	407	1.51	0.19200	11.5	0.06960	12.1	0.00273	8.1	0.00140	10.7	0.668	75	17.6	1.4	70.4	8.8	2750	120	17.6 ± 1.4
CR-5-5	173	237	1.37	0.13300	13.5	0.05040	12.1	0.00277	6.1	0.00110	10.0	0.507	64	17.8	1.1	49.8	5.9	2180	160	17.8 ± 1.1
CR-5-16	227	344	1.52	0.14000	17.1	0.05220	14.6	0.00279	6.1	0.00127	5.7	0.419	65	17.9	1.1	51.5	7.4	2130	200	17.9 ± 1.1
CR-5-14	205	347	1.69	0.12600	16.7	0.04740	14.6	0.00284	6.0	0.00111	8.5	0.411	61	18.3	1.1	46.9	6.6	2170	240	18.3 ± 1.1
CR-5-17	273	384	1.41	0.14000	20.0	0.05060	17.2	0.00284	6.3	0.00123	8.9	0.369	63	18.3	1.1	50.0	8.4	2210	210	18.3 ± 1.1
CR-5-6	226	347	1.54	0.21400	16.8	0.08300	16.9	0.00288	9.7	0.00155	6.5	0.576	77	18.6	1.8	81.0	13.0	2960	120	18.6 ± 1.8
CR-5-9	100	114	1.14	0.27000	14.1	0.10800	13.0	0.00299	8.4	0.00225	13.3	0.645	81	19.2	1.6	103.0	12.0	3240	150	19.2 ± 1.6
CR-5-11	118	147	1.25	0.21800	13.3	0.08900	12.4	0.00301	7.0	0.00173	9.2	0.564	77	19.4	1.3	85.8	9.9	3100	100	19.4 ± 1.3
CR-5-19	129	155	1.20	0.28800	12.2	0.13100	13.0	0.00346	5.5	0.00234	10.3	0.423	82	22.3	1.2	124.0	15.0	3420	150	22.3 ± 1.2
n = 19																			Concordia lower intercept Age =	**15.05 ± 0.94**
(2 sigma, MSWD = 2.5; all data)																				
Sample 5S-1 Cinco Señores intrusive (Tatatila de Las Minas, Veracruz)																				
5S-1-13	883	1600	1.81	0.08500	11.8	0.02500	9.6	0.00221	3.7	0.00075	4.1	0.381	43	14.2	0.5	25.1	2.3	1280	190	**14.2 ± 0.5**
5S-1-6	730	680	0.93	0.07900	16.5	0.02230	16.6	0.00223	5.8	0.00077	11.8	0.351	36	14.3	0.8	22.4	3.6	870	300	**14.3 ± 0.8**
5S-1-16	424	68	0.16	0.15400	16.9	0.05390	18.0	0.00229	6.6	0.00468	16.9	0.364	72	14.8	1.0	53.1	9.2	2500	210	14.8 ± 1.0
5S-1-11	424	402	1.45	0.08300	19.3	0.02660	19.2	0.00231	5.2	0.00102	7.0	0.271	44	14.9	0.8	26.6	5.0	1210	300	**14.9 ± 0.8**
5S-1-3	424	3630	2.84	0.08480	9.2	0.02690	7.8	0.00233	2.8	0.00074	3.5	0.358	45	15.0	0.4	27.0	2.1	1320	160	**15.0 ± 0.4**
5S-1-12	424	1200	1.96	0.08540	10.4	0.02780	10.4	0.00237	3.1	0.00082	4.0	0.295	45	15.3	0.5	27.8	2.8	1270	180	**15,3 ± 0,5**

http://dx.doi.org/10.18268/BSGM2020v72n3a110520

Appendix 3. (Continuation) U-Pb isotope data from zircons in the intrusive rocks associated with IOCG skarns in the Tatatila-Las Minas area.

				CORRECTED ISOTOPIC RATIOS												CORRECTED AGES (Ma)						
Analysis/Zircon	U# (ppm)	Th# (ppm)	Th/U	207Pb/206Pb†	err %*	207Pb/235U†	err %*	206Pb/238U†	err %*	208Pb/232Th†	err %*	Rho**	% disc.***	206Pb/238U	±2s*	207Pb/235U	±2s*	207Pb/206Pb	±2s*	Best Age (Ma) ± 2s				
5S-1-8	424	180	1.13	0.08900	19.1	0.03030	17.2	0.00238	5.5	0.00093	9.3	0.318	49	15.3	0.9	30.2	5.1	1330	310	**15,3 ± 0,9**		
5S-1-19	424	671	1.86	0.08100	16.0	0.02750	17.1	0.00241	3.7	0.00079	6.4	0.216	44	15.5	0.6	27.5	4.8	1180	240	**15.5 ± 0.6**		
5S-1-7	424	302	1.30	0.08750	9.1	0.02930	9.2	0.00249	3.7	0.00081	6.6	0.401	45	16.0	0.6	29.3	2.7	1410	180	**16.0 ± 0.6**		
5S-1-5	424	634	1.55	0.17200	17.4	0.05980	14.7	0.00257	8.2	0.00109	13.8	0.555	72	16.5	1.3	58.8	8.4	2530	270	16.5 ± 1.3		
5S-1-17	424	284	1.37	0.14700	10.9	0.05320	10.2	0.00260	4.2	0.00119	6.1	0.417	68	16.7	0.7	52.5	5.2	2240	170	16.7 ± 0.7		
5S-1-15	424	149	0.86	0.16000	23.8	0.05800	32.8	0.00264	7.6	0.00173	30.6	0.231	70	17.0	1.3	57.0	17.0	2410	310	17.0 ± 1.3		
5S-1-4	424	213	1.12	0.15000	10.7	0.05510	9.3	0.00265	4.2	0.00131	9.2	0.448	69	17.0	0.7	54.4	4.9	2330	160	17.0 ± 0.7		
5S-1-10	424	53	0.76	0.17900	21.8	0.07000	18.6	0.00272	8.8	0.00247	14.2	0.475	75	17.5	1.5	69.0	13.0	2480	450	17.5 ± 1.5		
5S-1-14	424	45	0.83	0.18300	27.3	0.06900	23.2	0.00277	9.4	0.00179	15.1	0.405	73	17.9	1.7	66.0	15.0	2010	570	17.9 ± 1.7		
5S-1-20	424	75	0.58	0.38200	12.6	0.13500	18.5	0.00278	8.6	0.00464	10.6	0.466	86	17.9	1.5	127.0	21.0	3730	180	17.9 ± 1.5		
5S-1-18	424	137	0.93	0.15600	17.3	0.06160	15.4	0.00281	6.4	0.00175	10.3	0.415	70	18.1	1.1	60.4	9.0	2410	240	18.1 ± 1.1		
5S-1-1	424	273	1.23	0.20700	20.8	0.08100	23.5	0.00282	6.4	0.00167	12.0	0.272	77	18.2	1.1	78.0	17.0	2670	340	18.2 ± 1.1		
5S-1-2	424	212	1.12	0.13200	23.5	0.05500	25.5	0.00287	7.3	0.00137	17.5	0.287	66	18.4	1.3	54.0	13.0	2070	350	18.4 ± 1.3		
5S-1-9	424	345	1.31	0.23700	15.2	0.09340	9.9	0.00302	6.6	0.00187	11.8	0.672	79	19.4	1.9	90.3	8.4	3030	250	19.4 ± 1.9		
n = 20																		Mean $^{206}Pb/^{238}U$ Age =		**15,09 ± 0,48**		
(2 sigma, MSWD = 4.0; n = 8)																						
Sample **SC-2b** — **Santa Cruz intrusive** (Tatatila de Las Minas, Veracruz)																						
SC-2b-6	318	178	0.56	0.27600	8.3	0.06680	7.0	0.00189	5.8	0.00195	7.7	0.827	81	12.1	0.7	65.6	4.4	3300	140	12.1 ± 0.7		
SC-2b-20	583	305	0.52	0.08300	13.3	0.02360	13.1	0.00199	3.6	0.00089	8.5	0.276	46	12.8	0.5	23.6	3.0	1260	210	12.8 ± 0.5		
SC-2b-7	365	405	1.11	0.06030	14.8	0.01670	16.2	0.00210	4.5	0.00067	11.8	0.279	19	13.5	0.6	16.8	2.7	230	260	**13.5 ± 0.6**		
SC-2b-5	275	194	0.71	0.07100	15.5	0.02060	13.1	0.00213	4.5	0.00079	7.9	0.340	34	13.7	0.6	20.7	2.7	840	270	**13.7 ± 0.6**		
SC-2b-8	259	208	0.80	0.08900	13.5	0.02570	11.7	0.00216	5.1	0.00098	9.2	0.436	46	13.9	0.7	25.7	3.0	1280	280	13.9 ± 0.7		
SC-2b-25	263	243	0.92	0.07000	15.7	0.02010	14.4	0.00217	4.6	0.00080	8.6	0.319	31	14.0	0.7	20.1	2.9	830	250	**14.0 ± 0.7**		
SC-2b-23	231	159	0.69	0.07100	21.1	0.02030	22.7	0.00223	4.4	0.00102	10.8	0.196	30	14.4	0.6	20.4	4.5	590	410	**14.4 ± 0.6**		
SC-2b-21	260	201	0.77	0.06200	16.1	0.01780	18.0	0.00225	5.3	0.00080	8.5	0.297	23	14.5	0.8	18.8	3.1	480	280	**14.5 ± 0.8**		
SC-2b-4	251	169	0.67	0.06800	17.6	0.02050	17.6	0.00225	3.5	0.00086	11.6	0.202	29	14.5	0.5	20.5	3.6	660	340	**14.5 ± 0.5**		
SC-2b-22	376	352	0.94	0.10800	11.1	0.03260	9.5	0.00226	3.9	0.00095	7.9	0.409	55	14.6	0.6	32.5	3.0	1740	190	14.6 ± 0.6		
SC-2b-10	227	151	0.67	0.06300	17.5	0.01900	16.8	0.00226	5.3	0.00084	13.1	0.315	24	14.6	0.8	19.1	3.2	560	350	**14.6 ± 0.8**		
SC-2b-18	350	266	0.76	0.13400	12.7	0.04150	12.3	0.00227	4.4	0.00131	9.2	0.358	64	14.6	0.7	41.1	4.9	2090	210	14.6 ± 0.7		
SC-2b-14	298	230	0.77	0.10400	12.5	0.03230	11.8	0.00228	5.3	0.00118	11.0	0.447	54	14.7	0.8	32.2	3.7	1640	210	14.7 ± 0.8		
SC-2b-9	266	181	0.68	0.07600	17.1	0.02480	13.7	0.00229	4.4	0.00098	8.9	0.319	41	14.7	0.7	24.8	3.4	870	290	14.7 ± 0.7		
SC-2b-2	266	174	0.65	0.05780	13.0	0.01820	12.6	0.00230	3.4	0.00087	9.6	0.268	19	14.8	0.5	18.3	2.3	410	260	**14.8 ± 0.5**		
SC-2b-3	366	311	0.85	0.11400	11.4	0.03500	11.7	0.00232	4.3	0.00108	7.9	0.368	57	14.9	0.7	34.8	4.0	1820	200	14.9 ± 0.7		
SC-2b-24	265	184	0.69	0.08700	13.8	0.02860	13.6	0.00233	4.7	0.00106	9.4	0.346	47	15.0	0.7	28.6	3.8	1220	270	15.0 ± 0.7		
SC-2b-15	219	150	0.68	0.06700	16.4	0.02050	18.5	0.00234	5.1	0.00085	10.4	0.277	29	15.1	0.8	21.2	3.8	740	320	**15.1 ± 0.8**		
SC-2b-13	219	170	0.78	0.12400	19.4	0.03900	30.8	0.00237	7.2	0.00108	39.8	0.233	60	15.2	1.1	38.0	11.0	1790	280	15.2 ± 1.1		
SC-2b-12	190	108	0.57	0.14300	12.6	0.04930	13.2	0.00241	4.1	0.00151	11.3	0.315	68	15.5	0.7	48.6	6.3	2220	250	15.5 ± 0.7		
SC-2b-19	278	191	0.69	0.10800	13.9	0.03480	14.4	0.00244	5.3	0.00103	12.6	0.371	55	15.7	0.8	34.6	4.8	1720	220	15.7 ± 0.8		
SC-2b-16	579	587	1.01	0.07530	10.5	0.02490	9.2	0.00245	4.5	0.00084	4.9	0.486	37	15.8	0.7	25.0	2.3	950	250	15.8 ± 0.7		
SC-2b-1	399	176	0.44	0.18800	7.4	0.06480	10.0	0.00248	4.0	0.00249	9.6	0.402	75	16.0	0.7	63.6	6.1	2740	130	16.0 ± 0.7		
SC-2b-11	176	105	0.59	0.06420	15.3	0.02580	19.8	0.00301	8.3	0.00110	12.7	0.420	25	19.4	1.6	25.7	5.0	540	300	19.4 ± 1.6		
SC-2b-17	280	207	0.74	0.24000	8.8	0.09510	6.9	0.00304	4.3	0.00272	4.8	0.616	79	19.6	0.9	92.1	6.0	3080	130	19.6 ± 0.9		
n = 23																		Mean $^{206}Pb/^{238}U$ Age =		**14,33 ± 0,38**		
(2 sigma, MSWD = 2.6; n = 9)																						
Sample **BO-1a** — **Boquillas intrusive** (Tatatila de Las Minas, Veracruz)																						
BO-1a-11	986	1860	1.89	0.05520	2.7	0.20090	3.4	0.02631	1.5	0.00803	2.1	0.443	10	167.4	2.5	185.8	5.9	431	58	167.4 ± 2.5		
BO-1a-18	716	651	0.91	0.05740	3.1	0.23740	3.0	0.03048	2.5	0.00823	3.4	0.811	10	193.6	4.7	216.2	6.0	496	64	193.6 ± 4.7		
BO-1a-20	900	820	0.91	0.05510	2.7	0.24630	3.9	0.03260	2.9	0.01198	3.3	0.748	8	206.8	5.9	223.6	7.9	414	61	206.8 ± 5.9		
BO-1a-9	302	133	0.44	0.05380	3.3	0.25160	3.6	0.03335	1.7	0.01286	3.5	0.473	7	211.5	3.5	227.5	7.4	400	75	211.5 ± 3.5		
BO-1a-8	504	131	0.26	0.05480	4.4	0.26100	4.2	0.03484	1.9	0.01255	4.0	0.443	6	220.8	4.0	235.4	9.0	391	95	220.8 ± 4.0		
BO-1a-14	541	196	0.36	0.05820	4.1	0.28000	4.3	0.03496	1.8	0.01299	3.6	0.420	12	221.5	3.9	250.7	9.2	513	89	221.5 ± 3.9		
BO-1a-17	532	240	0.45	0.05270	3.0	0.26300	3.3	0.03667	1.4	0.01336	2.5	0.424	2	232.1	3.2	236.9	7.1	299	68	232.1 ± 3.2		
BO-1a-12	306	81	0.26	0.05390	3.3	0.27300	3.7	0.03730	1.8	0.01297	4.1	0.483	4	236.0	4.1	244.7	8.3	369	75	236.0 ± 4.1		
BO-1a-23	248	15	0.06	0.05040	4.8	0.26200	5.0	0.03750	1.8	0.01704	5.7	0.365	1	237.3	4.2	240.0	10.0	190	100	237.3 ± 4.2		
BO-1a-10	382	166	0.43	0.05560	3.1	0.28200	3.9	0.03753	2.2	0.01296	3.9	0.553	6	237.5	5.0	252.1	9.0	414	74	237,5 ± 5,0		

http://dx.doi.org/10.18268/BSGM2020v72n3a110520

Appendix 3. (Continuation) U-Pb isotope data from zircons in the intrusive rocks associated with IOCG skarns in the Tatatila-Las Minas area.

				CORRECTED ISOTOPIC RATIOS											CORRECTED AGES (Ma)						
Analysis/Zircon	U# (ppm)	Th# (ppm)	Th/U	207Pb/206Pb†	err %*	207Pb/235U†	err %*	206Pb/238U†	err %*	208Pb/232Th†	err %*	Rho**	% disc.***	206Pb/238U	±2s *	207Pb/235U	±2s *	207Pb/206Pb	±2s*	Best Age (Ma) ± 2s	
BQ-1a-**4**	372	177	0.48	0.05330	4.7	0.27500	5.1	0.03759	2.5	0.01358	4.8	0.486	4	237.9	5.8	247.0	12.0	320	110	237,9	± 5,8
BO-1a-**6**	368	144	0.39	0.05350	3.9	0.28200	4.3	0.03861	1.9	0.01399	3.4	0.438	3	244.2	4.5	251.6	9.2	325	89	244.2	± 4.5
BO-1a-**24**	277	35	0.13	0.05230	4.4	0.27800	5.0	0.03875	2.1	0.01460	6.8	0.415	1	245.1	5.0	248.0	11.0	276	91	245.1	± 5.0
BO-1a-**2**	338	125	0.37	0.05380	3.5	0.28500	4.6	0.03933	2.2	0.01371	2.7	0.485	2	248.6	5.4	253.0	11.0	358	80	248.6	± 5.4
BO-1a-**7**	261	31	0.12	0.05670	3.9	0.30900	4.5	0.03994	1.9	0.01593	5.2	0.426	8	252.4	4.8	273.0	11.0	472	80	252.4	± 4.8
BO-1a-**25**	418	198	0.47	0.06810	7.5	0.38200	5.5	0.04060	3.4	0.01481	5.7	0.627	22	256.8	9.0	328.0	15.0	870	120	256.8	± 9.0
BO-1a-**19**	471	95	0.20	0.05230	2.9	0.29320	3.3	0.04118	1.5	0.01327	4.1	0.458	1	260.1	3.9	262.1	7.7	298	65	260.1	± 3.9
BO-1a-**13**	391	298	0.76	0.05250	4.4	0.32400	4.3	0.04479	1.9	0.01447	2.5	0.429	1	282.5	5.1	285.0	10.0	294	92	**282.5**	**± 5.1**
BO-1a-**15**	318	312	0.98	0.05260	3.4	0.32400	3.7	0.04492	1.8	0.01437	2.4	0.475	1	283.2	4.8	284.8	8.9	292	78	**283.2**	**± 4.8**
BO-1a-**3**	405	387	0.96	0.05190	3.5	0.33000	4.2	0.04582	2.1	0.01378	4.1	0.484	0	288.8	5.8	289.0	11.0	266	73	**288.8**	**± 5.8**
BO-1a-**5**	764	64	0.08	0.05950	2.9	0.38500	8.3	0.04690	7.9	0.01183	5.2	0.949	11	295.0	23.0	331.0	26.0	588	67	295.0	± 23.0
BO-1a-**16**	104	55	0.53	0.05450	4.8	0.37500	5.1	0.05100	1.8	0.01807	4.3	0.348	2	320.6	5.5	328.0	14.0	391	97	320.6	± 5.5
BO-1a-**1**	765	55	0.07	0.06470	1.7	0.46800	4.5	0.05210	3.5	0.01440	9.7	0.770	16	327.0	11.0	389.0	14.0	759	35	327.0	± 11.0
BO-1a-**26**	664	209	0.31	0.06600	2.4	0.49700	3.0	0.05424	1.8	0.01046	4.2	0.599	17	340.5	6.0	410.0	10.0	805	55	340.5	± 6.0
BO-1a-**21**	1069	120	0.11	0.07010	2.9	0.55900	7.0	0.05790	4.3	0.01490	24.8	0.619	20	363.0	15.0	451.0	23.0	928	52	363.0	± 15.0
BQ-1a-**22**	703	246	0.35	0.09140	1.9	1.86600	4.9	0.14920	3.9	0.06560	6.7	0.797	16	896.0	33.0	1069.0	35.0	1454	38	1454,0	± 38,0
n = 23																					
Sample **BQ-1b** **Boquillas intrusive** (Tatatila de Las Minas, Veracruz)																					
BQ-1b-**4**	322	97	0.30	0.08020	7.9	0.33700	5.9	0.03160	5.1	0.02010	9.0	0.853	33	201.0	12.0	299.0	18.0	1210	160	201,0	±
BO-1b-**1**	642	453	0.71	0.05120	3.9	0.26010	3.5	0.03683	1.9	0.01248	2.8	0.537	1	233.2	4.4	234.6	7.4	240	73	233.2	± 4,4
BO-1b-**16**	684	544	0.80	0.06170	4.1	0.31400	4.8	0.03699	1.8	0.01275	4.2	0.379	15	234.1	4.2	277.0	11.0	672	82	234.1	± 4.2
BO-1b-**11**	507	176	0.35	0.05630	2.8	0.28920	3.1	0.03715	1.5	0.01102	4.2	0.462	9	235.1	3.3	257.7	7.2	450	61	235.1	± 3.3
BO-1b-**3**	295	24	0.08	0.06660	3.8	0.35400	4.2	0.03849	1.7	0.03100	8.7	0.411	21	243.4	4.2	307.0	11.0	824	76	243.4	± 4.2
BO-1b-**14**	142	11	0.08	0.06070	4.8	0.33800	5.3	0.04043	1.9	0.01930	10.4	0.362	13	255.5	4.8	294.0	13.0	580	110	255.5	± 4.8
BO-1b-**10**	567	346	0.61	0.05570	2.9	0.34800	3.2	0.04471	1.8	0.01464	3.0	0.566	7	282.0	4.9	303.1	8.2	426	63	282.0	± 4.9
BO-1b-**6**	474	286	0.60	0.05360	3.0	0.33400	3.6	0.04500	2.2	0.01414	3.7	0.619	3	283.7	6.2	292.8	8.9	341	63	**283.7**	**± 6.2**
BO-1b-**15**	284	127	0.45	0.05910	3.0	0.36900	3.5	0.04521	1.5	0.01505	3.5	0.427	11	285.0	4.2	318.6	9.3	557	67	285.0	± 4.2
BO-1b-**13**	331	155	0.47	0.05390	3.5	0.34200	4.1	0.04553	1.5	0.01488	3.2	0.370	4	287.0	4.2	298.0	10.0	343	77	**287.0**	**± 4.2**
BO-1b-**5**	923	1400	1.52	0.05310	2.1	0.33080	2.4	0.04556	1.4	0.01457	1.7	0.599	1	287.2	4.1	290.0	6.1	342	45	**287.2**	**± 4.1**
BO-1b-**12**	301	151	0.50	0.06200	3.1	0.41500	3.4	0.04849	1.4	0.01651	2.7	0.422	13	305.2	4.2	352.0	10.0	662	63	305.2	± 4.2
BO-1b-**7**	263	199	0.76	0.05510	6.5	0.36800	6.0	0.04852	2.0	0.01566	4.5	0.334	4	305.4	6.0	317.0	17.0	390	150	305.4	± 6.0
BO-1b-**18**	185	138	0.75	0.05660	4.6	0.37200	4.8	0.04887	1.7	0.01557	3.4	0.351	4	307.6	5.1	321.0	13.0	444	99	307.6	± 5.1
BO-1b-**17**	151	74	0.49	0.07000	3.9	0.48400	3.9	0.04952	2.0	0.02109	3.1	0.499	23	311.5	6.0	402.0	13.0	920	80	311.5	± 6.0
BO-1b-**8**	395	80	0.20	0.05570	3.1	0.40300	4.0	0.05254	1.8	0.01546	4.6	0.465	4	330.1	6.0	343.0	11.0	412	59	330.1	± 6.0
BO-1b-**2**	1780	146	0.08	0.07330	1.9	0.84000	6.9	0.08380	5.4	0.02510	6.8	0.778	16	519.0	26.0	619.0	28.0	1018	37	519.0	±
BO-1b-**9**	637	312	0.49	0.08090	1.4	2.22700	2.0	0.20010	1.2	0.05960	1.7	0.632	1	1176.0	13.0	1191.0	14.0	1216	27	1216,0	± 27,0
n = 18																					

#U and Th concentrations (ppm) are calculated relative to analyses of trace-element glass standard NIST 610.

†Isotopic ratios are corrected relative to 91500 standard zircon for mass bias and down-hole fractionation (91500 with an age ~1065 Ma; Wiedenbeck *et al.*, 1995). Isotopic $^{207}Pb/^{206}Pb$ ratios, ages and errors are calculated following Paton *et al.* (2010).

*All errors in isotopic ratios are in percentage whereas ages are reported in absolute and given at the 2-sigma level. The weighted mean $^{206}Pb/^{238}U$ age is also reported in absolute values at the 2-sigma level. The uncertenties have been propagated following the methodology discussed by Paton *et al.* (2010).

**Rho is the error correlation value for the isotopic ratios $^{206}Pb/^{238}U$ and $^{207}Pb/^{235}U$ calculated by dividing these two percentage errors. The Rho value is required for plotting concordia diagrams.

http://dx.doi.org/10.18268/BSGM2020v72n3a110520

http://dx.doi.org/10.18268/BSGM2020v72n3a110520

Appendix 4. Age and trace element data for LA-ICPMS spot analyses on zircon grains for intrusive units in Tatatila-Las Minas, Veracruz, Mexico.

	Age (Ma) ± 2s	P	Ti	Y	Nb	La	Ce	Pr	Nd	Sm	Eu	Gd	Tb	Dy	Ho	Er	Yb	Lu	Hf	Pb	Th	U
Sample **ES-3** **Escalona dyke**																						
ES5-**1**	4,4 ± 0,4	530	11,3	2380	3,06	0,113	25,0	0,511	9,10	15,60	1,66	74,1	21,20	217	78,6	319	547	103	8880	0,45	497	384
ES5-**2**	4,7 ± 0,4	200	26,3	2290	2,08	0,057	12,7	0,456	5,99	11,71	1,67	60,5	18,40	204	74,2	316	549	108	7910	0,43	357	425
ES5-**3**	3,7 ± 0,2	-380	8,9	1162	1,77	0,038	16,6	0,080	2,14	4,65	0,82	25,0	7,70	93	36,6	166	331	69	9650	0,55	282	772
ES5-**4**	4,0 ± 0,4	-270	8,9	1240	2,91	0,000	20,5	0,087	1,51	2,40	0,54	20,2	6,91	87	38,1	188	409	88	9580	0,36	374	472
ES5-**5**	4,1 ± 0,3	580	10,4	2810	3,16	0,058	27,4	0,525	10,28	19,30	2,35	89,9	26,20	274	94,5	385	650	123	7750	0,49	893	730
ES5-**6**	14,2 ± 1,2	840	22,0	1170	1,42	0,102	16,6	0,127	3,20	5,10	0,92	30,9	10,50	100	36,8	160	290	60	9800	0,75	204	204
ES5-**7**	9,3 ± 0,8	350	20,0	3230	3,43	0,120	30,1	0,910	14,40	25,20	3,09	103,9	31,10	320	108,9	443	696	134	8620	1,09	622	468
ES5-**8**	6,0 ± 0,5	370	6,5	747	1,42	0,032	12,0	0,125	1,54	3,00	0,35	16,5	5,10	62	23,9	110	223	46	10810	0,37	140	342
ES5-**9**	5,5 ± 0,4	10	6,8	792	1,45	0,000	12,3	0,081	2,10	3,30	0,39	17,5	5,68	66	25,3	114	220	46	9990	0,36	135	272
ES5-**10**	5,1 ± 0,3	200	11,3	1880	2,44	0,026	20,7	0,316	7,29	14,55	1,80	59,9	18,20	183	62,3	256	420	82	9260	0,41	616	502
ES5-**11**	3,9 ± 0,3	370	10,1	2270	3,02	0,075	40,5	0,410	7,40	12,60	1,07	59,7	19,30	206	74,8	319	537	106	9770	0,75	1075	1045
ES5-**12**	4,2 ± 0,4	40	21,9	1561	1,43	0,031	10,3	0,378	5,70	10,60	1,32	44,6	13,90	145	50,8	218	381	77	7770	0,19	255	250
ES5-**13**	4,1 ± 0,3	730	6,5	3380	3,65	0,095	37,6	0,748	12,99	23,10	2,36	102,6	30,90	325	113,3	462	750	141	8350	0,71	1276	1031
ES5-**14**	4,2 ± 0,3	80	13,5	3070	2,78	0,076	27,1	0,690	10,48	20,50	2,26	93,7	28,40	289	102,7	421	721	139	7530	0,56	827	761
ES5-**15**	4,4 ± 0,3	50	13,4	2424	2,33	0,046	24,5	0,507	8,55	16,20	1,85	71,4	22,17	229	80,9	337	563	110	8950	0,47	798	717
ES5-**16**	5,1 ± 0,5	150	15,7	2930	2,74	0,064	18,2	0,520	6,46	15,91	2,50	90,8	26,50	284	98,1	404	656	129	8340	0,45	839	583
ES5-**17**	6,1 ± 0,4	70	126,0	1613	2,25	0,039	19,4	0,278	4,84	10,55	1,22	45,7	14,27	150	53,7	220	383	75	9110	0,54	512	454
ES5-**18**	4,2 ± 0,3	-310	7,9	1826	2,16	0,059	25,2	0,309	4,44	11,00	1,16	44,9	14,86	165	60,2	261	463	94	9260	0,53	762	830
ES5-**19**	4,4 ± 0,4	340	9,4	1552	1,50	0,139	13,9	0,349	5,00	8,99	1,19	42,8	13,11	141	50,7	220	400	80	7010	0,29	276	300
ES5-**20**	4,2 ± 0,4	-50	8,9	1001	1,18	0,004	15,2	0,126	1,63	4,28	0,70	21,9	7,23	85	32,3	146	281	59	10810	0,43	343	602
ES5-**21**	4,2 ± 0,3	420	14,3	3160	2,98	0,058	25,9	0,587	9,75	21,50	2,51	96,2	29,80	308	108,2	443	743	144	9780	0,55	946	818
ES5-**22**	4,6 ± 0,4	550	6,0	2160	2,32	0,077	23,4	0,420	5,30	10,20	1,45	67,4	20,20	210	73,3	310	531	103	10100	0,63	573	575
ES5-**23**	4,2 ± 0,4	900	12,4	2320	3,23	0,017	32,4	0,433	5,72	11,00	1,18	58,9	19,50	215	77,0	327	557	108	9010	0,76	1113	839
Sample **CR-5** **Carbonera intrusive**																						
CR5-**1**	17,3 ± 1,4	550	12,6	2120	2,57	0,028	51,7	0,540	6,80	12,00	4,58	47,4	14,80	163	63,5	298	731	164	7490	1,05	162	114
CR5-**2**	17,5 ± 1,4	540	3,4	1617	1,44	0,077	24,8	0,396	5,63	9,21	4,50	38,2	12,25	132	51,3	237	563	130	6860	0,51	238	179
CR5-**3**	16,0 ± 1,1	70	6,3	1894	1,76	0,026	33,6	0,365	5,84	9,39	4,58	40,3	13,19	149	57,4	272	643	146	7580	0,68	242	178
CR5-**4**	15,7 ± 1,5	180	3,6	1570	4,04	0,031	58,3	0,174	3,29	5,80	2,22	26,9	9,10	114	49,4	241	605	145	9130	1,68	341	264
CR5-**5**	17,8 ± 1,1	70	7,3	1595	1,43	0,046	21,8	0,334	4,48	7,83	3,97	36,8	11,88	133	50,7	238	554	126	7290	0,57	237	173
CR5-**6**	18,6 ± 1,8	-90	72,0	2102	1,95	0,272	27,8	0,396	5,70	9,72	4,63	48,3	15,00	172	66,0	309	702	158	7370	0,70	347	226
CR5-**7**	16,4 ± 1,2	300	6,0	3430	6,17	0,136	113,5	0,700	10,50	14,40	6,74	72,6	22,90	263	104,3	486	1157	253	8420	2,17	889	503
CR5-**8**	16,8 ± 0,7	380	11,0	2860	4,97	0,156	74,7	0,860	13,10	18,60	7,36	68,6	21,60	234	88,5	410	944	208	8210	1,51	1006	535
CR5-**9**	19,2 ± 1,6	-70	8,2	1019	0,98	0,044	15,8	0,263	3,15	5,43	2,42	22,1	6,85	79	31,3	152	377	85	6970	0,46	114	100
CR5-**10**	16,2 ± 0,8	130	4,3	2240	3,34	0,095	59,3	0,345	5,80	9,02	4,21	45,5	14,64	171	67,2	322	767	172	7840	1,36	524	368
CR5-**11**	19,4 ± 1,3	0	5,7	1184	1,05	0,037	19,2	0,295	4,96	7,38	3,30	28,4	8,76	99	38,3	177	426	97	7200	0,42	147	118
CR5-**12**	17,6 ± 1,0	150	5,4	2246	2,32	0,078	43,2	0,540	7,21	10,59	5,09	48,5	15,76	180	70,1	326	766	171	8330	0,97	438	283
CR5-**13**	17,5 ± 1,1	310	5,0	1803	1,22	0,057	27,7	0,417	7,25	10,90	4,80	43,2	13,12	150	55,6	256	606	136	7200	0,57	235	158
CR5-**14**	18,3 ± 1,1	1110	10,0	2830	2,72	0,081	54,6	0,940	13,20	20,40	8,65	72,7	22,00	235	88,8	407	918	198	7160	0,97	347	205
CR5-**15**	16,1 ± 1,1	440	9,0	2254	1,93	0,060	33,7	0,496	9,15	14,20	7,26	59,0	17,31	193	73,3	331	765	168	7190	0,60	321	188
CR5-**16**	17,9 ± 1,1	420	9,8	2180	1,89	0,202	37,3	0,647	9,04	14,38	6,01	53,5	16,27	182	69,7	320	750	167	7370	0,71	344	227
CR5-**17**	18,3 ± 1,1	450	3,5	2200	1,99	0,045	31,5	0,405	5,97	9,42	4,67	46,1	14,77	176	69,7	328	775	171	7870	0,81	384	273
CR5-**18**	17,6 ± 1,4	230	9,6	2360	2,13	0,118	39,5	0,538	8,10	11,40	5,65	55,0	16,70	189	73,6	346	806	179	8110	0,79	407	270
CR5-**19**	22,3 ± 1,2	170	3,3	1270	1,12	0,055	17,8	0,349	4,83	6,16	3,21	27,7	8,46	101	39,4	183	456	99	7680	0,54	155	129
Sample **5S-1** **Cinco Señores intrusive**																						
5S1-**1**	18,2 ± 1,1	90	15,2	1960	1,81	0,079	35,1	0,385	5,65	7,54	3,80	35,2	11,60	138	57,1	280	667	149	8650	0,61	273	222
5S1-**2**	18,4 ± 1,3	90	13,2	1490	1,58	0,216	28,0	0,381	4,35	5,21	2,44	25,0	8,00	98	40,6	221	563	129	7590	0,53	212	189
5S1-**3**	15,0 ± 0,4	200	18,8	2960	8,04	0,171	180,0	1,020	13,00	16,40	6,49	63,8	18,60	214	85,1	406	924	203	8400	2,82	3630	1280
5S1-**4**	17,0 ± 0,7	99	12,0	885	1,72	0,009	22,9	0,077	1,10	2,14	0,82	11,2	4,02	55	25,1	134	372	90	8300	0,50	213	190
5S1-**5**	16,5 ± 1,3	140	15,4	2070	3,26	0,018	57,1	0,073	1,19	2,87	1,73	26,1	9,40	128	58,0	301	752	171	8810	0,95	634	409
5S1-**6**	14,3 ± 0,8	110	11,9	930	1,47	0,103	15,5	0,156	1,82	3,46	1,20	15,9	5,05	65	27,4	140	382	104	10900	1,62	680	730
5S1-**7**	16,0 ± 0,6	110	12,8	1164	1,90	0,001	30,6	0,090	1,29	2,26	1,31	14,6	5,28	72	32,7	177	475	113	8000	0,57	302	233
5S1-**8**	15,3 ± 0,9	299	12,3	944	1,31	0,023	19,0	0,092	1,56	2,22	1,01	12,4	4,29	58	26,2	142	378	90	7930	0,39	180	159
5S1-**9**	19,4 ± 1,9	140	15,2	980	1,60	0,112	27,5	0,063	0,89	1,83	0,74	9,4	3,85	54	26,0	141	420	98	8800	0,81	345	264
5S1-**10**	17,5 ± 1,5	183	13,1	817	1,06	0,006	10,6	0,145	2,12	3,19	1,08	16,9	5,50	67	26,0	123	280	64	9820	0,20	53	70
5S1-**11**	14,9 ± 0,8	100	16,1	1300	2,21	0,250	32,9	0,143	1,59	2,48	1,38	17,9	6,61	88	38,3	196	474	109	8850	0,63	402	278

Appendix 4. (Continuation) Age and trace element data for LA-ICPMS spot analyses on zircon grains for intrusive units in Tatatila-Las Minas, Veracruz, Mexico.

	Age (Ma) ± 2s	P	Ti	Y	Nb	La	Ce	Pr	Nd	Sm	Eu	Gd	Tb	Dy	Ho	Er	Yb	Lu	Hf	Pb	Th	U
5S1-**12**	15,3 ± 0,5	215	14,5	1820	2,94	0,015	63,6	0,164	2,28	4,38	2,36	28,9	9,72	123	51,7	259	631	144	8300	1,48	1200	611
5S1-**13**	14,2 ± 0,5	234	15,0	2380	4,53	0,207	78,6	0,217	3,76	7,28	3,37	39,8	13,10	157	68,8	335	836	197	9430	1,86	1600	883
5S1-**14**	17,9 ± 1,7	302	19,1	1240	1,83	0,137	14,6	0,174	2,43	4,30	1,52	22,3	7,65	98	39,4	192	416	92	8520	0,15	45	55
5S1-**15**	17,0 ± 1,3	138	10,0	813	1,12	0,014	16,6	0,068	1,27	2,27	1,04	11,0	3,89	50	23,0	123	347	86	8540	0,44	149	174
5S1-**16**	14,8 ± 1,0	90	32,7	1080	1,76	0,189	15,5	0,199	2,43	3,33	1,23	18,7	6,26	82	33,0	168	388	86	10000	0,93	68	424
5S1-**17**	16,7 ± 0,7	199	12,4	1120	1,56	0,349	27,5	0,187	1,94	3,03	1,56	17,0	5,78	75	32,6	169	422	99	8230	0,53	284	207
5S1-**18**	18,1 ± 1,1	218	11,8	986	1,37	0,017	19,4	0,066	1,00	2,33	0,95	13,3	4,66	65	29,0	150	373	87	7880	0,41	137	147
5S1-**19**	15,5 ± 0,6	90	13,5	1208	1,91	0,150	42,0	0,111	1,35	2,50	1,30	14,3	5,26	71	32,6	180	506	124	8040	0,86	671	361
5S1-**20**	17,9 ± 1,5	250	22,5	1030	1,31	2,350	17,4	0,545	3,70	3,68	1,31	20,2	6,79	79	32,6	157	352	79	9760	0,38	75	130
Sample **SC-2b**	**Santa Cruz intrusive**																					
SC2b-**1**	16,0 ± 0,7	113	11,8	434	1,86	0,406	16,4	0,131	0,97	1,30	0,41	6,2	2,41	31	13,3	69	174	42	10040	0,96	176	399
SC2b-**2**	14,8 ± 0,5	205	11,8	771	1,70	0,013	13,7	0,083	1,28	2,26	0,84	13,2	4,71	59	24,4	121	278	65	9290	0,58	174	266
SC2b-**3**	14,9 ± 0,7	350	15,1	728	1,81	0,790	18,6	0,340	2,69	2,97	1,00	12,5	4,36	54	22,5	113	285	68	9620	0,83	311	366
SC2b-**4**	14,5 ± 0,5	179	10,9	409	1,27	0,000	10,8	0,015	0,43	0,99	0,40	6,4	2,31	30	12,3	62	159	39	9040	0,56	169	251
SC2b-**5**	13,7 ± 0,6	239	10,9	693	1,55	0,156	13,0	0,113	1,33	2,48	0,82	11,9	4,12	52	21,7	107	262	64	8880	0,59	194	275
SC2b-**6**	12,1 ± 0,7	4610	16,8	8460	1,21	2,940	39,0	13,100	157,00	228,00	71,60	629,0	145,00	1140	270,0	830	913	154	8870	0,60	178	318
SC2b-**7**	13,5 ± 0,6	310	12,4	967	2,14	0,129	19,0	0,121	2,18	3,91	1,31	18,8	6,33	74	30,6	148	326	78	9080	0,76	405	365
SC2b-**8**	13,9 ± 0,7	252	10,6	882	1,37	0,024	13,7	0,127	1,88	3,44	1,16	17,8	5,95	71	28,4	133	287	69	9030	0,55	208	259
SC2b-**9**	14,7 ± 0,7	367	12,0	1078	1,68	0,085	15,1	0,443	6,26	10,10	3,05	33,3	9,42	108	33,5	152	311	69	8420	0,60	181	266
SC2b-**10**	14,6 ± 0,8	212	10,9	441	1,46	0,028	10,9	0,043	0,61	1,03	0,45	6,4	2,35	32	13,6	69	177	43	8780	0,51	151	227
SC2b-**11**	19,4 ± 1,6	274	12,0	516	1,38	0,014	9,3	0,040	0,67	1,25	0,60	8,2	3,15	39	16,4	81	191	45	7950	0,57	105	176
SC2b-**12**	15,5 ± 0,7	420	12,3	426	1,32	0,690	11,8	0,200	1,03	1,02	0,39	6,6	2,39	30	12,4	66	171	42	9140	0,44	108	190
SC2b-**13**	15,2 ± 1,1	2770	26,7	780	1,49	27,000	62,5	5,750	26,70	10,00	2,67	23,8	6,92	76	26,1	115	246	52	9250	0,47	170	219
SC2b-**14**	14,7 ± 0,8	220	36,9	692	1,88	0,220	15,1	0,096	0,99	1,76	0,80	10,3	3,72	47	20,4	103	267	65	8460	0,65	230	298
SC2b-**15**	15,1 ± 0,8	230	10,3	453	1,35	0,146	11,6	0,050	0,81	1,21	0,46	7,1	2,60	33	14,1	69	177	43	8020	0,52	150	219
SC2b-**16**	15,8 ± 0,7	480	12,8	885	2,63	3,100	26,4	0,660	3,24	3,26	1,04	15,6	5,57	67	27,9	137	327	78	8870	1,35	587	579
SC2b-**17**	19,6 ± 0,9	179	10,9	685	1,52	0,070	13,2	0,100	1,26	2,56	0,99	13,0	4,20	51	21,0	103	264	65	9080	0,83	207	280
SC2b-**18**	14,6 ± 0,7	252	12,9	1189	2,43	0,045	20,3	0,111	1,64	3,50	1,20	20,4	7,20	95	37,8	181	393	90	8850	0,79	266	350
SC2b-**19**	15,7 ± 0,8	298	18,9	988	1,98	0,080	15,5	0,265	2,84	5,10	1,90	23,2	7,31	83	31,6	147	326	75	9110	0,67	191	278
SC2b-**20**	12,8 ± 0,5	170	11,7	988	3,53	0,106	23,1	0,069	1,52	2,35	0,78	15,7	5,67	73	30,4	152	353	82	10080	1,19	305	583
SC2b-**21**	14,5 ± 0,8	203	11,5	643	1,76	0,091	15,2	0,052	0,72	1,62	0,54	10,2	3,72	51	20,5	101	225	53	8940	0,59	201	260
SC2b-**22**	14,6 ± 0,6	223	14,6	1009	2,32	0,226	20,2	0,132	1,84	3,25	1,00	17,4	6,19	79	31,7	155	350	81	9030	0,84	352	376
SC2b-**23**	14,4 ± 0,6	160	9,9	688	1,39	0,072	11,7	0,068	1,38	1,99	0,78	11,9	3,90	51	21,6	107	255	62	8330	0,52	159	231
SC2b-**24**	15,0 ± 0,7	566	12,7	724	1,39	5,170	21,3	0,980	4,92	2,85	0,92	13,8	4,59	55	22,9	114	279	65	9120	0,64	184	265
SC2b-**25**	14,0 ± 0,7	232	10,8	1170	1,61	0,048	19,3	0,157	2,69	4,52	1,75	23,2	8,00	94	35,5	173	383	85	10230	0,59	243	263
Sample **BQ-1a**	**Boquillas intrusive**																					
BQ1a-**1**	327 ± 11	205	11,5	591	4,34	0,870	8,3	0,392	2,54	2,28	1,13	11,9	4,12	47	17,4	83	198	47	13390	40,50	55	765
BQ1a-**2**	249 ± 5	480	11,7	1050	1,98	0,080	8,7	0,077	1,13	2,25	0,95	15,0	5,66	78	33,2	170	453	106	10830	13,38	125	338
BQ1a-**3**	289 ± 6	385	16,7	1082	5,31	0,081	16,4	0,117	1,62	3,96	1,46	19,2	6,83	86	34,1	175	428	105	9010	18,75	387	405
BQ1a-**4**	238 ± 6	1250	47,0	4170	4,80	0,156	19,5	0,218	4,90	12,60	3,58	78,0	29,20	362	141,0	620	1130	229	10500	14,00	177	372
BQ1a-**5**	295 ± 23	204	11,6	647	3,03	0,699	7,8	0,349	2,57	2,61	1,55	16,3	5,63	60	19,3	81	168	38	13370	33,95	64	764
BQ1a-**6**	244 ± 5	125	10,5	946	1,94	0,044	10,0	0,113	1,78	3,96	1,30	20,9	6,69	77	29,7	140	324	71	11430	13,93	144	368
BQ1a-**7**	252 ± 5	56	15,8	550	1,92	0,043	4,5	0,073	1,49	3,76	2,61	22,9	6,97	62	16,9	58	87	17	13140	10,43	31	261
BQ1a-**8**	221 ± 4	290	18,9	1650	3,93	0,087	12,9	0,372	5,80	13,50	8,80	79,5	23,20	197	52,2	167	207	38	11700	17,38	131	504
BQ1a-**9**	212 ± 4	182	15,7	1110	1,52	0,088	9,4	0,160	2,07	3,81	0,91	20,3	7,01	83	35,4	173	390	90	10460	10,15	133	302
BQ1a-**10**	238 ± 5	120	11,0	1025	2,39	0,105	11,4	0,089	2,30	4,74	1,75	23,0	7,59	87	31,3	146	352	82	10310	13,73	166	382
BQ1a-**11**	167 ± 3	510	22,1	3490	14,00	1,010	80,0	1,100	12,70	21,10	7,13	96,1	29,70	315	110,9	478	907	188	9720	26,70	1860	986
BQ1a-**12**	236 ± 4	214	17,5	910	2,98	0,020	10,0	0,092	1,67	4,84	2,84	26,8	8,63	88	28,3	115	211	45	9600	11,43	81	306
BQ1a-**13**	283 ± 5	273	12,1	1185	3,00	0,160	19,4	0,097	1,25	3,26	1,88	20,5	7,18	90	37,7	183	461	109	10130	16,63	298	391
BQ1a-**14**	222 ± 4	150	26,2	1218	4,76	0,136	16,3	0,136	1,98	4,17	1,63	25,6	8,59	101	39,0	182	388	89	12450	18,38	196	541
BQ1a-**15**	283 ± 5	255	11,1	1545	2,65	0,049	20,8	0,161	2,27	4,99	2,31	29,8	10,04	121	49,2	237	553	129	11050	14,13	312	318
BQ1a-**16**	321 ± 6	180	9,6	535	0,79	0,007	5,2	0,028	0,56	1,30	0,59	7,5	2,89	38	16,6	89	240	61	9810	5,40	55	104
BQ1a-**17**	232 ± 3	160	9,8	1180	3,28	0,087	14,5	0,113	1,23	3,05	1,51	20,2	7,32	88	36,0	176	414	95	11270	19,30	240	532
BQ1a-**18**	194 ± 5	82	15,2	748	1,44	0,560	14,7	0,290	1,83	2,38	1,22	14,1	4,65	56	22,7	110	272	71	11490	21,53	651	716
BQ1a-**19**	260 ± 4	62	9,7	815	3,86	0,000	8,9	0,026	0,55	2,00	1,50	20,0	6,75	73	25,0	107	239	55	13220	19,43	95	471
BQ1a-**20**	207 ± 6	390	14,8	2100	8,33	0,490	48,2	0,239	1,86	4,89	1,82	32,8	11,80	156	68,5	346	820	189	13200	27,00	820	900
BQ1a-**21**	363 ± 15	197	45,0	639	2,60	0,664	8,0	0,347	2,97	2,69	1,39	13,9	5,46	60	19,7	79	149	32	13790	59,25	120	1069

http://dx.doi.org/10.18268/BSGM2020v72n3a110520

Appendix 4. (Continuation) Age and trace element data for LA-ICPMS spot analyses on zircon grains for intrusive units in Tatatila-Las Minas, Veracruz, Mexico.

	Age (Ma) ± 2s	P	Ti	Y	Nb	La	Ce	Pr	Nd	Sm	Eu	Gd	Tb	Dy	Ho	Er	Yb	Lu	Hf	Pb	Th	U
BQ1a-**22**	1454 ± 38	327	15,2	1570	2,80	0,427	25,6	0,591	6,19	8,42	2,94	40,6	13,41	147	50,9	209	378	77	11230	106,50	246	703
BQ1a-**23**	237 ± 4	168	26,4	760	1,91	0,118	1,9	0,075	0,93	3,13	2,49	25,4	8,27	76	22,0	73	103	20	9670	9,33	15	248
BQ1a-**24**	245 ± 5	108	10,3	870	2,60	0,033	6,5	0,078	0,87	3,63	2,46	27,2	9,01	90	26,4	95	145	28	12550	10,68	35	277
BQ1a-**25**	257 ± 9	154	20,0	1450	3,23	0,165	27,3	0,465	7,99	15,40	7,84	68,2	17,90	161	48,4	180	287	61	12660	16,18	198	418
BQ1a-**26**	341 ± 6	174	14,0	776	3,58	0,059	10,6	0,132	1,98	5,41	2,86	28,2	8,52	81	25,2	97	226	51	12500	34,53	209	664
Sample **BQ-1b**	**Boquillas intrusive**																					
BQ1b-**1**	233 ± 4	293	16,5	1440	7,37	0,145	27,6	0,294	4,70	7,01	2,86	31,7	9,17	114	45,7	223	539	131	10500	23,58	453	642
BQ1b-**2**	519 ± 26	228	19,0	682	8,30	1,740	12,7	0,496	3,46	2,76	0,70	11,5	3,31	47	21,3	120	357	88	14700	153,00	146	1780
BQ1b-**3**	243 ± 4	80	17,5	330	1,54	0,204	2,6	0,119	0,92	1,68	1,12	9,7	3,09	32	9,2	34	56	12	10340	11,50	24	295
BQ1b-**4**	201 ± 12	150	75,0	1260	2,66	0,146	11,6	0,246	3,25	5,34	2,75	32,7	11,20	116	38,1	169	361	83	12400	10,13	97	322
BQ1b-**5**	287 ± 4	520	14,1	3520	7,58	0,074	74,2	0,209	3,79	10,65	5,74	71,7	24,10	281	112,4	551	1187	265	9720	42,75	1400	923
BQ1b-**6**	284 ± 6	166	8,9	1149	3,82	0,075	17,6	0,078	1,63	4,53	1,90	29,0	9,52	106	36,0	152	305	66	11780	20,85	286	474
BQ1b-**7**	305 ± 6	340	11,4	1340	1,65	0,640	15,9	0,270	3,16	4,69	1,06	23,6	8,20	100	42,2	205	488	112	9830	12,48	199	263
BQ1b-**8**	330 ± 6	280	14,4	545	2,89	0,052	6,0	0,051	1,09	3,68	1,05	21,0	5,73	56	16,8	61	99	20	13200	21,28	80	395
BQ1b-**9**	1216 ± 27	403	22,0	1451	3,15	0,165	25,1	0,166	3,17	6,44	2,37	37,5	12,13	132	45,8	197	347	70	8550	127,00	312	637
BQ1b-**10**	282 ± 5	631	11,9	2610	4,01	0,053	20,8	0,219	4,71	9,70	3,77	56,1	19,00	221	83,4	384	806	180	11700	24,50	346	567
BQ1b-**11**	235 ± 3	175	11,2	1168	3,42	0,167	13,8	0,151	2,14	4,55	2,08	26,3	8,88	101	37,6	165	366	85	11240	18,63	176	507
BQ1b-**12**	305 ± 4	2870	29,3	1197	2,39	16,800	45,4	4,450	21,30	7,85	1,89	26,2	8,27	96	37,1	176	406	94	9800	14,75	151	301
BQ1b-**13**	287 ± 4	381	10,3	928	1,88	0,007	9,6	0,068	0,59	2,47	1,25	15,3	5,37	72	28,7	143	376	95	11720	15,30	155	331
BQ1b-**14**	256 ± 5	223	11,0	600	0,74	0,013	1,4	0,015	0,58	2,03	1,72	16,4	5,43	58	18,7	73	116	23	8830	5,98	11	142
BQ1b-**15**	285 ± 4	238	9,6	842	2,30	0,023	11,5	0,068	1,14	2,85	1,09	16,2	5,80	65	26,6	124	287	66	10500	12,80	127	284
BQ1b-**16**	234 ± 4	316	9,9	1387	4,20	0,093	26,1	0,113	1,47	3,74	1,05	23,3	8,09	102	42,1	209	512	118	11550	24,28	544	684
BQ1b-**17**	312 ± 6	334	29,9	847	1,79	0,151	7,9	0,059	1,15	2,21	0,65	14,0	5,15	68	27,7	132	306	69	9100	7,38	74	151
BQ1b-**18**	308 ± 5	410	8,1	1165	2,61	0,011	10,3	0,067	0,83	2,46	0,66	19,0	7,20	92	38,5	178	385	85	9760	9,23	138	185

Element concentrations (ppm) are calculated relative to analyses of trace-element glass standard NIST 610.

http://dx.doi.org/10.18268/BSGM2020v72n3a110520